

UNIVERSIDADE FEDERAL DE MINAS GERAIS
Instituto de Ciências Biológicas
Programa de Pós-Graduação em Bioquímica e Imunologia

Carlos Felipe Estevez Castro

***Trypanosoma cruzi* Inositol Phosphorylceramide Synthase as a Potential Drug Target for
Chagas Disease**

Belo Horizonte,
2020

Carlos Felipe Estevez Castro

***Trypanosoma cruzi* Inositol Phosphorylceramide Synthase as a Potential Drug Target for
Chagas Disease**

Versão final

Dissertação apresentada ao Programa de Pós-Graduação em Bioquímica e Imunologia da Universidade Federal de Minas Gerais como requisito parcial para obtenção do título de Mestre em Bioquímica e Imunologia.

Orientadora: Profa. Dra. Santuza Maria Ribeiro Teixeira

Belo Horizonte
2020

043 Castro, Carlos Felipe Estevez.
Trypanosoma cruzi inositol phosphorylceramide synthase as a potential drug target for Chagas disease [manuscrito] / Carlos Felipe Estevez Castro. – 2020.
95 f. : il. ; 29,5 cm.

Orientadora: Profa. Dra. Santuza Maria Ribeiro Teixeira.
Dissertação (mestrado) – Universidade Federal de Minas Gerais, Instituto de Ciências Biológicas. Programa de Pós-Graduação em Bioquímica e Imunologia.

1. Bioquímica e imunologia. 2. Doença de Chagas. 3. Trypanosoma cruzi. 4. Inositol. 5. Sistemas CRISPR-Cas. I. Teixeira, Santuza Maria Ribeiro. II. Universidade Federal de Minas Gerais. Instituto de Ciências Biológicas. III. Título.

CDU: 577.1



Universidade Federal de Minas Gerais
 Curso de Pós-Graduação em Bioquímica e Imunologia ICB/UFMG
 Av. Antônio Carlos, 6627 – Pampulha
 31270-901 – Belo Horizonte – MG
 e-mail: pg-biq@icb.ufmg.br (31)3409-2615



ATA DA DEFESA DA DISSERTAÇÃO DE MESTRADO DE CARLOS FELIPE ESTEVEZ CASTRO. Aos vinte e um dias do mês de fevereiro de 2020 às 09:00 horas, reuniu-se no Instituto de Ciências Biológicas da Universidade Federal de Minas Gerais, a Comissão Examinadora da dissertação de Mestrado, indicada *ad referendum* do Colegiado do Curso, para julgar, em exame final, o trabalho intitulado *Trypanosoma cruzi* inositol phosphorylceramide synthase as a potential drug target for chagas disease", requisito final para a obtenção do grau de Mestre em Bioquímica e Imunologia, área de concentração: Bioquímica. Abrindo a sessão, a Presidente da Comissão, Prof^a. Santuza Maria Ribeiro Teixeira, da Universidade Federal de Minas Gerais, após dar a conhecer aos presentes o teor das Normas Regulamentares do Trabalho Final, passou a palavra ao candidato para apresentação de seu trabalho. Seguiu-se a arguição pelos examinadores, com a respectiva defesa do candidato. Logo após a Comissão se reuniu, sem a presença do candidato e do público, para julgamento e expedição do resultado final. Foram atribuídas as seguintes indicações: Dr. Rafaela Salgado Ferreira (Universidade Federal de Minas Gerais), aprovado; Dr. Ana Paula Fernandes (Universidade Federal de Minas Gerais), aprovado; Dr. Santuza Maria Ribeiro Teixeira - Orientadora (Universidade Federal de Minas Gerais), aprovado. Pelas indicações o candidato foi considerado:

APROVADO
 REPROVADO

O resultado final foi comunicado publicamente ao candidato pela Presidente da Comissão. Nada mais havendo a tratar, a Presidente da Comissão encerrou a reunião e lavrou a presente Ata que será assinada por todos os membros participantes da Comissão Examinadora. Belo Horizonte, 21 de fevereiro de 2020.

Dr. Rafaela Salgado Ferreira (UFMG) *Rafaela S. Ferreira*

Dr. Ana Paula Fernandes (UFMG) *Ana Paula Fernandes*

Dr. Santuza Maria Ribeiro Teixeira - Orientadora (UFMG) *Santuza M. R. Teixeira*

Lida Quercia
 Prof^a Lida Quercia
 Coordenadora do Curso de Pós-Graduação
 em Bioquímica e Imunologia
 ICB - UFMG

Acknowledgments

To You, my God, Lord of my life.

To my family, the one I chose and the one that didn't, here in Brazil and Colombia, for their unconditional love.

To Professor Santuza Teixeira, for all the teachings, from pipetting to molecular biology.

To Dani for its unconditional friendship and help during literally this whole process.

To Mari, Gabi, Edson, Heli, Vivi, Thais, Nailma, Fernanda, Renata, Wannessa, Rafael, Carlos, and Melissa, more than colleagues and guides, friends.

To Professor Paul Denny, for the Benzazepanes, support, and valuable discussions.

To Professor Patiu, for her dear friendship.

To Professor Elaine Souza-Fagundes, and her students, for the friendship and help to use the microplate reader.

To Professor Silvane Murta for donating the Benznidazole used in this work.

To Professor Silvia Uliana, for donating the Tamoxifen used in this work.

To Jamil, for his friendship and valuable help in the lipid extractions.

To the friends from other ICB laboratories, for their good energy and willingness to help.

To the UFMG and the postgraduate program in Biochemistry and Immunology for the valuable opportunity to take this course.

To the financing agencies CNPq, CAPES, and GCRF, for the funding to carry out this work.

To FAPEMIG, for the granting of the scholarship.

And to all those who somehow contributed to the realization of this work.



O importante é a Rosa.

Resumo

Os esfingolipídios (SLs) são uma parte essencial de todas as membranas celulares eucarióticas. A inositol fosforilceramida (IPC) é um SL presente em numerosos protozoários, porém ausente em mamíferos. No *Trypanosoma cruzi*, este SL complexo é sintetizado pela IPC sintase, uma proteína integral de membrana expressa em todas as formas do parasito. Em consequência, a IPC sintase constitui um alvo ideal para o desenvolvimento de novas quimioterapias para a doença de Chagas; afecção causada pelo *T. cruzi* que carece de tratamento eficaz. Assim, neste estudo o nosso objetivo foi validar a IPC sintase do *T. cruzi* (TcIPCS) como potencial alvo terapêutico para a doença de Chagas, através da geração e caracterização de parasitos geneticamente modificados. Além disso, a avaliação de potenciais compostos anti-TcIPCS também foram analisados para verificar o potencial da enzima como alvo de fármacos. Utilizando a tecnologia CRISPR-Cas9, geramos mutantes nocautes do gene da *TcIPCS*, refutando a suposição sobre a essencialidade desse gene em *T. cruzi*. No entanto, as caracterizações fenotípicas dos parasitos nocautes da *TcIPCS* demonstraram a importância da *TcIPCS* para o *fitness* do *T. cruzi*. A deleção do *TcIPCS* afetou negativamente a proliferação de epimastigotas e a metaciclo gênese. Além disso, os parasitos nocautes apresentaram diminuição das capacidades de infecção *in vitro*, replicação intracelular das amastigotas e liberação de tripomastigotas das células hospedeiras. Curiosamente, o sobrenadante de células infectadas com os mutantes mostrou a predominância de amastigotas extracelulares (EA), provavelmente como resultado de alterações metabólicas que desencadeiam a diferenciação das tripomastigotas liberadas para as formas EA. Também visando caracterizar o papel do TcIPCS em *T. cruzi*, geramos parasitos que superexpressam o *TcIPCS* usando o vetor de expressão pROCK-Hygro. Esses parasitos apresentaram *in vitro* uma metaciclo gênese precoce e aumentada. Embora várias tentativas de obter a proteína completa expressa em *E. coli* tenham sido malsucedidas, fomos capazes de expressar e purificar uma fração C-terminal antigênica da proteína que será usada para imunizar camundongos. Finalmente, testamos inibidores específicos da IPCS da *L. major* identificados recentemente, contra os parasitos nocautes e selvagens usando um ensaio de viabilidade celular baseado na resazurina. Os resultados dos ensaios de dose-resposta com quatro compostos selecionados não mostraram atividade anti-TcIPCS significativa contra as formas epimastigotas. Em conclusão, embora a TcIPCS tenha demonstrado ser não essencial para a viabilidade do *T. cruzi*, a caracterização fenotípica tanto dos parasitos nocautes como dos superexpressores sugerem que esta enzima é um alvo interessante para o desenvolvimento de drogas.

Palavras-chave: Doença de Chagas, *Trypanosoma cruzi*, Inositol fosforilceramida sintase, alvo terapêutico, CRISPR-Cas9.

Abstract

Sphingolipids (SLs) are an essential part of all eukaryotic cellular membranes. Inositol phosphorylceramide (IPC) is an SL present in numerous protozoa but absent in mammals. In *Trypanosoma cruzi*, this complex SL is synthesized by the IPC synthase, an integral membrane protein expressed in all parasite forms. Thus, IPC synthase constitutes an ideal target for the development of new chemotherapy for Chagas disease, an illness caused by *T. cruzi* infection, which still lacks effective treatment. In this study, we aimed to validate the *T. cruzi* IPC synthase (TcIPCS) as a potential therapeutic target for Chagas disease, through the generation and characterization of genetically modified parasites. We also evaluated potential anti-TcIPCS compounds to verify the tractability of the enzyme for drug screening. Using the CRISPR-Cas9 technology, we generated *TcIPCS* null mutants, disproving an assumption about the essentiality of this gene in *T. cruzi*. Nevertheless, phenotypic characterizations of *TcIPCS* null mutants demonstrated the importance of TcIPCS for the fitness of this parasite. *TcIPCS* deletion affected epimastigote proliferation and metacyclogenesis. Moreover, Knock-out (KO) parasites showed decreased *in vitro* infection capacities, intracellular amastigote replication and trypomastigote release from host-cells. Interestingly, the supernatant of cells infected with the mutants showed the predominance of extracellular amastigotes (EA), most likely as a result of metabolic changes that trigger differentiation of the released trypomastigotes into EA forms. Also aimed at characterizing the TcIPCS role in *T. cruzi*, we generated transfected cell lines overexpressing *TcIPCS* using the pROCK-Hygro expression vector. *TcIPCS* overexpressors showed early and enhanced metacyclogenesis *in vitro*. Although several attempts to obtain the full-length protein expressed in *E. coli* were unsuccessful, we were able to express and purify a recombinant antigenic C-terminal fraction of the protein that will be used to immunize mice. Finally, we tested recently identified specific inhibitors of the *L. major* IPCS, against wild type *T. cruzi* and *TcIPCS* null mutants using a resazurin cell viability assay. The results of dose-response assays with four selected compounds showed no significant activity against epimastigotes. In conclusion, although *TcIPCS* was proven to be non-essential for the viability of *T. cruzi*, the phenotypic characterization of both knockout parasites and overexpressors suggests that this enzyme is still an attractive target for drug development.

Keywords: Chagas disease, *Trypanosoma cruzi*, Inositol phosphorylceramide synthase, therapeutic target, CRISPR-Cas9.

List of Figures

Figure 1. Global distribution of Chagas disease cases according to official estimates and status of vector transmission.....	16
Figure 2. Vector-borne transmission and life cycle of <i>Trypanosoma cruzi</i>	18
Figure 3. Illustration of representative species of complex sphingolipids in Mammals and <i>T. cruzi</i>	20
Figure 4. Schematic representation of de novo sphingolipid biosynthesis.....	22
Figure 5. Form dependent sphingolipid signatures in <i>T. cruzi</i> Y-strain epimastigotes and Tissue-culture cell-derived trypomastigotes.	23
Figure 6. Schematic representation of the PredMP workflow.....	46
Figure 7. TcIPCS2 topology and 3D model predicted with PredMP	47
Figure 8. Alignment of kinetoplastid Inositol phosphorylceramide synthases.....	49
Figure 9. <i>TcIPCS</i> null mutants' generation by a single nucleofection with two specific sgRNAs complexed with the recombinant <i>Staphylococcus aureus Cas9</i> (rSaCas9) and an HDR DNA donor.....	51
Figure 10. PCR genotyping and quantitative PCR analysis of <i>TcIPCS</i> null mutants	54
Figure 11. Phenotypic characterization of <i>TcIPCS</i> null mutants.....	56
Figure 12. Generation of <i>TcIPCS</i> overexpressor parasites and preliminary characterization.	66
Figure 13. pET28a-TcIPCS1 and pET28a-C-terminal-TcIPCS1 vector construction and <i>in silico</i> analysis of the expected rC-terminal-TcIPCS1	69
Figure 14. Heterologous expression of rTcIPCS1 (38.68 kDa) and rC-terminal-TcIPCS1 (23.87 kDa), and purification by affinity chromatography.....	71
Figure 15. Establishment of a resazurin cell viability assay to evaluate <i>TcIPCS</i> KO epimastigote sensitivity to potential TcIPCS inhibitory molecules.	73
Figure 16. Effect of benzazepanes against wild type and <i>TcIPCS</i> KO epimastigotes	77

List of Tables

Table 1. Primers used in this study..	30
Table 2. <i>E. coli</i> strains used in this study.....	33
Table 3. Chemical compounds evaluated in this study.....	42

Abbreviations

aa	Amino acid
AAPI	Alkylacyl-phosphatidylinositol
AE	ArcticExpress (DE3)
AEPnC	Aminoethylphosphonate
BZ	benznidazole
CD	Chagas disease
CDS	Coding sequence
CER	Ceramide
CerS	Ceramide synthase
CNS	Crystallography & NMR System
DAG	Diacylglycerol
DMEM	Dulbecco's Modified Eagle Medium
DMEM-2	DMEM medium supplemented with 2% FBS
dpi	Days post-infection
DSB	Double-stranded break
DTL	Deep Transfer Learning
EA	Extracellular amastigotes
EPC	Phosphoethanolamine ceramide
ER	Endoplasmic reticulum
EuPaGDT	Eukaryotic Pathogen CRISPR guide RNA/DNA design tool
FBS	Fetal bovine serum
FT	Flow-through
GA	Golgi apparatus
GIPL	Glycoinositolphospholipid
GluCer	Glucosylceramides
GPI	Glycosylphosphatidylinositol
HA-tag	Human influenza hemagglutinin tag
HDR	Homology-directed repair
hpi	Hours post-infection

HR	Homologous recombination
HTS	High throughput screening
IC50	Half maximal inhibitory concentration
INS	Insoluble
IPC	Inositol phosphorylceramide
IPL	Inositolphospholipid
KO	Knockout
LIT	Liver infusion tryptose
LLC-MK2	Rhesus Monkey Kidney Epithelial Cells
LPP	Lipid phosphate phosphatase
MOI	Multiplicity of infection
MP	Transmembrane protein
MSA	Multiple sequence alignment
MW	Molecular weight
NF	Nifurtimox
NI	Non-induced
OE	Overexpressor
OR	Origami2 (DE3)
PC	Phosphatidylcholine
PI	Phosphatidylinositol
PI-PLC	Phosphoinositide phospholipase C
PLB	Phosphate lysis buffer
PP	Purified protein extract
RIPA buffer	Radioimmunoprecipitation assay buffer
rSaCas9	Recombinant Staphylococcus aureus Cas9
SB	Solubilization buffer
SDS-PAGE	Sodium dodecyl sulfate–polyacrylamide gel electrophoresis
sgRNA	Single-guided RNAs
SIA	Sialic acid
SL	Sphingolipid
SLS	Sphingolipid synthase

SM	Sphingomyelin
SMS	Sphingomyelin synthase
SOL	Soluble
SPH	Sphingosine
SPT	Serine palmitoyltransferase
Ssp4	Stage-specific surface protein 4
TAM	Tamoxifen
TCT	Tissue-culture cell-derived trypomastigotes
TM	Transmembrane
TMD	Transmembrane domain
TS	Trans-sialidases
WHO	World Health Organization
WT	Wild type

Table of Content

1. Introduction	16
1.1 <i>Trypanosoma cruzi</i> , the causative agent of Chagas disease	16
1.2 Available treatment, putative drug targets against CD and vaccine development	19
1.3 Sphingolipids and their biological significance	20
1.4 The sphingolipid biosynthetic pathway	21
1.5 The sphingolipid biosynthetic pathway as a potential target for chemotherapy against CD	22
1.6 The <i>T. cruzi</i> inositol phosphorylceramide synthase and its biological significance	23
1.7 TcIPCS as drug target	24
2. Objectives	26
2.1 General objective	26
2.2 Specific objectives	26
3. Materials and Methods	27
3.1 Parasite cultures	27
3.2 Gene characterization, expression pattern, and topology and 3D structure prediction of the <i>T. cruzi</i> Inositol Phosphorylceramide Synthase	28
3.3 Genomic DNA extraction of <i>T. cruzi</i> CL Brener	28
3.4 Total RNA isolation from <i>T. cruzi</i> epimastigotes	29
3.5 PCR and quantitative real-time PCR primer design	29
3.6 PCR amplification	31
3.7 Cloning of <i>T. cruzi</i> and <i>E. coli</i> expression vectors	32
3.8 Transformation of <i>E. coli</i> competent cells	33
3.9 Plasmid DNA extraction and endonuclease restriction cleavage	34
3.10 Transfection and cloning of <i>T. cruzi</i> epimastigote forms	34

3.11	CRISPR-Cas9 knockout of the <i>T. cruzi</i> <i>IPCS</i> gene	35
3.12	Generation of <i>T. cruzi</i> <i>IPCS</i> overexpressing parasites	36
3.13	Quantitative PCR	37
3.14	Recombinant TcIPCS1 and C-terminal-TcIPCS1 induction and purification	38
3.15	SDS-PAGE and western blot analysis	39
3.16	Growth curve and <i>in vitro</i> metacyclogenesis assays	40
3.17	<i>In vitro</i> infections	40
3.18	Chemical compounds with potential anti-TcIPCS activity and resazurin sodium salt ...	41
3.19	Resazurin cell viability assays and determination of the half maximal inhibitory concentration (IC ₅₀) of each compound	42
3.20	Statistical analyses and graphics	43
4.	Results and Discussion	44
4.1	<i>TcIPCS</i> gene characterization	44
4.2	Topology and 3D structure predictions of the <i>T. cruzi</i> Inositol Phosphorylceramide Synthase protein and its comparison with related orthologues	44
4.3	Generation of <i>T. cruzi</i> <i>IPCS</i> knockout parasites using the CRISPR-Cas9 system	50
4.4	Phenotypic characterization of <i>TcIPCS</i> null mutants	55
4.5	Generation of <i>T. cruzi</i> <i>IPCS</i> overexpressors and preliminary characterization	63
4.6	Recombinant <i>TcIPCS1</i> and <i>C-terminal-TcIPCS1</i> heterologous expression and purification for anti-TcIPCS polyclonal antiserum generation	67
4.7	Determination of inhibitory concentrations (IC ₅₀) of tamoxifen and benzazepanes for <i>TcIPCS</i> KO and wild type epimastigotes	72
5.	Concluding Remarks and Perspectives	79
6.	Bibliography	81

1. Introduction

1.1 *Trypanosoma cruzi*, the causative agent of Chagas disease

Trypanosoma cruzi is a vector-borne flagellated parasite that belongs to the order Kinetoplastida, family Trypanosomatidae (Levine et al. 1980). It is the causative agent of Chagas disease (CD), an anthroponozoonosis that affects about 6-8 million people worldwide and causes approximately 50,000 deaths per year (Lidani et al. 2019). Although CD was once entirely confined to the 21 Central and South America's countries in which the parasite is endemic, today mostly due to migration it has spread to non-endemic regions such as North America, Europe, and Western Pacific regions, making Chagas disease an important public health problem of global concern (Gascon, Bern, and Pinazo 2010; Jackson, Pinto, and Pett 2014). Currently, it is estimated that around 65 – 100 million people worldwide are at risk of contract CD (Engels and Savioli 2006; WHO 2015).

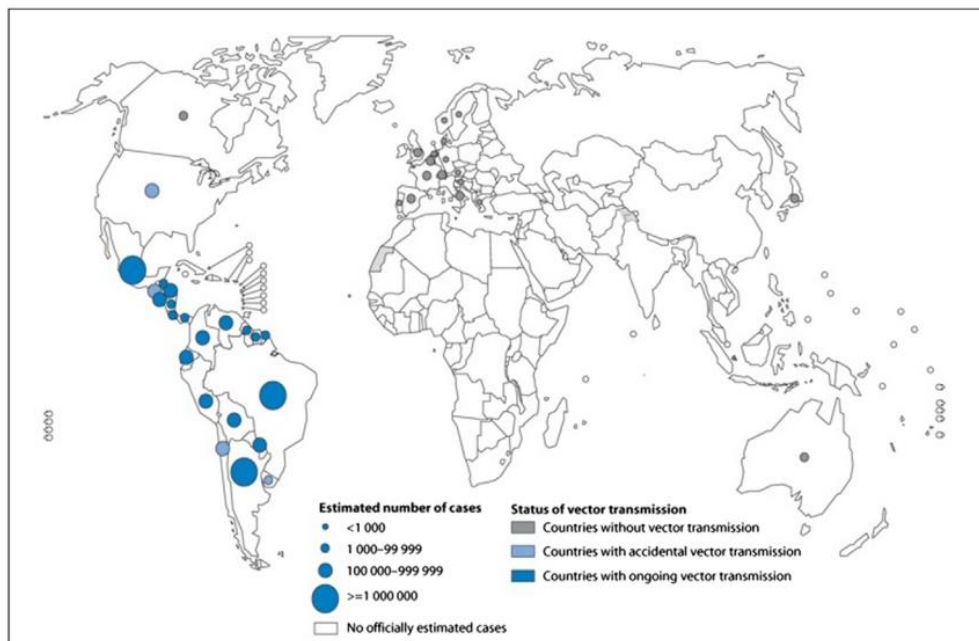


Figure 1. Global distribution of Chagas disease cases according to official estimates and status of vector transmission. Taken from Guhl and collaborators (2017).

T. cruzi is primarily transmitted to humans by the feces of blood-sucking triatomine insect vectors, widely known as “kissing bugs”, however non-vectorial mechanisms of infection can occur through organ transplantations, blood transfusions, oral and congenital transmission (Rassi Jr, Rassi, and Marin-Neto 2010). CD has two characteristic clinical phases: acute phase, characterized by high parasitemia and inflammation, and chronic phase, which can be asymptomatic, with no apparent pathology that may be extended during the rest of the host’s lifespan, or symptomatic, which occurs usually 10-30 years after infection in 30 - 40% of the patients and may result in severe digestive and/or cardiac damage. Symptomatic chronic phase can be deadly if untreated (Rassi, Rassi, and Marcondes de Rezende 2012).

T. cruzi has a complex life cycle with mainly four different morphologically and biochemically forms that involve the blood-sucking triatomine insect vectors and a broad range of mammalian hosts. Inside the midgut of the bug, epimastigote form proliferates until reaching the insect’s hindgut, where it differentiates into a non-dividing infectious metacyclic trypomastigote. During an insect blood meal, these metacyclic trypomastigotes are transmitted to mammals by the contaminated feces that passes through the skin lesions caused by the insect vector as it eats (Rassi Jr, Rassi, and Marin-Neto 2010). After infection, these metacyclic parasites penetrate host cells and transform into replicative amastigote form. Inside host cells, these amastigotes multiply by binary fission and differentiate into non-replicative trypomastigotes (tissue-culture cell-derived trypomastigotes when obtained *in vitro*), which are released to the bloodstream upon host cell lysis. Consequently, infective trypomastigotes spread and invade a range of nucleated cells and tissues. Finally, infected blood is taken up by another insect, which restarts the parasite’s life cycle (Figure 2) (M. C. Fernandes and Andrews 2012).

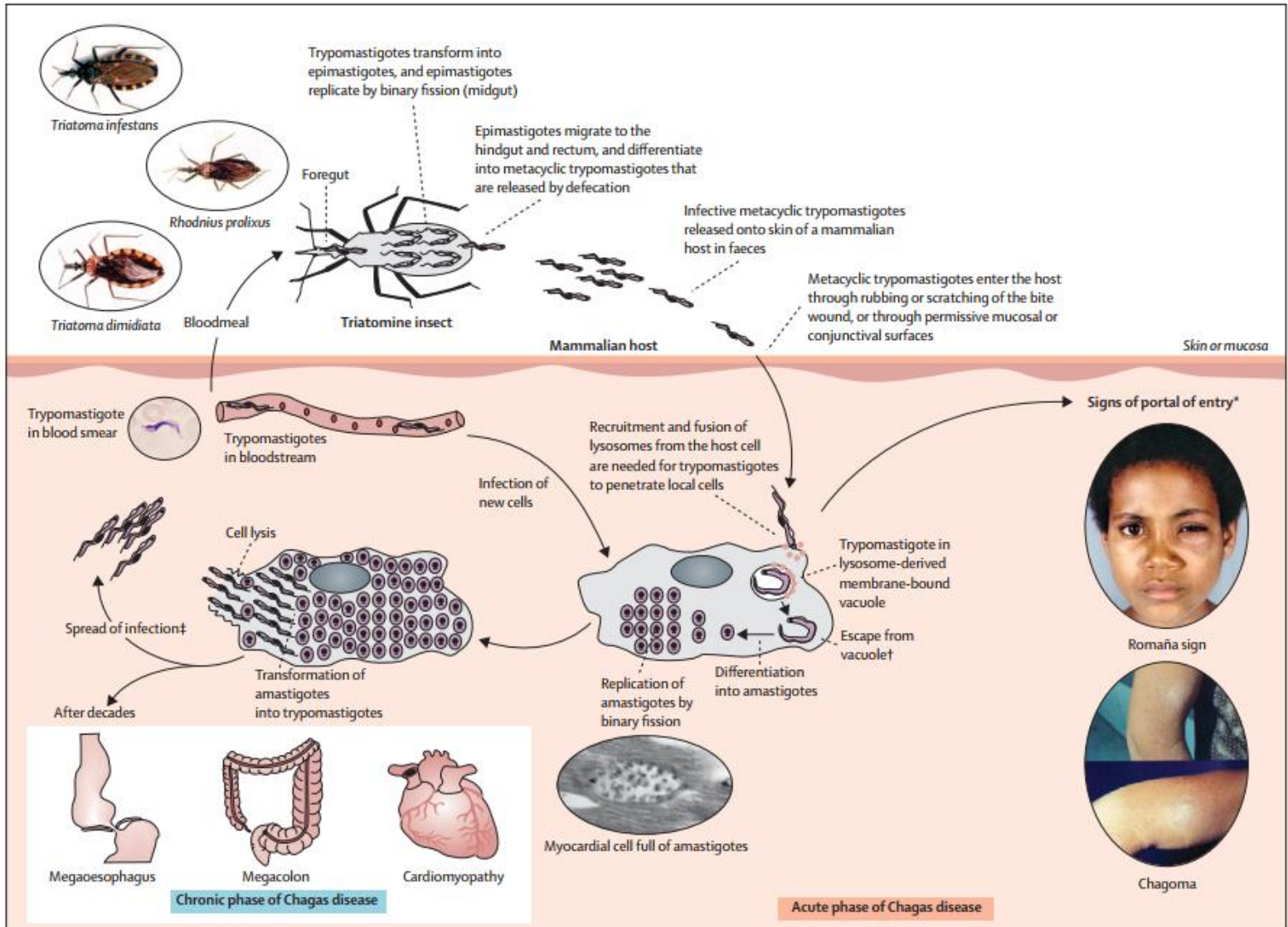


Figure 2. Vector-borne transmission and life cycle of *Trypanosoma cruzi*. Taken from Rassi Jr et al. (2010)

1.2 Available treatment, putative drug targets against CD and vaccine development

Despite more than a hundred years of research, a vaccine to prevent CD is not available, and treatment relies on two drugs with substantial limitations and severe side effects. According to the World Health Organization (WHO), the goal of treatment for CD is to eliminate the parasite from infected patients, hence decreasing the probability of developing symptomatic CD and hindering parasite transmission (WHO 2012).

Currently, there are only two approved drugs for chemotherapy for CD, benznidazole (BZ) and nifurtimox (NF). Both drugs require prolonged treatment (60-90 days) and are mainly useful for acute infections, congenital cases, and cases of reactivation during the chronic phase (Müller Kratz et al. 2018) However, treatment is often discontinued due to adverse side effects (Menna-barreto and Castro 2017) and inefficacy against the genetic background of the infecting strain (Zingales 2018).

As these treatments for CD were developed many decades ago, are ineffective, and possess toxic side effects, there has been an increasing demand for the identification of exploitable macromolecular targets for therapeutic development. Thus, diverse pathways and enzymes have attracted attention as possible drug targets such as the sterol biosynthetic pathway, the lysosomal cysteine protease cruzipain, the trypanothione reductase, and the N-myristoylome (Fernando Villalta and Rachakonda 2019). Nevertheless, none of these studies have been entirely successful.

Besides chemical treatments, immunological protection against experimental infection has also been extensively studied (Rodríguez-Morales et al. 2015). Although a broad spectrum of immunogens has been evaluated, the development of an effective human vaccine against CD remains an open question. However, over the last years, the prospect of a potential vaccine for CD has started to improve. Such potential has been boosted by the greater understanding of the immune mechanisms responsible for control of infection, the identification of targets involved in the parasite infectivity, and the development of molecular tools, like CRISPR, to study such targets, making the production of strong and safe immune therapies a more feasible task (Rios et al. 2019).

Overall, the lack of effective therapy or vaccine demands an intensive search for alternative anti-trypanosomal therapies with alternative molecular targets that may allow developing effective treatment and control.

1.3 Sphingolipids and their biological significance

Sphingolipids (SLs) represent one of the major classes of eukaryotic lipids. They were first isolated in the late 19th century by Johann L. W. Thudichum, and since then, SLs have been a subject of intense studies. Initially, they were considered of structural importance only; but, over the last two decades, numerous studies have shown their roles in diverse aspects of cell growth regulation, polarized cellular trafficking, signal transduction, differentiation and apoptosis (Cuvillier 2002; Hannun and Obeid 2018; Huwiler et al. 2000; Ohanian and Ohanian 2001).

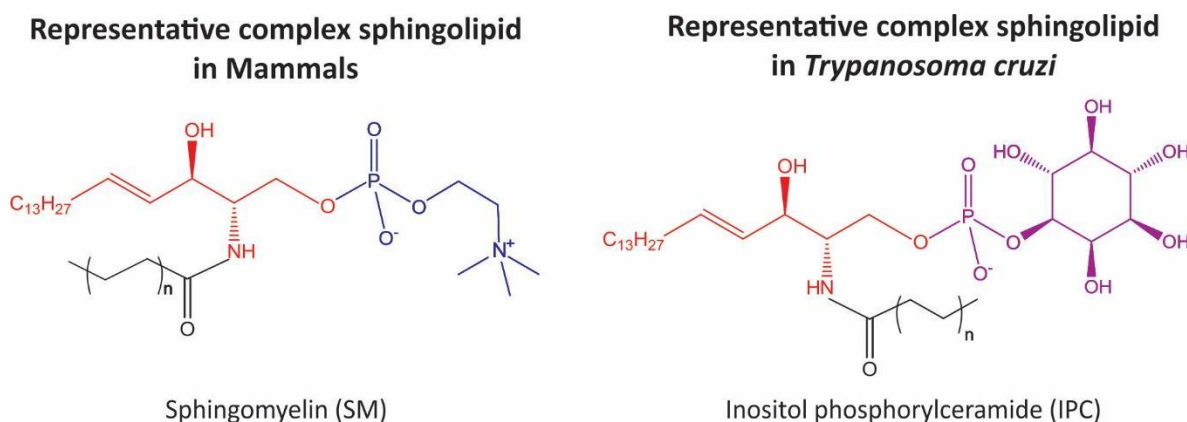


Figure 3. Illustration of representative species of complex sphingolipids in Mammals and *T. cruzi*. Sphingosine backbones are colored in red. Phosphocholine and inositol-phosphate head groups are colored in blue and purple, respectively. Fatty acids are colored in black. Sphingolipid head group and fatty acid chain may vary, producing alternative sphingolipid classes.

Structurally, SLs can be distinguished from other lipids by the presence of a sphingoid base backbone (e.g., sphingosine (SPH)) linked by an amide bond to an acyl group of a fatty acid to form *N*-acyl-sphingosines commonly named “ceramides.” To the latter, numerous head groups can be attached, i.e., neutral, charged, phosphorylated, and or glycosylated, to form complex SLs as

sphingomyelin (SM), the predominant complex SL in mammals, or inositol phosphorylceramide (IPC), that predominates in fungi, plants, and various protozoa, including *T. cruzi* (J. G. M. Mina and Denny 2018). Such structure confers the SLs with an amphipathic character that gives rise to their tendency to aggregate into membranous structures. Moreover, the diversity of the attached chemical groups allows for their distinct roles within cellular metabolism (Hannun and Obeid 2018).

1.4 The sphingolipid biosynthetic pathway

SL metabolism constitutes a highly complex matrix of associated pathways where ceramide occupies a central position in biosynthesis and catabolism (Hannun and Obeid 2018). As SLs are indispensable for multiple cellular processes and functions, their biosynthesis is highly conserved among eukaryotes and is considered to be essential (Li et al. 2018; Sutterwala et al. 2007). The mammalian sphingolipid metabolism has been extensively studied, and all key enzymes have now been molecularly identified. Briefly, *de novo* biosynthesis takes place in the endoplasmic reticulum (ER) and Golgi apparatus (GA) (Van Meer and Lisman 2002) (Figure 4) and can be simplified into three crucial steps. The first, which constitutes the rate-limiting step, involves the condensation of Acyl-CoA and L-serine in the ER via serine palmitoyltransferase (SPT) to produce 3-ketodihydrosphingosine. At the crucial second step, in animal and kinetoplastid cells, dihydrosphingosine is acylated to dihydroceramide by the action of the Ceramide synthase, which is later desaturated to form ceramide. The last key step occurs after the ceramide transport to the GA, where the synthesis of complex SLs takes place. These final products vary depending on the species and are formed under the catalysis of what could be named SL synthases. In mammals, ceramide is mainly the substrate of Sphingomyelin synthase to produce sphingomyelin. In contrast, in *T. cruzi*, such ceramide is thought to be primarily used for the synthesis of Inositol phosphorylceramide (IPC) by the IPC synthase (Mina and Denny 2018). As this phosphoinositol-containing SL is absent from mammalian cells, the IPC synthase enzyme represents an attractive molecular target for drug or vaccine development.

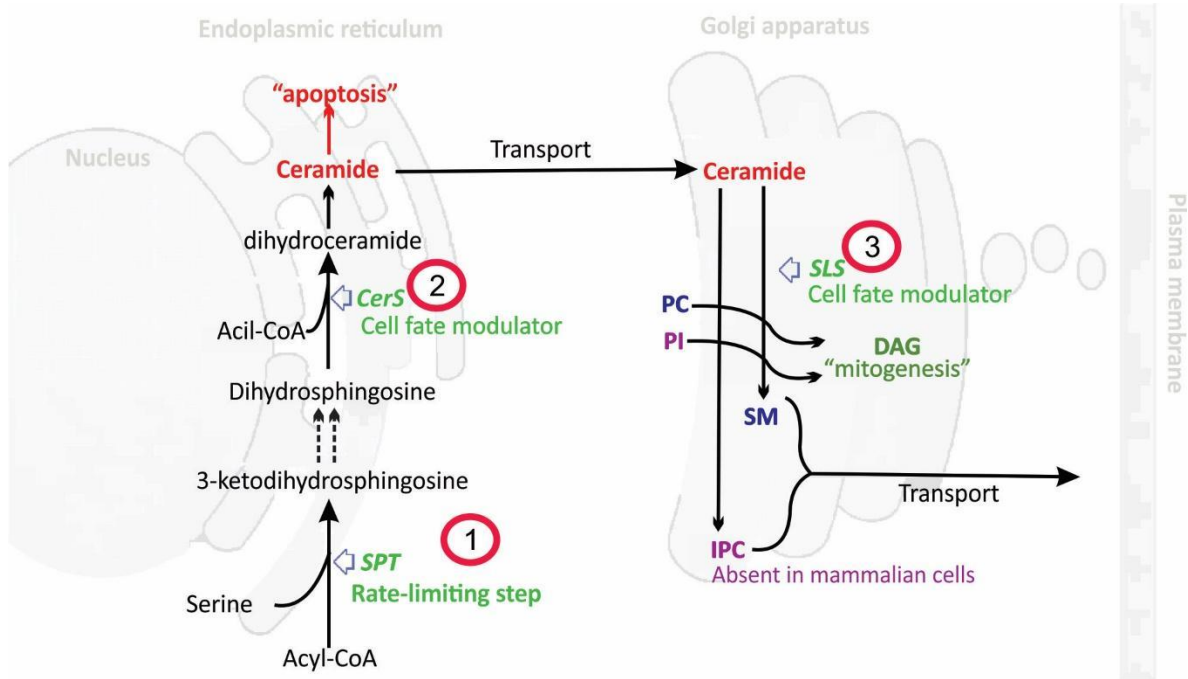


Figure 4. Schematic representation of de novo sphingolipid biosynthesis. Three crucial steps are highlighted. See the text for more details. SPT, serine palmitoyltransferase; CerS, ceramide synthase; SLS, sphingolipid synthase; PC, phosphatidylcholine; PI, phosphatidylinositol; DAG, diacylglycerol; SM, sphingomyelin; and IPC, inositol phosphorylceramide. Modified from Mina and Denny (2018)

1.5 The sphingolipid biosynthetic pathway as a potential target for chemotherapy against CD

Recent reports strongly suggest that *T. cruzi* has a lifecycle form-dependent specific lipid signature (Gazos-Lopes et al. 2017), including the SL signature (Guan and Mäser 2017) (Figure 5). *T. cruzi* synthesizes the same complex SLs, albeit, in different proportions. In tissue-culture cell-derived trypomastigotes (TCTs), aminoethylphosphonate ceramides (AEPnC) and phosphoethanolamine ceramides (EPC) are highly enriched, while in the epimastigote form, these two phospho-SLs are found quite low. In contrast, IPC and sphingomyelin (SM) are found in both parasite forms, but more abundant in the insect stage. A single orthologue of the gene encoding the sphingolipid synthase, TcIPCS, has been reported in *T. cruzi*. TcIPCS is a dedicated inositol phosphorylceramide synthase (Sevova et al. 2010), which cannot account entirely for the SL profile reported. As it has been demonstrated that several parasites, including *Leishmania* and *Toxoplasma gondii*, are able to scavenge host SLs (Romano et al. 2013; Zhang et al. 2009), this could also be

the case of *T. cruzi*. In fact, as *T. cruzi* amastigotes have been reported to scavenge host fatty acids (Gazos-Lopes et al. 2017), it is also possible that other lipid forms are subject to scavenging. This assumption would explain the EPC and SM detection, but not the AEPnC identification since it is absent in the mammal host (Guan and Mäser 2017).

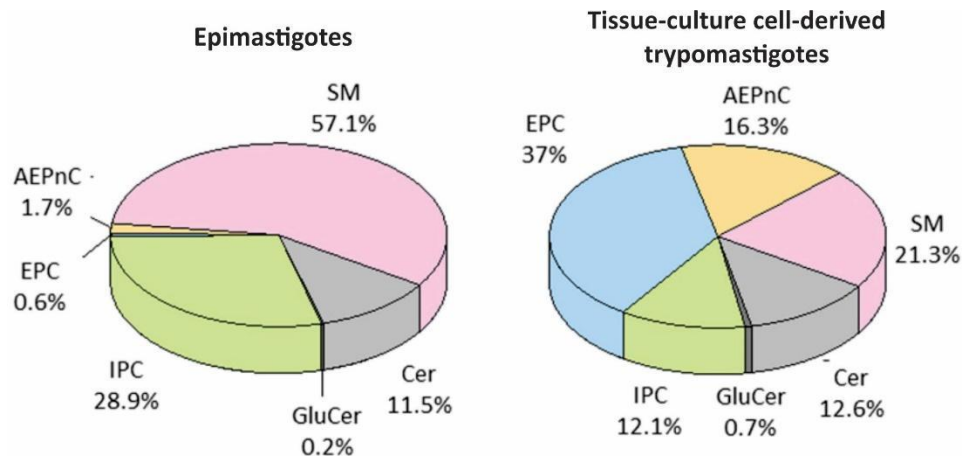


Figure 5. Form dependent sphingolipid signatures in *T. cruzi* Y-strain epimastigotes and Tissue-culture cell-derived trypomastigotes. Pie charts represent the relative distribution of SL subclasses in these parasite forms. Abbreviations: Cer, ceramides; EPC, phosphoethanolamine ceramides; GluCer, glucosylceramides; IPC, inositol phosphorylceramides; SM, sphingomyelins; AEPnC, aminoethylphosphonate ceramides. Taken from Guan and Mäser (2017).

1.6 The *T. cruzi* inositol phosphorylceramide synthase and its biological significance

The presence of IPC synthase activity in all *T. cruzi* forms was first demonstrated by metabolic labeling (L. E. Bertello et al. 1995; Figueiredo et al. 2005; Uhrig et al. 1996). More recently, the *TcIPCS* gene was identified (Denny et al. 2006), presenting two alleles with 97% shared identity. Such a gene codifies a membrane-bound protein of 335 amino acids with MW of approximately 38 kDa. According to the literature, the kinetoplastid SLSs, including *TcIPCS*, are GA localized proteins with six predicted transmembrane domains (TMDs) (Denny et al. 2006; Sutterwala et al. 2008). Moreover, *TcIPCS* belongs to the sphingomyelin synthase (SMS) family, which presents a conserved catalytic triad that in the case of the *T. cruzi* orthologue catalyzes the transfer of inositol-phosphate from phosphatidylinositol (PI) to the C-1 hydroxyl group of ceramide (CER), releasing

diacylglycerol (DAG) as a by-product (J. G. Mina et al. 2010). This active site is predicted to be located in the second and third luminal loops of the protein and comprises the His202, His245, and Asp249 (Huitema et al. 2004).

In Eukaryotes, sphingolipid synthases (SLS) play a central role in the intersection between phosphoglycerolipids (e.g., PI in and DAG out) and SLs (e.g., CER in and IPC out), regulating the balance between pro-apoptotic CER and pro-mitogenic DAG (Tafesse, Ternes, and Holthuis 2006) (Figure 4). Thus, specific inhibitors of fungus IPC synthase have been shown to induce programmed cell death by CER accumulation (Georgopapadakou 2000), an analogous effect to the apoptotic CER function in mammalian cells (Hernández-Corbacho et al. 2017).

In *T. cruzi*, IPC is found in free glycoinositolphospholipids (GIPLs) and as part of the glycosylphosphatidylinositol (GPI) anchor of many surface glycoproteins (De Lederkremer and Bertello 2001). In epimastigotes, IPC is found in 92-98% of GIPLs (Nakayasu et al. 2009). In TCTs, IPC has been detected in the GPI anchor of trans-sialidases and Tc-85 glycoproteins (Agusti et al. 1997; Couto et al. 1993), as well as in the anchor of the Ssp4 antigen of amastigotes (Laura E. Bertello, Andrews, and De Lederkremer 1996), and mucins and 1G7-AG proteins (in metacyclic trypomastigote forms)(Guther et al. 1992; Heise, de Almeida, and Ferguson 1995; Serrano et al. 1995). Both, GIPLs and GPI anchors, highly abundant in the plasma membrane of the parasite, are profoundly involved in various aspects of host-parasite interaction, including adhesion and invasion of host cells, modulation and evasion from the host immune response, and pathogenesis itself (DosReis et al. 2002; Previato et al. 2004; Sergio Schenkman et al. 1993). Therefore, any molecule or mechanism that interferes with the surface expression of free GIPLs and GPI-anchored is expected to impact the parasite fitness hardly and would be a very attractive treatment against CD.

1.7 TcIPCS as drug target

In *T. cruzi*, other protozoa and fungi, IPC is one of their primary SLs (J. G. M. Mina and Denny 2018). Even if IPC makes up a relatively low proportion of the SLs, its synthesis is essential in fungi (Nagiec et al. 1997). RNAi silencing of *T. brucei* *TbSLS* genes inhibited parasite growth, demonstrating the essentiality of these genes (Sutterwala et al. 2008).

As a result of its attractiveness as a drug target, IPCS has been extensively used as a chemotherapy target against fungi and parasites. Such efforts led to the discovery of the Aureobasidin A, a depsipeptide that inhibits the IPCS fungal orthologue (AUR1p) explicitly at a low nanomolar concentration (Sugimoto, Sakoh, and Yamada 2004). Unfortunately, this drug was not significantly effective against the kinetoplastid IPCS orthologues from *Leishmania major*, *T. cruzi*, or *Toxoplasma gondii* (Denny et al. 2006; Figueiredo et al. 2005; Pratt et al. 2013); probably reflecting the evolutionary divergence between the enzymes. The *Leishmania* IPCS was recently the subject of a high throughput screening (HTS) assay that resulted in the identification of the antileishmanial benzazepanes, which shown specific inhibitory effect at the low nanomolar level (Norcliffe et al. 2018). Furthermore, as a result of an *in vitro* enzymatic assay, a breast cancer drug named tamoxifen was also identified as a specific inhibitor of the *Leishmania* IPCS enzyme (Trinconi et al. 2018). Although no similar study has been carried out in *T. cruzi*, as the TcIPCS predicted protein share 69-70% sequence similarity and present predicted TMD and active site conservation (Denny et al. 2006), it is possible that the benzazepanes and the tamoxifen also display inhibitory activity against the *T. cruzi* IPCS protein.

2. Objectives

2.1 General objective

- To validate *T. cruzi* IPC synthase as a potential therapeutic target for Chagas disease.

2.2 Specific objectives

- To generate and characterize knockout mutants for IPC synthase.
- To generate and characterize IPC synthase over-expressing parasites.
- To induce and purify recombinant TcIPCS protein for polyclonal sera production.
- To determine the effect of potential anti-TcIPCS compounds in wild type and genetically modified parasites.

3. Materials and Methods

3.1 Parasite cultures

Epimastigote forms of the cloned strain *Trypanosoma cruzi* CL Brener were maintained at 28 °C in liver infusion tryptose (LIT) medium (10 g/L liver infusion; 4 g/L NaCl; 400 mg/L KCl; 8 g/L Na₂HPO₄; 1 g/L glucose; 5 g/L tryptose; 10 mL of hemine at 0,2% NaOH (m/v); pH 7,2) supplemented with 10% heat-inactivated fetal bovine serum (GIBCO) and penicillin (100 U/mL)/streptomycin (100 u/mL) (GIBCO) as described by Camargo (1964). To preserve cultures in their logarithmic growth phase, they were passaged every four days in a fresh supplemented LIT medium. Such conditions were used for all the experiments unless stated otherwise. Additionally, genetically modified parasites were cultured after transfection in the presence of the appropriate antibiotic at 200 µg/mL for selection and subsequent maintenance. To establish *in vitro* infections metacyclic trypomastigotes were obtained after 12 - 15 days of culture in LIT medium (Camargo 1964) and used to infect Rhesus Monkey Kidney Epithelial Cells (LLC-MK2) grown in Dulbecco's Modified Eagle Medium (DMEM) supplemented with 5% inactivated fetal bovine serum (FBS) at 37°C and 5% CO₂ as described by Belew et al. (2017). After 4 hours of infection, the infected cells were washed with PBS 1X (132 mM NaCl; 3 mM KCl; 8 mM Na₂HPO₄; 1,5 mM KH₂PO₄; pH 7,2) and maintained in fresh DMEM medium supplemented with 5% non-inactivated horse serum (GIBCO) to lyse epimastigote forms. After four days post-infection (dpi), infected cultures were washed and maintained in DMEM medium supplemented with 2% FBS (DMEM-2) at 34°C and 5% CO₂. After approximately six days, tissue-culture cell-derived trypomastigotes (TCT) were collected from the infected monolayers, centrifuged for 10 min at 600g, and then allowed to swim up from the pellet overnight. The pure highly motile fraction in the supernatant was used for the controlled *in vitro* infection assays.

3.2 Gene characterization, expression pattern, and topology and 3D structure prediction of the *T. cruzi* Inositol Phosphorylceramide Synthase

Sequence analyses were conducted using the *T. cruzi* CL Brener genome database (www.tritrypdb.org). Sequences of the known kinetoplastid SLSs from *L. major*, *T. brucei*, and *T. cruzi* were used as queries in Blastn analyses. Tritrypdb (www.tritrydb.org), accession numbers: *L. major* IPCS: LmjF.35.4990; *T. brucei* SLS1-4: Tb927.9.9410, Tb927.9.9400, Tb927.9.9390 and Tb927.9.9380; and *TcIPCS1* - 2: TcCLB.506885.124, TcCLB.510729.290. To evaluate the expression pattern of the *TcIPCS* alleles over the parasite forms was used the RNA-seq data recently published by our group (Belew et al. 2017). For topology and 3D structure *de novo* prediction of the protein embedded into a bilayer membrane, it was used the PredMP software (S. Wang et al. 2018). As TcIPCS1 (Esmeraldo-like allele) and TcIPCS2 (Non-Esmeraldo-like allele) present 96% of amino acid identity, it was selected only the Non-Esmeraldo-like allele for these predictions. Moreover, the TcIPCS1, LmjF.IPCS and TbSLS1 proteins, were aligned by using the multiple sequence alignment tool for transmembrane proteins TM-Aligner (Bhat et al. 2017), and transmembrane domains and active site were indicated according to the PredMP topology predictions and the conserved signatures predicted by Huitema and collaborators (2004), respectively.

3.3 Genomic DNA extraction of *T. cruzi* CL Brener

Exponentially growing 10^8 epimastigotes, cultivated in LIT medium, were collected by centrifugation (3000 rpm/10 min) and washed twice with PBS 1X. The DNA extractions were performed by using the *Illustra blood GenomicPrep Mini Spin Kit* (GE Healthcare) following the manufacturer's recommendations. Extracted DNA samples were quantified by spectrophotometry in a NanoDrop. Furthermore, their quality was assessed by their migration in a 1% agarose gel electrophoresis in TAE buffer 1x with 0,005% SYBR safe (1:20000). Band profile was visualized in a UV transilluminator.

3.4 Total RNA isolation from *T. cruzi* epimastigotes

Total RNA was isolated from 2×10^8 log-phase epimastigotes using the TRIzol reagent protocol (Invitrogen) as recommended by the manufacturer. Briefly, parasites were centrifuged (3000 rpm/10 min), resuspended with 500 μ L of cold TRIzol reagent and incubated at room temperature for 5 minutes. Then, 100 μ L of chloroform was added, the solution was vigorously mixed, incubated (2 – 3 min) and centrifuged at 12000xg for 15 min at 4°C. Subsequently, the aqueous phase (located at the upper part) was transferred to a new tube and purified by isopropanol/ethanol precipitation. Afterward, the RNA was quantified by absorbance at 260nm. Also, RNA quality was verified by 1,2% agarose gel electrophoresis in MOPS buffer pH 7.0 (20 mM MOPS; 5 mM sodium acetate; 1 mM EDTA) and 5% of formaldehyde (Teixeira, Kirchhoff, & Donelson, 1995). Before adding to the gel, each sample of at least 500 ng of RNA was prepared with 2.5 μ L of loading buffer (MOPS 1x; 50% of formamide; 17% of formaldehyde; 5% of glycerol; 0.25% de bromophenol blue) and incubated for 15 min at 65°C. Then, it was added 1 μ L of ethidium bromide (1 mg/mL) to each sample before gel loading. Samples were run at 100 V for 45 min and visualized in a UV transilluminator.

3.5 PCR and quantitative real-time PCR primer design

Available DNA sequences deposited in the TritypDB were used as a template for designing and synthesis of different primer sets for various purposes (Table 1). As both TcIPCS alleles share 97% of sequence identity, the Esmeraldo allele was selected for the designing of primers directed for the amplification of the gene coding sequence (CDS). For the overexpression strategy, forward and reverse primers were constructed with the flanking restriction sites *XbaI* and *XhoI*, respectively, to facilitate the cloning of the CDS into the *XbaI/XhoI* sites of the *T. cruzi* expression vector pROCK-Hygro (DaRocha et al. 2004). In the case of the reverse primer, before the *XhoI* site and the stop codon, it was added a sequence that codifies the human influenza hemagglutinin tag (HA-tag) for immunoblotting purposes. To heterologous express in *E. coli*, the *TcIPCS* and a C-terminal fragment of the gene, both sets of primers were designed with the flanking restriction sites *EcoRI* and *XhoI*, so the amplified sequences could be cloned into the

plasmid pET-28a (+) (Novagen), at the *EcoRI/XhoI* sites. For the construction of the plasmid containing the homology-directed repair (HDR) DNA donor used in the knockout (KO) strategy, it was designed two sets of primers; each set directed for the amplification of around 370 nucleotides upstream and downstream of the *TcIPCS* CDS. For the upstream sequence, the forward and reverse primers were flanked by *KpnI* and *SpeI*, respectively, and, for the downstream sequence, the primers were flanked by the restriction sites *EcoRV* and *XhoI*. These amplified regions were sequentially cloned into the restriction sites *KpnI/SpeI* and *EcoRV/XhoI* of the plasmid Topo-HX1-Neo-GAPDH (Cardoso et al. 2013). This last construction was carried out by the former students Rafael Greco and Mariana S. Cardoso. For genotyping of the *TcIPCS* knockout parasites, it was designed a set of primers that anneal, in both alleles, upstream and downstream of the inserted *NeoR* cassette. Moreover, it was also designed a forward and reverse primers that anneal inside the *neomycin* gene. For quantitative PCR analyses of the *TcIPCS* mRNA levels, a set of primers was also designed.

Table 1. Primers used in this study. Annealing direction of each primer is indicated by the letter F (Forward) and R (Reverse). Underlined bases indicate the restriction sites for cleavage.

Purpose	Primer: number and name	Sequence (5'-3')
sgRNA amplification	1: TcIPCS-sgRNA-5'-1 F	GGAGGCCGGAGAATTGTAATACG ACTCACTATAGGAAGCAAAAACA GCAGCAAAAAGTTTTAGTACTCT GGAAACAGAATC
	2: TcIPCS-sgRNA-5'-2 F	GGAGGCCGGAGAATTGTAATACG ACTCACTATAGGTTGTCCGGCCGC TGCCAGACAGTTTTAGTACTCTGG AAACAGAATC
	3: TcIPCS-sgRNA-3' F	GGAGGCCGGAGAATTGTAATACG ACTCACTATAGGACGACGGTTGG ACCAGCCTGTGTTTTAGTACTCTG GAAACAGAATC
	4: Sa-sgRNA scaffold R	TTGAACAACCGCTCTAAAAAAA

HDR DNA donor construction and amplification	5: TcIPCS-HDR- <i>KpnI</i> -5' F	TTTGGTACCTACCCTTCTTGTCCTG TCCTG
	6: TcIPCS-HDR- <i>SpeI</i> -5' R	GGGACTAGTATAGCCTGCGTTTTTC AGTGG
	7: TcIPCS-HDR- <i>EcoRV</i> -3' F	TTTGATATCGTGGGAATTTTGGAC ACTGG
	8: TcIPCS-HDR- <i>XhoI</i> -3' R	TATCTCGAGCTGCGACTCCCTTCA CAAATC
	9: TcIPCS-HDR-5' F	TACCCTTCTTGTCCTGTCCTG
	10: TcIPCS-HDR-3' R	TGCGACTCCCTTCACAAATC
TcIPCS KO genotyping	11: TcIPCS-Ext-5' F	TTCTTGACTTGTGCGGGTGA
	12: TcIPCS-Int-5' R	TGG GTT CTG GCA ATG GTT GT
	13: TcIPCS-Ext-3' R	TGCGTCACCTACGACTTACTTCC
	14: Neo (+694) F	CTGAAGAGCTTGGCGGCGAAT
	15: Neo (+804) R	TCAGAAGAACTCGTCAAGAAGGC G
pROCK-Hygro-IPCS::HA construction and sequencing	16: TcIPCS1- <i>XbaI</i> -5' F	TCTAGAATGGTTTTAATGGGGCCT CATTCTG
	17: TcIPCS1::HA- <i>XhoI</i> -3' R	CTCGAGTCAAGCGTAATCTGGTA CGTCGTATGGGTA
Quantitative real-time PCR	18: TcIPCS-mRNA F	CGGTCTCCATCACGCTCAGT
	19: TcIPCS-mRNA R	TCGTCCGTGTAGTGGGAACG
	20: TcL9-mRNA F	CCTTCACTGCCGTTTCGTTGGTTTG
	21: TcL9-mRNA R	ATGCGAGAGTGCCGTGTTGATGG T
pET-28a(+)-TcIPCS1 and pET-28a(+)-C-terminal-TcIPCS1 construction	22: TcIPCS1- <i>EcoRI</i> -5' F	GGGGAATTCATGGTTTTAATGGG GCC
	23: C-terminal-TcIPCS1- <i>EcoRI</i> -5' F	GGGGAATTCTCGTATCCTGCAAC GGACAA
	24: TcIPCS1- <i>XhoI</i> -3' R	TCTCTCGAGTCACCAGTGTCCTCAA AT

3.6 PCR amplification

Genomic *T. cruzi* CL Brener DNA was used as the template for PCR amplification for the plasmid constructions and genotyping. For the HDR DNA donor amplification, the resultant plasmid construction, TOPO-IPCS_UTR-HX1-Neo-GAPDH-IPCS_UTR, was used as the template. Each PCR reaction was made in a final volume of 20 μ L, with 35 ng of genomic DNA

or 15 ng of plasmid DNA, 0,5 μ M of each primer, 0,2mM of each nucleotide (dATP, dCTP, dGTP and dTTP), 4 μ L of 5x GoTaq reaction buffer (Promega), 1 U of GoTaq DNA Polymerase and nuclease-free water to complete the final volume. In the cases where the expected product was longer than 3 Kb, it was used a Taq DNA polymerase of high processivity. For this particular reactions, with a final volume of 50 μ L, it was used 35ng of DNA, 0,5 μ M of each primer, 2,5 mM of each nucleotide, 2,5mM of MgCl₂, 5 μ L of 10X LA PCR Buffer II (TAKARA), 0,8 U of TaKaRa LA Taq DNA polymerase (TAKARA) and nuclease-free water to complete the final volume. The PCR reactions were incubated in the ProFlex™ PCR System (Applied Biosystems) with the following program: *i*) initial denaturation at 95°C for 1 min; *ii*) 30 cycles of denaturation at 95°C for 30 s, primer annealing at 50 – 64°C for 30 s, and extension time (1 min/Kb) either at 72°C for GoTaq or 68°C for TaKaRa LA Taq; and *iii*) final extension at 72°C for 10 min. The amplified products were analyzed by 1% agarose gel electrophoresis, as previously described in item 3.3.

3.7 Cloning of *T. cruzi* and *E. coli* expression vectors

PCR products from item 3.6 were purified by using the NucleoSpin Gel and PCR Clean-up kit (Macherey-Nagel) following the manufacturer's recommendations. After DNA purification, PCR products were ligated in the plasmid pGEM-T-easy vector (Promega). Each ligation reaction was made in a final volume of 10 μ L containing 5 μ L of 2X rapid ligation buffer, 50 ng of the linearized plasmid pGEM-T-easy vector, 90 ng of the selected purified PCR product, 3 Weiss units of T4 DNA ligase and nuclease-free water to complete the final volume. Finally, the resultant solution was incubated overnight at 4°C and used to transform *E. coli* XL1-Blue competent cells (described on the next item). Cloned PCR products were subcloned by specific restriction cleavage of the pGEM-T-easy-PCR_product followed by fragment purification and insert ligation into the linearized desired plasmid. These ligation reactions were made in a final volume of 10 μ L, containing three Weiss units of T4 DNA ligase (Promega), 1 μ L of 10X ligase buffer (300mM Tris-HCl, pH 7.8; 100mM MgCl₂, 100mM DTT and 10mM ATP), 100 ng of the selected vector, 500 ng of the purified DNA insert and nuclease-free water to complete the volume. Reactions were incubated at 15°C overnight and used to transform *E. coli* XL1-Blue competent cells.

3.8 Transformation of *E. coli* competent cells

Different strains of *E. coli* competent cells (table 2) were transformed by heat shock, as described by Sambrook et al. (2001). In brief, 10 µL of the ligation reaction or 20 ng of plasmid DNA were added to 100 µL of competent cells and incubated at 4°C for 30 min. Next, the solution was heat-pulsed in a 42°C water bath for 50 s and incubated on ice for 2 minutes. Then, it was added to the solution 400 µL of 2xYT media (1,6% bacto-tryptone, 1% yeast extract, 0,5% NaCl, pH 7,4), and cultured for 45 min at 37°C with agitation (180 rpm). Subsequently, the culture was plated in 2xYT solid medium supplemented with the selected antibiotic, e. g. ampicillin (100 µg/mL) and incubated overnight at 37°C. A few resistant colonies were selected, and the integration of the desired insert was confirmed by PCR, using specific primers that anneal in the flanking region where the insertion occurs, being easy to identify the positive transformants. After this first analysis, the positive transformants were confirmed by restriction mapping (item 3.9), and aliquots of these colonies were conserved in glycerol 10% and stocked at -80°C.

Table 2. *E. coli* strains used in this study

Strain	Genotype	Source/reference
XL1-Blue Competent Cells	<i>recA1 endA1 gyrA96 thi-1 hsdR17 supE44 relA1 lac [F' proAB lacIqZΔM15 Tn10 (Tetr)]</i>	Agilent
BL21(DE3) Competent Cells	<i>fhuA2 [lon] ompT gal (λ DE3) [dcm] ΔhsdS λ DE3 = λ sBamHIo ΔEcoRI-B int::(lacI::PlacUV5::T7 gene1) i21 Δnin5</i>	(Studier and Moffatt 1986)
Shuffle® T7 Competent Cells	<i>F' lac, pro, lacIQ / Δ(ara-leu)7697 araD139 fhuA2 lacZ::T7 gene1 Δ(phoA) PvuII phoR ahpC* galE (or U) galK λatt::pNEB3-r1-cDsbC (SpecR, lacIq) ΔtrxB rpsL150(StrR) Δgor Δ(malF)3</i>	NEB
Origami™ 2(DE3) Competent Cells	<i>Δ(ara-leu)7697 ΔlacX74 ΔphoA PvuII phoR araD139 ahpC galE galK rpsL F'[lac+ lacIq pro] (DE3) gor522::Tn10 trxB (StrR, TetR)</i>	Novagen

OverExpress™ C41(DE3) Chemically Competent Cells	F- <i>ompT hsdSB (rB - mB -) gal dcm (DE3)</i>	Lucigen
ArcticExpress (DE3) Competent Cells	<i>E. coli</i> B F- <i>ompT hsdS(rB- mB-) dcm+ Tetr</i> <i>gal λ(DE3) endA Hte [cpn10</i> <i>cpn60 Gentr]</i>	Agilent

3.9 Plasmid DNA extraction and endonuclease restriction cleavage

A fresh colony was inoculated in 5mL of 2xYT medium supplemented with the selective antibiotic and incubated overnight at 37°C with agitation. Plasmid DNA extraction was made with the NucleoSpin Plasmid miniprep kit (Macherey-Nagel) as recommended by the manufacturer. DNA quantity and quality were evaluated as described above (item 3.3). Plasmid DNA was used for different applications, as template for PCR reactions, for restriction enzyme cleavage, or to transform other *E. coli* strains. The restriction cleavage reactions were performed with 1 – 10 µg of DNA, 1 – 10 U of each restriction enzyme (Promega), 3 µL of 10X manufacturer's suggested buffer and incubation at the recommended temperature for 4 to 16 hours. DNA digestions were analyzed by 1% agarose gel electrophoresis.

3.10 Transfection and cloning of *T. cruzi* epimastigote forms

Transfections were performed as described by Burle-Caldas et al. (2017), with some modifications. For transfection, 2×10^7 log-phase parasites were collected by centrifugation (3000 rpm, 10 min, 4°C), washed twice with PBS 1X and resuspended in 100 µL of sterile nucleofection buffer (90 mM sodium phosphate, five mM potassium chloride, 0.15 mM calcium chloride, 50 mM HEPES, pH 7.3) containing 5 – 10 µg of the desired DNA or water for the negative control (mock culture). Electroporation was performed using 2 mm gap cuvettes (BioRad) with one or two pulses of the program U-033 of the Amaxa Nucleofector (Lonza, Switzerland). Subsequently, the electroporated culture was transferred to 5 mL of supplemented LIT medium and cultured at 28°C. Twenty-four hours after each transfection, the medium was supplemented with 200 µg/mL of the antibiotic G418 (neomycin) or hygromycin, and stable transformants were selected after 15 – 20

days of culture. The selected population was diluted in supplemented LIT medium containing 200 µg/mL of the specific antibiotic and transferred to 96-well plates at two different densities: 1 parasite/well and 0,5 parasites/well. 96-well plates were maintained in a humid chamber at 28°C, and after 15-20 days of incubation, the obtained clones were expanded and characterized.

3.11 CRISPR-Cas9 knockout of the *T. cruzi* *IPCS* gene

To knockout (KO) both alleles of the *TcIPCS* gene, it was designed a strategy based on the proposed by Beneke et al. (2017). The strategy was based on the simultaneous transfection of wild type parasites with rSaCas9 complexed with either one of two single-guided RNAs and the homology-directed repair (HDR) double-stranded DNA donor containing a neomycin resistance cassette flanked by the 5' and 3' *TcIPCS* regions. Before transfecting the parasites, to achieve complexation between the recombinant *Staphylococcus aureus* Cas9 (rSaCas9) and the single-guided RNAs (sgRNA), 15 µg of the recombinant protein was incubated with 20 µg of each sgRNA for 10 min at room temperature followed by incubation for 10 min at 37°C. Then, wild type parasites (3×10^6) were simultaneously transfected with the complexed rSaCas9/sgRNAs, and the 10 µg of PCR amplified HDR DNA donor. Electroporation, selection, and cloning were performed as described in item 3.11.

The rSaCas9 was expressed and purified from an *Escherichia coli* Rosetta-Gami 2 (Novagen, Germany) transformed with the pET32eKLIC plasmid containing the coding sequence of the SaCas9 as described by Burle-Caldas et al. (2018). The sgRNAs were designed using the Eukaryotic Pathogen CRISPR guide RNA/DNA design tool (EuPaGDT), available at <http://grna.ctegd.uga.edu/>. Each sgRNA was designed to direct the SaCas9 double-stranded break (DSB) in both *TcIPCS* alleles, either a few nucleotides after the translation initiation codon or a few nucleotides before the translation stop codon. Therefore, the action of both sgRNA produced the deletion of a significant fraction of the *TcIPCS* gene. To *in vitro* synthesize these sgRNAs, PCR reactions were performed with a specific forward primer containing a T7 RNA promoter followed by the 21 nucleotides complementary to the target site and a reverse primer that anneals to the sequence of the SaCas9 scaffold. The pTZSaCasScaffold plasmid was used as the template for the PCR reactions (Burle-Caldas et al. 2018) (see table 1 for primer details). Next, each PCR product

was *in vitro* transcribed using the MEGAshortscript™ T7 Transcription kit (Thermo Fischer Scientific, USA), at 37 °C for 16 h and purified with acidic-phenol: chloroform followed by ethanol precipitation, as described by the manufacturer. Purified sgRNAs were quantified by absorbance at 260nm, and the RNA quality was verified by 2% agarose gel electrophoresis in MOPS buffer pH 7.0, as described in item 3.4. As a DNA donor sequence for DSB repair by homologous recombination (HDR DNA donor), it was prepared a plasmid containing the *NeoR* cassette flanked by the upstream and downstream flanking regions of the expected cleavage sites described above (see item 3.5 for the construction details). This plasmid was used as the template for the amplification of the HDR DNA donor (*IPCS_UTR-HX1-Neo-GAPDH-IPCS_UTR*), which is expected to be used by the transfected parasites as its homologous recombination repair template after the DNA breakages caused by the rSaCas9/sgRNA endonuclease. After electroporation, antibiotic selection, and cloning, genomic DNA was extracted from selected clones. It was used as the template for PCR genotyping reactions with specific primers that allow verifying the integration of the resistance cassette in the *TcIPCS* loci and the specific gene deletion (see primer details in table 1). Furthermore, total RNA was extracted to evaluate the mRNA levels of the *TcIPCS* by quantitative PCR (see item 3.4, for RNA isolation details, and 3.13 for quantitative PCR details).

3.12 Generation of *T. cruzi* *IPCS* overexpressing parasites

To generate *T. cruzi* *IPCS1* overexpressing stable clones was prepared a pROCK-Hygro-IPCS::HA expression vector (DaRocha et al. 2004) (see item 3.5 for construction details) and verified by restriction mapping (see item 3.9). As this plasmid presents a *T. cruzi* β -*tubulin* sequence that the parasite can integrate into its tubulin loci, the expression vector was linearized before transfection. Thus, 10 μ g of the prepared plasmid was linearized with the restriction enzyme *NotI* and gel-purified with the NucleoSpin Gel and PCR Clean-up kit (Macherey-Nagel), as recommended by the manufacturer. At least 5 μ g of pure linearized pROCK-Hygro-IPCS::HA was transfected, selected, and cloned as described above (item 3.10). The stable expression of the TcIPCS::HA was confirmed at the mRNA level by quantitative PCR.

3.13 Quantitative PCR

For quantitative PCR reactions, total RNA samples were treated with DNase I (Thermo Scientific™) as recommended by the manufacturer. For a final volume of 10 μ L was added 1 μ g of RNA, 1 μ L of 10X DNase buffer (100 mM Tris-HCl (pH 7.5 at 25 °C), 25 mM MgCl₂, 1 mM CaCl₂), 1 μ L of DNase I (1 U/ μ L) and DEPC-treated water to complete the final volume. Each reaction was incubated at room temperature for 15 minutes, followed by the enzyme inactivation by the addition of 1 μ L of 25 mM EDTA and heating for 10 min at 65°C. The resultant RNA was quantified using the Qubit RNA BR assay kit in a Qubit® 4 Fluorometer (Invitrogen), according to the recommendations.

To synthesize the first-strand cDNA of each RNA sample was used the SuperScript™ IV kit (Invitrogen), following the manufacturer's recommendations with few modifications. First, to anneal the oligo d(T)18 primer to the treated RNA, it was prepared a solution containing 0.5 μ g of the RNA sample, 0.5 μ L of 50 μ M oligo d(T)18 primer, 2.5 μ L of 2mM dNTP mix and DEPC-treated water to complete a final volume of 6.5 μ L. The resultant solution was heated at 65°C for 5 min and incubated on ice for at least 1 minute. Reverse transcriptase (RT) reaction mix was prepared with 2 μ L of 5x SuperScript IV RT buffer, 0.5 μ L of 100 mM DTT, 0.5 μ L of RNaseOUT Recombinant RNase Inhibitor and 0.5 μ L of SuperScript IV RT (200 U/ μ L). This reaction was added to the RNA-primer mix, the combined reaction mixture incubated at 53°C for 10 min and inactivated at 80°C for 10 min. Each RNA sample was made with a negative control without the RT enzyme (RT-). Resultant cDNA solutions were diluted 1:10 in DNase free water and used as the template for the quantitative PCR reactions. To verify the DNase treatment, the RT- and RT+ dilutions were subject to a PCR reaction with primers that amplify the control gene *TcL9* that are expected to amplify only in the RT+ reactions (see item 3.6 for PCR conditions). To quantify the *TcIPCS* mRNA levels by quantitative real-time PCR (qPCR) was used the SSO SYBR Green Supermix (Bio-rad) with primers specific for the *TcIPCS* and the control gene *TcL9* (Nardelli et al., 2007) (Table 1). Each qPCR reaction solution of 10 μ L contained 5 μ L of 2X SSO SYBR Green Supermix, 0.5 μ L of each primer, 2 μ L of the diluted cDNA sample and 2 μ L of DNase free water. Reactions were run in 96-well plates on an Applied Biosystems 7900HT Fast Real-Time PCR System (Life Technologies) with the following PCR conditions: 30 s at 95°C, 40 cycles of 95°C for 15 s and 60°C for 30 s. After each run, thermal dissociation confirmed that each qPCR reaction

generated a single amplicon. Relative *TcIPCS* mRNA levels were normalized to Ct values for the gene encoding for constitutive 60S ribosomal protein L9(*TcL9*) (TcCLB.504181.10), following the $2^{-\Delta\Delta Ct}$ method (Livak and Schmittgen 2001). These experiments were conducted in collaboration with the post-doctoral fellow Heliana Fernandes.

3.14 Recombinant TcIPCS1 and C-terminal-TcIPCS1 induction and purification

The gene sequences of the *TcIPCS1* or the *C-terminal-TcIPCS1* were cloned in the expression vector pET-28a (+) (Novagen), and different *E. coli* expression strains were transformed (Table 2). The *C-terminal-TcIPCS1* sequence was determined by using the B-cell epitopes prediction web server, BepiPred-2.0 (Jespersen et al. 2017). As the main goal of this section was to produce recombinant protein for antibody production, we envisioned to also induce the most immunogenic half of the protein as an alternative to use in the case of non-induction of the complete protein under the evaluated conditions. Recombinant protein expression of each strain was induced as described next. Each *E. coli* strain was plated in 2xYT solid medium supplemented with kanamycin (50 $\mu\text{g/ml}$) (KAN) and incubated at 37°C for 24 hours. Then, a fresh colony was used to inoculate 5mL of 2xYT liquid medium supplemented with KAN and cultured overnight at 37°C with agitation (200 rpm). At the next day, the culture was diluted 1:20 in 25 mL of fresh 2xYT supplemented broth and incubated with agitation at 37°C. When the culture reached an optic density (OD600) between 0.4 and 0.6, an aliquot of 1 mL was collected (non-induced control). Afterward, recombinant protein expression was induced in the rest of the culture by the addition of Isopropyl β - d-1-thiogalactopyranoside (IPTG) at a final concentration of 0.01 or 0.5 mM. The best conditions of inductions were optimized by modifying the following variables: IPTG concentration, incubation time, temperature, and cell lysis conditions. After the induction, an aliquot of the culture was centrifuged at 4°C and 12000 rpm for 10 min and lysed in Laemmli sample buffer (62,5 mM Tris-HCl, pH 6,8; 10% of glycerol; 2% of SDS; 5% of β - mercaptoethanol; 0,002% of bromophenol blue). Each sample was syringed eight times to shred the genomic DNA. After shredding, the samples were analyzed by 12,5% polyacrylamide gel electrophoresis (SDS-PAGE) and stained with coomassie blue. The induced protein extracts were compared with the non-induced extract to evaluate the efficiency of the induction. As the pET-28a (+) expression

vector produces a His-tag fused to the N-terminal region of the recombinant protein, the expression of the recombinant His-tagged protein was also confirmed by western blot analysis, using an anti-His antibody (Invitrogen). After the confirmation of the protein expression, the induction was performed on a larger scale (250 mL – 1L), during 24 h at 13°C with a final concentration of 0.5 mM IPTG. The cultures were harvested by centrifugation (12000 rpm for 10 min), resuspended in phosphate lysis buffer (PLB) (500 mM NaCl, 20 mM phosphate buffer pH 8, 30 mM imidazole, supplemented with 5 mM DTT, 1 mM PMSF, and 5 mM benzamidine), and lysed either by high-pressure homogenization with the EmulsiFlex-C3 (Avestin, Inc) or by sonication. The sonication was performed on ice using a Fisherbrand Dismembrator with three pulses of 30 seconds each. Subsequently, the lysates were centrifuged at 12000 rpm at 4°C for 30 min and an aliquot from the pellet and from the supernatant was resuspended in PBS and analyzed by 12.5% SDS-PAGE to verify the efficiency of the lysis method and the fraction, soluble or insoluble, in which the recombinant protein was located. As the protein was insoluble, solubility was assessed with Laemmli sample buffer, RIPA buffer (150 mM NaCl, 20 mM Tris-HCl [pH 7.5], 1 mM EDTA, 1% SDS, 0.1% Triton X-100) and a solubilization protocol described by Schlager and collaborators (2012), which worked best. Thus, the insoluble fraction of PLB lysed cells was centrifuged and resuspended in the solubilization buffer (8 mM Na₂HPO₄, 286 mM NaCl, 1.4 mM KH₂PO₄, 2.6 mM KCl and 1% SDS at pH 7.4). The solubilized lysates were chilled and incubated for 30 minutes in ice, and then centrifuged at 12000 rpm for 30 minutes at 4°C. The cleared supernatant was poured off and filtered through a 0.25 µm syringe before applying it to affinity purification. The soluble His-tagged protein was purified by affinity chromatography using His-Trap columns and the ÄKTA prime system (GE Healthcare, USA), following the manufacturer's recommendations. The fractions obtained were analyzed by 12.5% SDS-PAGE, and protein concentration was estimated by Lowry's method. These experiments were conducted in collaboration with the post-doctoral fellow Daniela F. Chame.

3.15 SDS-PAGE and western blot analysis

The protein lysate was subjected to 12.5% SDS-PAGE. Then, proteins were transferred to a nitrocellulose membrane for western blotting, blocked for 1 h with PBS supplemented with 5% bovine serum albumin (BSA) and then incubated overnight with a primary anti-His-probe antibody

(Invitrogen) diluted (1/10,000) in PBS supplemented with 3% BSA and 0.05% Tween 20. The membranes were washed three times with 0.05% Tween 20 in PBS and then incubated for 1.5 h with the secondary antibody (Amersham™ ECL™ Anti-Mouse IgG, horseradish peroxidase-linked whole antibody, GE healthcare life sciences) at a dilution of 1/10,000 in PBS supplemented with 3% BSA and 0.05% Tween 20. Nitrocellulose membranes were rewashed, and signal detection was performed using an Immobilon Western Chemiluminescent HRP Substrate (Merck-Millipore). Immunostaining was performed using a Gel Logic 1500 imaging system (Kodak).

3.16 Growth curve and *in vitro* metacyclogenesis assays

Log-phase epimastigotes were diluted in fresh supplemented LIT medium to an initial density of $2,5 \times 10^6$ parasites/mL. Then, 1 mL of the diluted parasites was plated in triplicate in 24-well plates. Parasite density was determined over nine days by direct counting in a hemocytometer chamber. Metacyclogenesis *in vitro* analyses were performed in cultures of 5 mL of diluted parasites transferred to a T25 flask and incubated at 28°C for 7 or 9 days to allow differentiation by nutritional stress (Camargo 1964). After these days, the cultures were homogenized, and 10 μ L samples were smeared in poli-L-lysine coated glass slides. After the samples were air-dried, the slides were incubated at 80°C for 1 hour. Then, samples were fixed with methanol for 5 minutes, followed by the addition of 100 μ L of Giemsa stain solution. Slides were incubated at room temperature for 30 minutes and gently washed with deionized water. When dried, the samples were mounted with a drop of Entellan (Merck) and a glass coverslip. Samples were analyzed by light microscopy, and the parasite differentiation stage was determined according to the model proposed by Gonçalves and collaborators (2018). Any parasite belonging to any differentiation stage was considered part of the metacyclic trypomastigotes. At least 400 parasites were counted, per replicate, to determine the metacyclic trypomastigote percentage.

3.17 *In vitro* infections


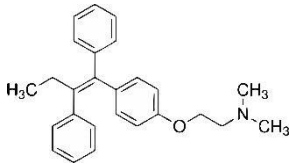
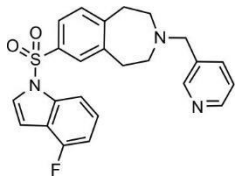
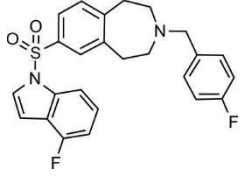
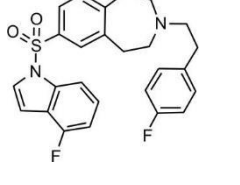
Vero cells were plated in 24-well plates and infected with purified tissue-culture cell-derived trypomastigotes (TCT) at a multiplicity of infection (MOI) of 10:1. Cell infection assays were

performed in plated monolayers at a density of 2.5×10^4 cells/well with for 4 h of infection, washed three times with PBS 1X, and incubated with DMEM-2 at 37°C for 24 h. Intracellular amastigote proliferation was evaluated as above, with two additional incubation times (i.e., 48 and 72 h). After incubation, infected monolayers were fixed and stained with a hematoxylin-eosin panoptic stain kit (RenyLab) and mounted on microscope slides with Entellan (Merk). Infection was quantified at each time post-infection by direct counting of at least 20 different fields of vision at the 100x microscope objective that accounted for at least 800 cells. It was quantified the percentage of infected cells or the number of amastigotes per cell. To evaluate amastigote differentiation into TCTs and its release to the culture supernatant, 24-well plates containing 5×10^4 cells/well were prepared and infected for 24 hours to achieve maximum cell infection. Afterward, infected monolayers were washed three times with PBS 1X and incubated with DMEM-2 at 37°C. Supernatant TCTs or extracellular amastigotes were determined over 12 days by direct counting in a hemocytometer chamber. These experiments were conducted in collaboration with the post-doctoral fellow Daniela F. Chame.

3.18 Chemical compounds with potential anti-TcIPCS activity and resazurin sodium salt

Tamoxifen (T5648, Sigma-Aldrich), benzazepanes (number 2, 7, 7a), and benznidazole (positive control) were kindly provided by the professors Silvia R. B. Uliana (University of São Paulo), Paul W. Denny (Durham University) and Silvane M. F. Murta (René Rachou Institute, FIOCRUZ), respectively. Tamoxifen, benzazepanes, and benznidazole were prepared in DMSO at 40mM, 50mM, and 50mM, respectively. Compounds were stored as recommended by manufacturers (table 3). Resazurin sodium salt was obtained from Sigma-Aldrich (St. Louis, USA). The resazurin working solution was prepared in PBS 1X at 2,5mM and filter-sterilized before use.

Table 3. Chemical compounds evaluated in this study

Name	Structure	Chemical Formula	Molecular Weight	Source
Benznidazole		C ₁₂ H ₁₂ N ₄ O ₃	260.249 g/mol	NORTEC
Tamoxifen		C ₂₆ H ₂₉ NO	371.515 g/mol	Sigma- Aldrich
Benzazepane #2		C ₂₄ H ₂₂ FN ₃ O ₂ S	435.52 g/mol	(Norcliffe et al. 2018)
Benzazepane #7		C ₂₅ H ₂₂ F ₂ N ₂ O ₂ S	452.52 g/mol	(Norcliffe et al. 2018)
Benzazepane #7a		C ₂₆ H ₂₄ F ₂ N ₂ O ₂ S	466.55 g/mol	(Norcliffe et al. 2018)

3.19 Resazurin cell viability assays and determination of the half maximal inhibitory concentration (IC₅₀) of each compound

A fluorescent resazurin cell viability assay was standardized to evaluate the anti-TcIPCS activity of each selected compound (item 3.18). The initial parasite density was optimized as follows. 2-fold serial dilutions of log-phase culture ranging from 0.25 to 0.039 x 10⁶ parasites/well were seeded in 96-well plates in a final volume of 100 µL and incubated for 72 or 96 hours at 28°C. After incubation time, 10 µL of resazurin solution was added to each sample and incubated, under light protection, at 28°C for 4 hours. Emitted fluorescence was measured at Ex528/Em590, using

a Varioskan™ LUX microplate reader (Thermo Scientific™). Resultant data were analyzed using the software GraphPad Prism 7.3

Log-phase epimastigotes were added to 96-well plates at $0,125 \times 10^6$ parasites/well in supplemented LIT media with appropriate concentrations of compounds and controls (vehicle and assay media alone) in a final volume of 100 μ L and incubated at 28°C for 72 hours. Each molecule was assayed in at least ten 1:2 serial dilutions (250 – 0,48 μ M) and normalized against the corresponding vehicle concentration. Cell viability was evaluated by the standardized resazurin assay (item 3.19). IC50 values were calculated using sigmoidal regression analysis in GraphPad Prism 7 (log (inhibitor) vs. normalized response - Variable slope).

3.20 Statistical analyses and graphics

All statistical analyses were performed using GraphPad Prism 7 (GraphPad Software, San Diego California USA). Reported values are means \pm SD of *n* biological experiments, as indicated in the Figure legends. Significant differences using either one-way ANOVA or two-way ANOVA, followed by Bonferroni post-test, with a level of significance set at $P < 0.05$, were used. All plasmid diagrams were performed using Benchling [Biology Software]. (2020). Retrieved from <https://benchling.com>. Protein alignment was plotted using the ESPript server 3.0. Retrieved from <http://esprpt.ibcp.fr/>.

4. Results and Discussion

4.1 *TcIPCS* gene characterization

TcIPCS gene was firstly identified in the *T. cruzi* CL Brener reference genome (El-sayed et al. 2005) by Denny and collaborators (2006). Since CL Brener is a hybrid clone with two different haplotypes, named Esmeraldo-like and Non-Esmeraldo-like, *TcIPCS* was found as a single copy gene with two alleles, each corresponding one haplotype. In the TritrypDB, (www.tritrydb.org), the *TcIPCS* Esmeraldo-like and Non-Esmeraldo-like alleles can be identified by the accession numbers TcCLB.506885.124 and TcCLB.510729.290, respectively. At the nucleotide level, the two *TcIPCS* alleles present 97% of sequence identity. Moreover, both alleles are expressed at constitutive levels along the parasite life cycle according to the RNA-seq data recently published by our group (Belew et al. 2017) (Figure 7F).

4.2 Topology and 3D structure predictions of the *T. cruzi* Inositol Phosphorylceramide Synthase protein and its comparison with related orthologues

Due to the *TcIPCS* properties as a transmembrane protein (MP), no crystal structure has been determined from this protein or any other protein belonging to the sphingomyelin synthase (SMS) family (Tafesse et al. 2006). The first attempt to predict the topology of any protein of the family was made by Huitema et al. (2004) using a comparative hydrophobicity analysis of SMS homologs predicted a six transmembrane domains (TMD) protein with four highly conserved sequence motifs, they designated D1, D2, D3 and D4. Furthermore, by comparing motifs D3 (C-G-D-X3-S-G-H-T) and D4 (H-Y-T-X-D-V-X3-Y-X6-F-X2-Y-H) with the C2 and C3 motifs of the lipid phosphate phosphatase (LPP) family (Neuwald 1997), they also identified the catalytic triad of the SMS enzymes (denoted by the bold residues above). On the other hand, motifs D1 (P-L-P-D) and D2 (R-R-X8-Y-X2-R-X6-T) were predicted as entirely unique to the SMS. This active site was recently validated in human SMS enzymes (Kol et al. 2017). By performing protease protection assays, Huitema et al. (2004) also predicted a cytosolic carboxyl terminus of the SMS proteins positioning the active site residues on the exoplasmic leaflet of the membrane. Currently, only

topology predictions of the kinetoplastid SMS have been made, which showed conservation of the 4 motifs, including the catalytic triad (Sutterwala et al. 2008), but no structural model has been published.

Recently, the ability to accurately predict three-dimensional contacts between pairs of residues has markedly advanced, which dramatically improved the accuracy of protein models without available template (Moult et al. 2018) In particular, for MPs, one of the most recent approaches to de novo predict 3D structure from sequence information is PredMP (S. Wang et al. 2018). This approach is based on a high-throughput Deep Transfer Learning (DTL) method that predicts MP contacts as distance restraints by learning from the existent non-MPs, overcoming the challenge that limited solved MP structures (510 non-redundant MP) present for the training of the deep learning model. This DTL framework serves as a key module for 3D model generation, which uses the predicted contacts as distance restraints to construct the 3D model by the Crystallography & NMR System (CNS) suite (Brünger et al. 1998). Another great advantage of the software is that, guided by the predicted transmembrane topology, it embeds the predicted 3D structure into a lipid bilayer using a depth- and residue-dependent membrane burial potential (Z. Wang et al. 2016). Figure 6 depicts the workflow of PredMP software.

To model the topology and 3D structure of the TcIPCS, we selected the Non-Esmeraldo-like allele protein sequence (TcIPCS2), as both alleles present 96% of amino acid (aa) identity (Figure 7E). The remaining 4% accounts to 15 mismatches, six of them being conservative amino acid substitutions (Figure 7E, green residues). The other aa mismatches are mainly located in places that are not expected to cause significant modifications to the protein function (Figure 7E, orange residues). Nevertheless, there are two mismatches (i.e., F191S and P205S; Figure 7E, light blue residues), located close to the active site, which may be causing a structural modification that might influence the TcIPCS activity. However, testing this hypothesis goes beyond the objectives of the present work.

Therefore, parting from the TcIPCS2 amino acid (aa) sequence, PredMP predicted, a 3D structure model with a reliable quality (Ln(Neff): 1.582099) (Figure 7A-E). The topology predictions, based on multiple sequence alignment (MSA) of the protein homologs, retrieved the same six TMDs reported previously, but with redefined boundaries (Sutterwala et al. 2008).

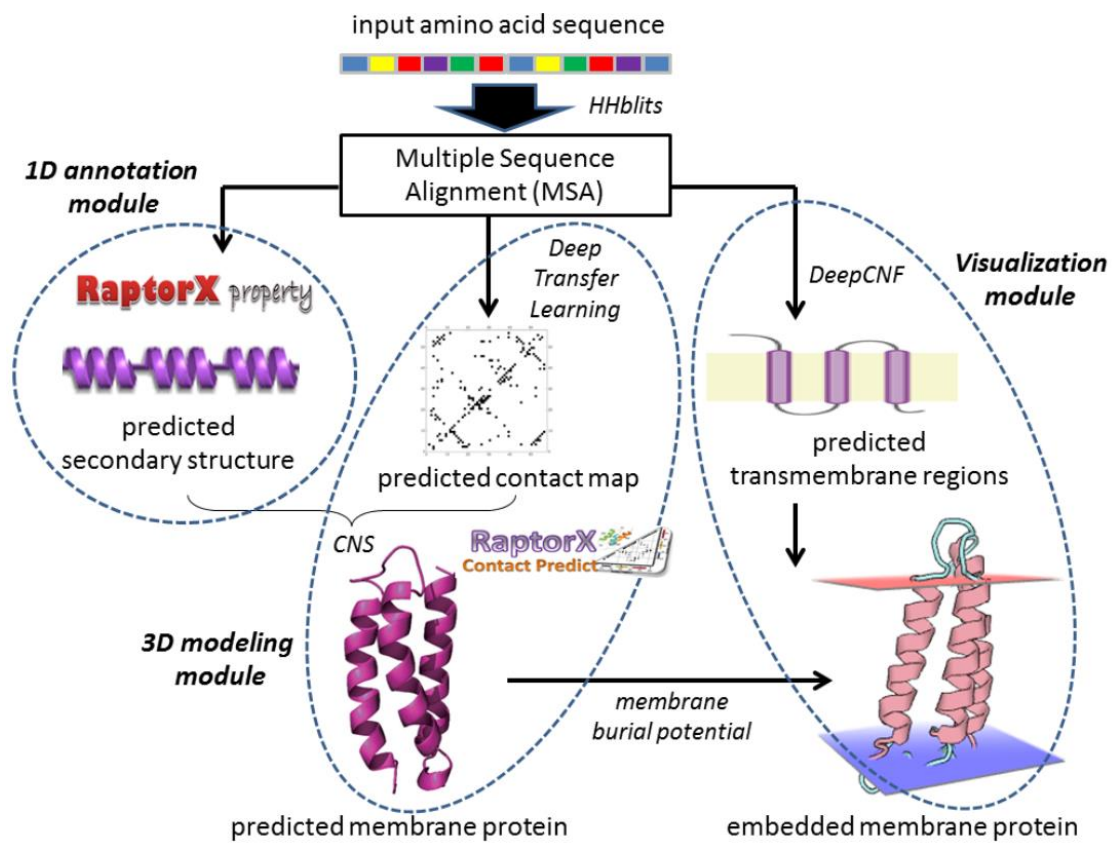


Figure 6. Schematic representation of the PredMP workflow. The software processes a protein sequence by three general modules. First, it generates a multiple sequence alignment (MSA) to predict transmembrane (TM) regions, secondary structure and contact map. Then, predicted secondary structures and contacts are used to de novo fold the 3D model by the CNS, and the resultant model is embedded into a bilayer membrane guided by the predicted TM regions and the membrane burial potential. Taken from Wang et al. supplemental material (2018).

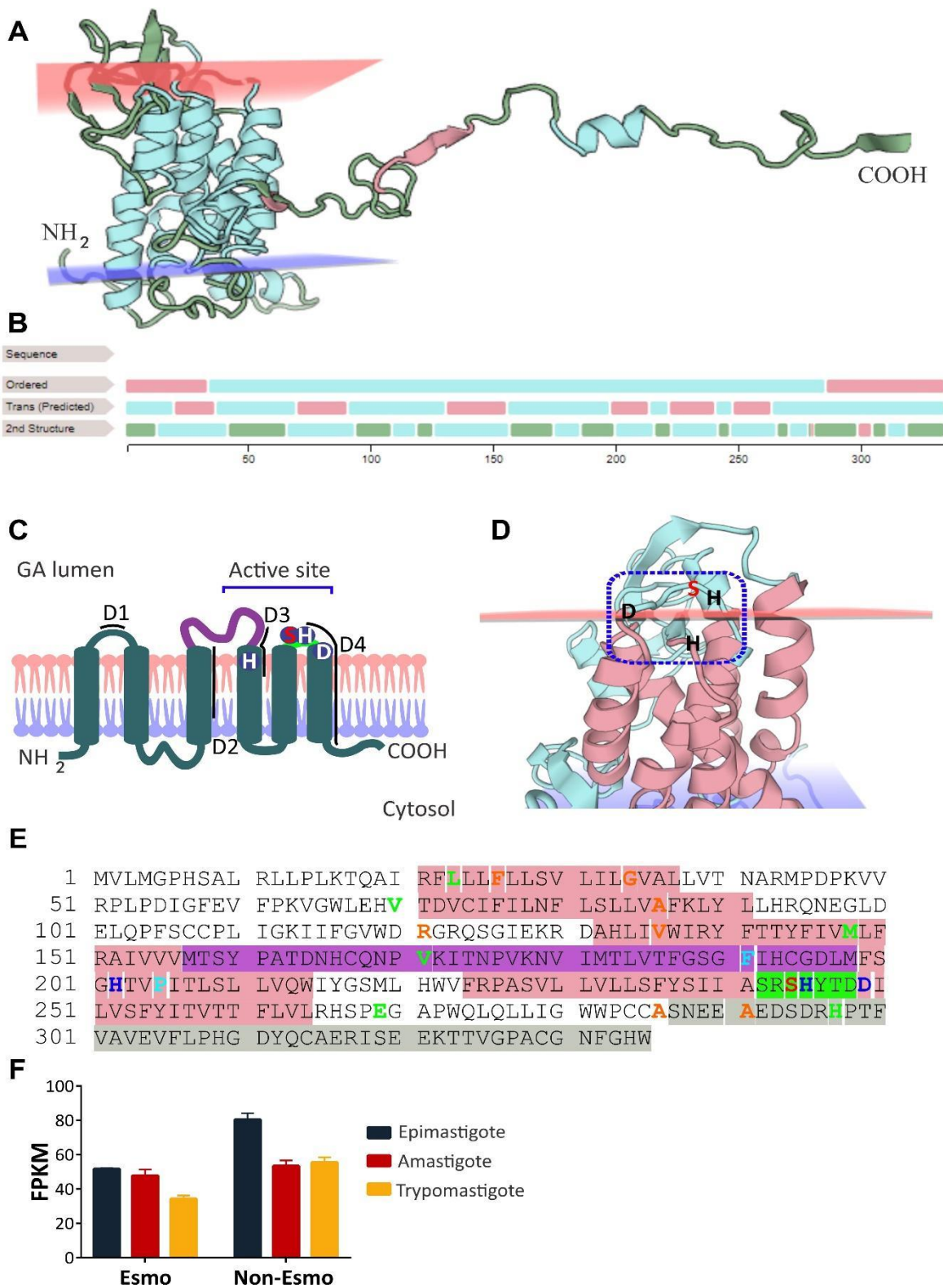


Figure 7. TcIPCS2 topology and 3D model predicted with PredMP. **A.** Best *de novo* constructed 3D model according to the energy function of CNS. To see the five predicted models with their information access to <http://www.predmp.com:3001/#/detail/1810246514101>. Color palette illustrates the 3-state secondary structure prediction. Light blue: α -helix; pink: β -strand; green: coil. **B.** Summary of the topology prediction results. The first-

row shows ordered (light blue) and disordered regions (pink). The second row shows transmembrane domains (pink). The third row shows the protein secondary structure, as described in point A. **C.** Topology diagram (not to scale) of TcIPCS. Conserved regions of SMS sequences as defined by Huitema et al. (2004) (D1-D4) are indicated by black bars. Key residues for the catalytic triad (H202, H245, D249) and substrate selectivity (S244), in loop b (purple) and loop c (green), are indicated in silhouette. **D.** Predicted location and disposition of the catalytic triad. **E.** The amino acid sequence of the TcIPCS2. The exact position of each TMD, loop b, loop c, and C-terminal region, are indicated in pink, purple, green, and grey, respectively. Blue letters indicate the catalytic triad. Red letter indicates the S244, determinant of the substrate selectivity. Green letters indicate functionally equivalent mismatches with TcIPCS1 aa sequence. Light blue and orange letters indicate non-equivalent mismatches with TcIPCS1 aa sequence. **F.** *TcIPCS* Esmeraldo-like (Esmo) and Non-Esmeraldo (Non-Esmo) expression pattern. Transcript expression values were extracted from the S4 Table of Belew et al. (2017).

Moreover, this analysis also displayed an intrinsically disordered C-terminal region of 49 aa, which could be playing a regulatory role of the protein metabolism, perhaps as a site of interaction with other proteins. According to the 3D model, the catalytic triad (H-H-D) was located partially buried on the exoplasmic leaflet of the membrane (Figure 7D), forming a binding pocket-like structure (Stank et al. 2016) Such an arrangement appears to be flanked by the H202, positioned below the membrane, and the H245 and D249, at each side. Interestingly, the S244, which have been found to determine phospholipid head group selectivity in SMS enzymes from *T. brucei* (Goren, Fox, and Bangs 2011) and human (Kol et al. 2017), was positioned above the catalytic triad, restricting any substrate interaction. In the absence of more experimental data, this hypothesis remains to be tested.

Based on primary sequence identity, orthologues of the *IPCS* gene were identified in the related parasites *T. cruzi*, *L. major* and *T. brucei* (Denny et al. 2006), and its SLS activity was characterized by cell-free synthesis (Sevova et al. 2010). Only one orthologue was identified for *T. cruzi* and *L. major*, both with IPC synthase activity. In the case of *T. brucei*, four different orthologues were identified, only one presenting IPCS activity. Taking the *T. cruzi* enzyme as a reference, the *L. major* and *T. brucei* IPCS share 70 and 65% amino acid similarity with the TcIPCS, respectively (Figure 8). Besides the sequence similarity, these proteins also present active site conservation.

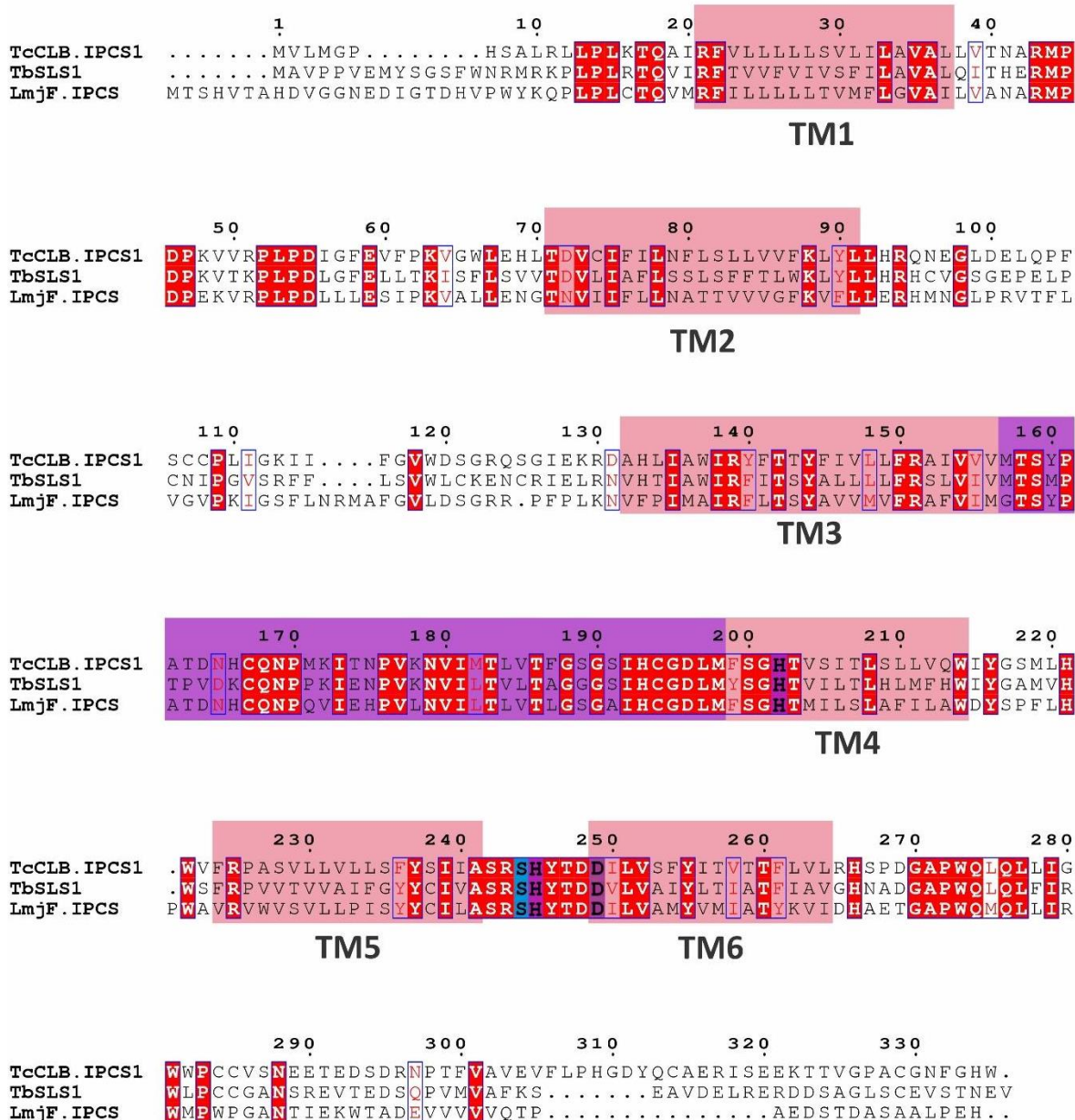


Figure 8. Alignment of kinetoplastid Inositol phosphorylceramide synthases. The sequence alignment was created with TM aligner (Bhat et al. 2017) and plotted by ESPrnt 3.0. Transmembrane domains (pink boxes) and loop (purple box) are depicted as predicted by PredMP (S. Wang et al. 2018). Catalytic triad is highlighted purple. S244, determinant of the substrate selectivity, is highlighted blue. Residues are numbered according to their position in the TcIPCS1 sequence. Residues highlighted red (white text) are conserved and residues in red text are functionally equivalent. Protein sequence identities with respective TcCLB.IPSC1 were 52% for the LmjF.IPSC and 49% for the TbSLS1. Tritypdb accession numbers: TcCLB.IPSC1: TcCLB.506885.124; TbSLS1: Tb927.9.9410; and LmjF.IPSC: LmjF.35.4990.

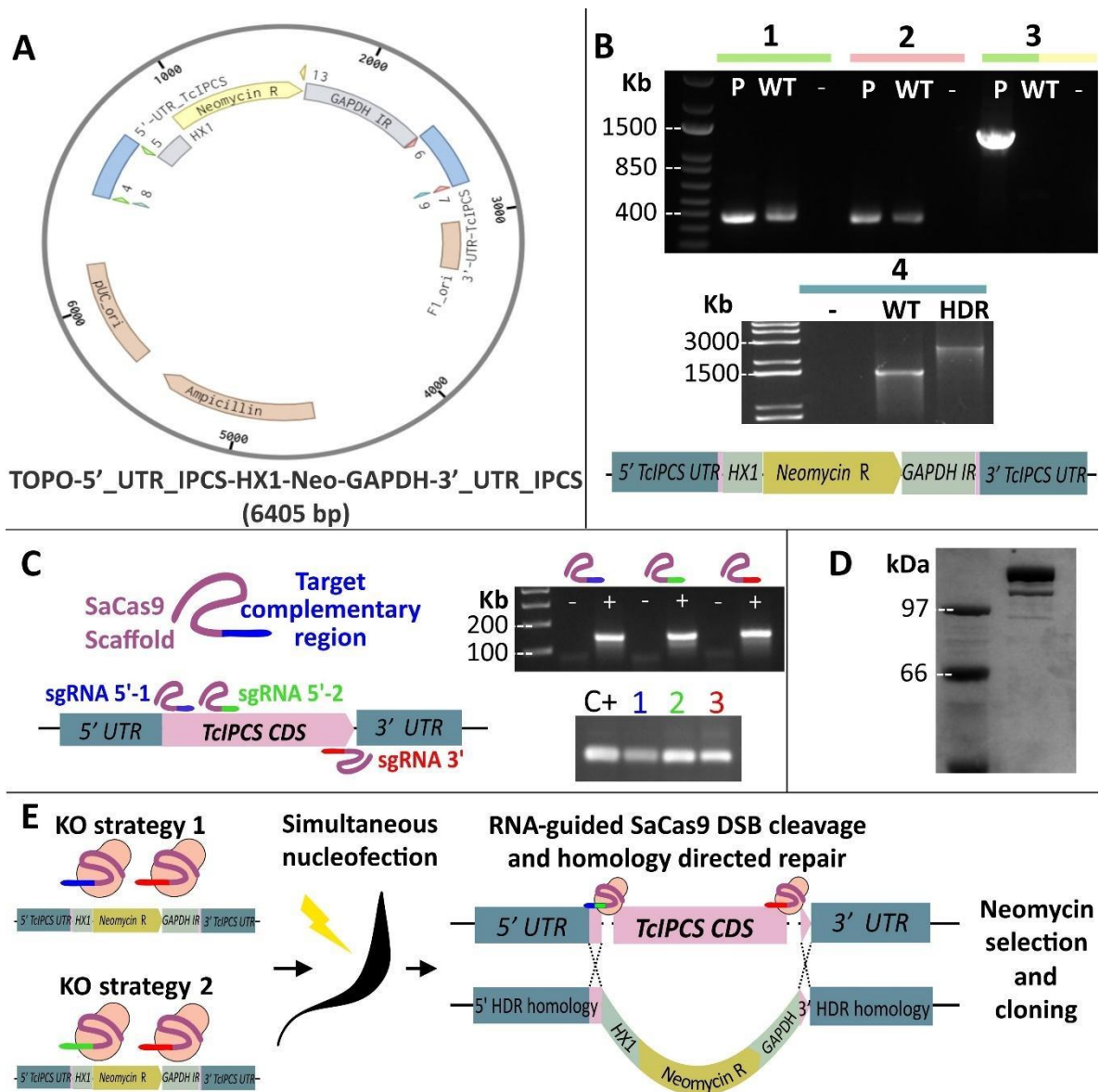
4.3 Generation of *T. cruzi* IPCS knockout parasites using the CRISPR-Cas9 system

As the *Leishmania* and *T. cruzi* IPCS enzymes share 70% similarity, the availability of recently identified anti-*Leishmania* IPCS compounds led us to hypothesize their possible anti-TcIPCS effect. Since one of the strategies used to assess the specificity of a compound for a molecular target is by the resistance caused after its gene deletion, we decided to generate *TcIPCS* null mutants to test the potential anti-TcIPCS activity of these compounds.

Therefore, we used the CRISPR-Cas9 technology (reviewed in Knott and Doudna 2018) to specifically cleave and edit both alleles of the *TcIPCS* gene using a donor DNA sequence for homologous recombination repair (HDR DNA donor, this strategy is described in item 3.11).

The vector used to generate the HDR DNA donor, named TOPO-5' _UTR_IPCS-HX1-Neo-GAPDH-3' _UTR_IPCS (Figure 9A), was constructed by PCR amplification and sequential cloning of the 5' and 3' untranslated regions (UTR) plus a small portion of the *TcIPCS* CDS into the plasmid Topo-HX1-Neo-GAPDH (described in item 3.5). Vector construction was verified by PCR amplification with different primer sets (Figure 9B). The HDR DNA donor fragment was PCR amplified using primers 9 and 10 (Table 1) and purified before parasite nucleofection. Originally, this PCR amplified sequence (5'-*IPCS_UTR-HX1-Neo-GAPDH-3'-IPCS_UTR*) was intended to be inserted by the parasite into the desired locus by homologous recombination of the flanking homology arms (UTR regions) with the endogenous regions without using CRISPR/Cas9. However, several attempts to obtain *TcIPCS* KO using this method failed. Since our lab has recently implemented the CRISPR-Cas9 technology, this new powerful protocol has overcome this obstacle, by the induction of site-specific double-strand breaks (DSBs) caused by the RNA-guided Cas9 endonuclease, which are repaired by the parasite using the HDR DNA donor as the template for homologous recombination (Reviewed in Lander and Chiurillo 2019).

As described previously by Beneke et al. (2017), we designed a two single-guided RNA (sgRNA) strategy to direct the Cas9 endonuclease activity for cleavage, in both alleles, of the 5' and 3' ends of the *TcIPCS* CDS (Figure 9C). These two sgRNAs were designed looking for two parameters: cut site located as close as possible to the junction of the homology arm (ideally less than ten bp away) and maximal homology of the sgRNA with both *TcIPCS* alleles.



scaffold sequence. A vector containing the whole SaCas9 scaffold (pTZSaCasScaffold) sequence was used as the PCR template (Burle-Caldas et al. 2018). Each column shows the amplification product of the sgRNAs represented at the left. (Bottom part) In vitro transcription of each sgRNA PCR product analyzed on 2% agarose gel electrophoresis. C+ represents a positive control, and each number and color are related to each of the sgRNAs schematized on the left side. **D.** Purified rSaCas9 protein separated in 10% SDS-PAGE and stained with coomassie blue. **E.** Diagrammatic representation of the strategy used to generate *TcIPCS* knockout (KO) using CRISPR-Cas9.

We were able to design a sgRNA that meets those two requirements only in the 3' end of the CDS (sgRNA 3'). For the 5' end we found a sgRNA that matches the first condition, but presents two mismatches with the Esmeraldo-like allele (sgRNA 5'-1). The closest sgRNA fitting the second condition was located 107 nucleotides away from the homology arm (sgRNA 5'-2). Consequently, we decided to test the sgRNA 3' with each of the 5' sgRNAs in separate experiments to maximize the chances of success (Figure 9E). *In vitro* synthesis of the sgRNAs is described in item 3.11. We used the heterologous expressed recombinant *Staphylococcus aureus* Cas9 (rSaCas9) produced in our lab as described by Burle-Caldas et al. (2018) (Figure 9D. See item 3.11 for more details). The enzyme was complexed with the sgRNAs, and the RNP (ribonucleoprotein) complex transfected into the parasites together with the HDR DNA donor using the Amaxa nucleofactor. After nucleofection, G418 selection, cloning and genotyping using PCR (Figure 10A), we observed that both KO strategies generated *TcIPCS* null mutants in only one round of transfection. These results demonstrated the high efficiency of the CRISPR-Cas9 technology, being the first time, to our knowledge, that a null mutant is obtained in *T. cruzi* with only one selection marker and the use of recombinant Cas9. In fact, even for KO generation with CRISPR-Cas9, it is common to use two different HDR DNA donors, each with a different selection marker, intended to be inserted in each allele (Costa et al. 2018). This result also showed that, different from the suggested by the literature, the *TcIPCS* is not an essential gene in *T. cruzi*.

For each KO strategy, six clones were randomly selected and genotyped by PCR reactions using the primer combinations shown in Figure 10A (PCR 1 and 2). From the six genotyped parasites belonging to KO strategy 1 (KO-1), three were null mutants (CL3, 4 and 8 = 50%), two single allele mutants (CL9 and 10 = 33.3%) and only one appeared to be wild type (CL11 = 16.7%). On the other hand, from the evaluated parasites of the KO strategy two (KO-2), only one showed null mutant genotype (CL10 = 33.3%), two single allele KO (CL1 and 11 = 66.7%) and three were inconclusive due to the lack of amplification in both PCRs (CL3, 4 and 12 = Excluded from analysis). Even though both strategies generated null mutants, this preliminary data showed higher efficiency for the KO-1, as this strategy generated 16% more double KOs than the other one. These

results suggest that a cutting site closer to the homology arm is more critical for KO generation than a complete homology of the sgRNAs with the intended DNA target. Clones 4 and 8 were further genotyped by the primer combinations shown in PCR 3 (Figure 10A). Relative quantification of the *TcIPCS* mRNA expression levels of each clone, assessed by quantitative PCR, confirmed their null mutant genotype (Figure 10B), as no *TcIPCS* mRNA was amplified. Thus, these two clones were selected for phenotypic characterization.

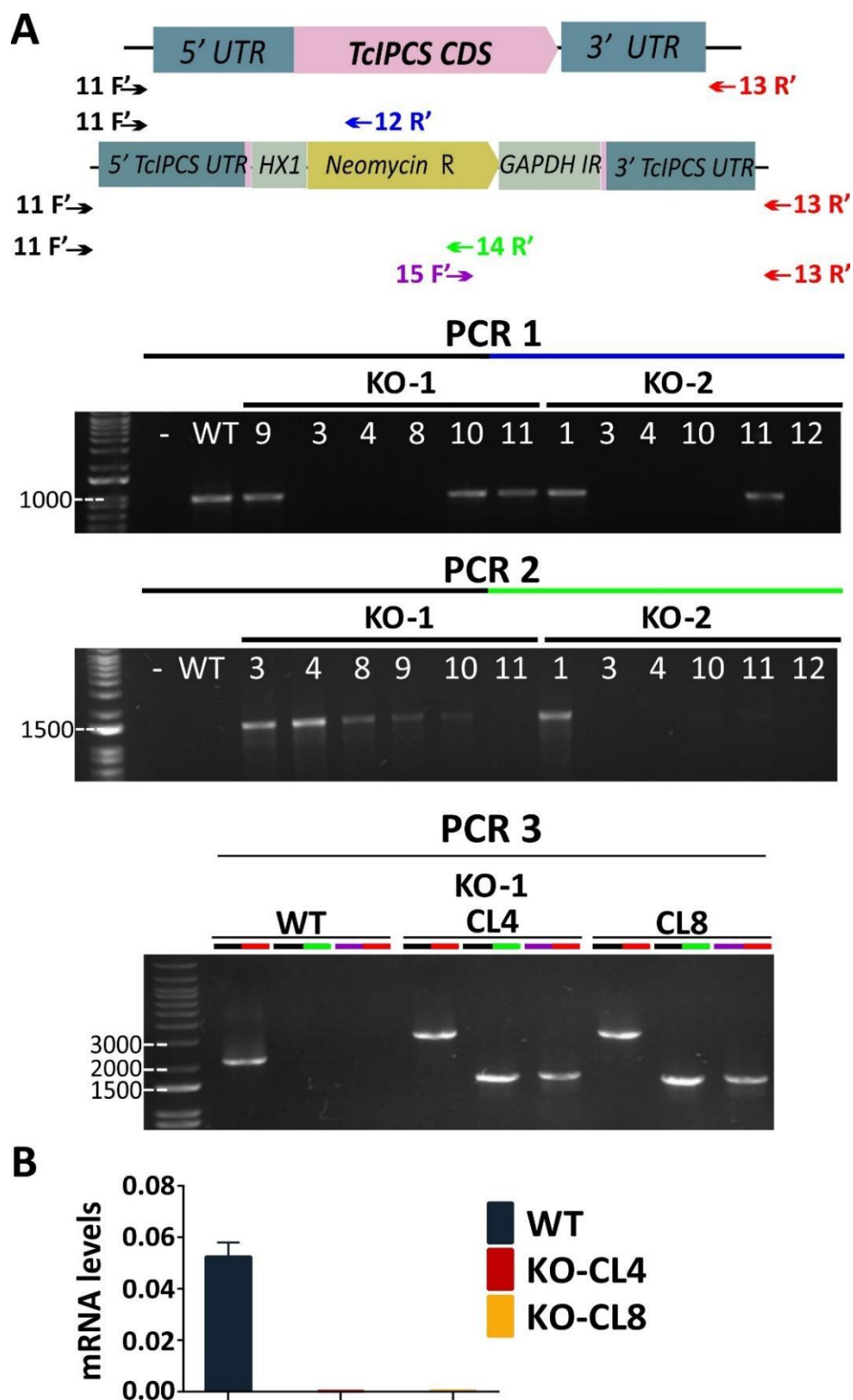


Figure 10. PCR genotyping and quantitative PCR analysis of *TcIPCS* null mutants. A. PCR analysis of DNA extracted from different nucleofected clones from both KO strategies. (On top). Representative diagram of the anneal location, in wild type (WT) and KO *TcIPCS* locus, of each used primer. PCR 1 and PCR 2 show the amplification product of two different primer combinations evaluated with genomic DNA from 6 different clones per KO strategy.

PCR 3 displays further genotyping of two selected clones from KO strategy 1 with additional primer sets. All PCR products were analyzed on 1% agarose gel electrophoresis and primer combinations were determined by the bar colors as above. B. Quantitative PCR analysis of *TcIPCS* mRNA levels of wild type (WT) and *TcIPCS* KO clone 4 (CL4) and clone 8 (CL8) epimastigotes. Results were normalized against the TcL9 control gene.

4.4 Phenotypic characterization of *TcIPCS* null mutants

In eukaryotes, sphingolipids (SL) are essential for multiple cellular processes and functions, including cell growth regulation, signal transduction, differentiation, and apoptosis (Cuvillier 2002; Hannun and Obeid 2018; Huwiler et al. 2000; Ohanian and Ohanian 2001) Moreover, SLSs play a central role in the intersection between phosphoglycerolipids (e.g., PI in and DAG out) and SLs (e.g., CER in and IPC out), controlling the balance between pro-apoptotic CER and pro-mitogenic DAG (Tafesse et al. 2006). Therefore, as previously showed in fungi by specific IPC synthase inhibitors (Georgopapadakou 2000), and in *T. brucei* by RNAi SLS silencing (Sutterwala et al. 2008), it was expected that the deletion of *TcIPCS* produces DAG - CER imbalances that ends up disturbing essential cell regulation processes. This disequilibrium was expected to cause cell cycle arrest, aberrant morphology, and cell death. Unexpectedly, this was not the case for the *TcIPCS* null mutants, which are viable parasites with normal epimastigote morphology (Figure 11A). It is thus possible that, as shown by recent sphingolipidomics study that revealed that *T. cruzi* epimastigotes have in their membranes other SLs besides IPC (Guan and Mäser 2017), these yet uncharacterized TcSLSs other than TcIPCS may be responsible for parasite viability in the absence of the deleted gene.

Even though *TcIPCS* null mutants showed normal morphology, as SLs have been related to cell growth regulation due to the CER/DAG balance, we asked if the gene deletion impaired in any way the KO epimastigote proliferation. Thus, we performed growth curves of log-phase parasites in supplemented LIT medium comparing KO clones 4 and 8, with wild type (WT) parasites. As shown in Figure 9B, we observed a significant growth rate reduction in the KO parasites during the end of the log phase.

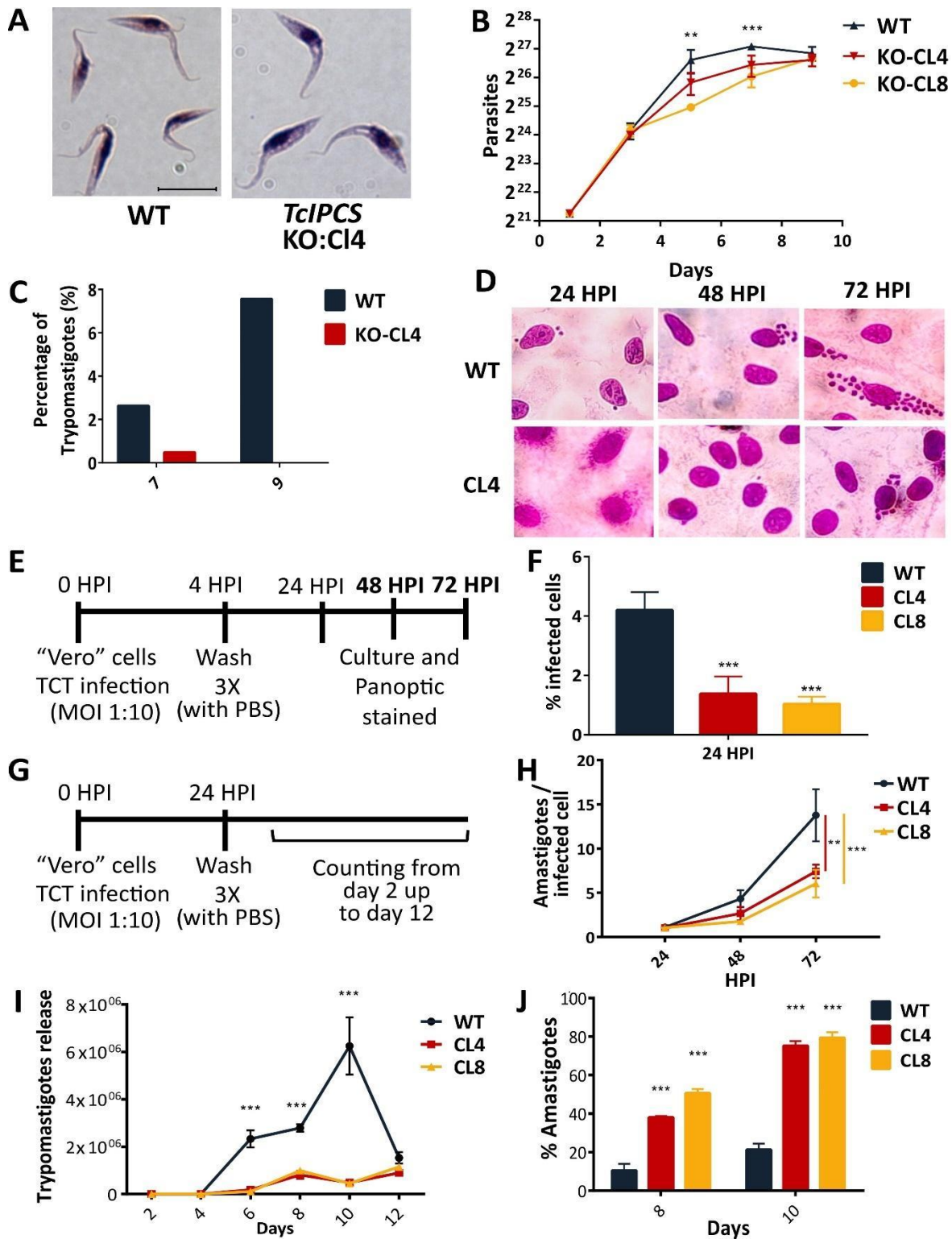


Figure 11. Phenotypic characterization of *TcIPCS* null mutants. **A.** *TcIPCS* KO epimastigotes present normal morphology. Log-phase wild type (WT) and *TcIPCS* KO-CL4 epimastigotes were fixed, stained with Giemsa, and analyzed by light microscopy using a BX60 Upright Compound Fluorescence Microscope (Olympus). Images were obtained using Q-CapturePro Software. Bar = 10 μ m. **B.** Growth of WT, *TcIPCS* KO CL4, and CL8 epimastigotes in LIT medium. Parasites were diluted to a concentration of 2.5×10^6 cells/mL, and parasite density was determined over

9 days. Significant differences in growth rates were found at days 5 and 7, using two-way ANOVA followed by Bonferroni post-test. WT and CL4 values are mean \pm SD; $n=3$. CL8 shows the result of only one replicate. $**p < 0.01$, $***p < 0.001$. **C.** Percentage of metacyclic trypomastigotes differentiated by nutritional stress in aged epimastigote cultures. Metacyclic differentiation was quantified by Giemsa staining to distinguish the position of the kinetoplastid by light microscopy. Values are the mean of two technical replicates. **D, E, F, G, H, I, J.** Vero cells infection assays with tissue-culture cell-derived trypomastigotes (TCT) from WT and *TcIPCS* KO CL4 and CL8 parasites. **E.** Schematic representation of the experiment workflow to evaluate the percentage of infection and the amastigotes per infected cell (includes legends in bold). **G.** Schematic representation of the experiment workflow to evaluate the trypomastigote release to the supernatant. **D** Representative pictures of the panoptic stained infected cells used to make quantifications for F and H. **F, H.** There were significant differences in the percentage of infected Vero cells at 24 h post-infection (hpi) (F) as well as in the number of intracellular amastigotes per infected host cell determined 72 hpi (H). **I, J.** There were significant differences in the released trypomastigotes to the supernatant (I) as well as in the percentage of extracellular amastigotes from the total number of released parasites (J). Values are mean \pm SD; $n=3$; $**p < 0.01$, $***p < 0.001$. One-way ANOVA was used in F, and two-way ANOVA used in H, I and J. All statistical analyses were followed by Bonferroni post-test for multiple comparisons.

Such a phenotype probably occurred because WT parasites reached the stationary-phase faster than the KO parasites. This difference may be due to the lack of CER/DAG regulation from *TcIPCS*, which may produce an unbalance in the CER level that slows down the KO cell cycle but is not sufficient for growth arrest. Furthermore, as these analyses were performed in rich media, the effects of IPC absence could be aggravated in a less supplemented medium. In regards to the final part of the curves, such stabilization of the cultures at similar cell densities probably happened due to the onset of metacyclogenesis in WT parasites. In contrast, KO parasites continue growing for a more extended period, reaching similar cell densities as attained by WT cultures. These observations drove us to hypothesize that *TcIPCS* deletion could be impairing metacyclic differentiation. To evaluate this hypothesis, we determined the effect that *TcIPCS* deletion causes in the metacyclic differentiation *in vitro* (methods described in item 3.16, Figure 8C). As expected, the percentage of metacyclic trypomastigotes in WT parasites increased as the parasites entered in the stationary phase of growth (Camargo 1964), reaching almost 8% of metacyclic trypomastigotes at day 9 of culture. In contrast, KO parasites displayed a significant decrease in the percentage of metacyclic trypomastigotes in days 7 and 9. Such a different phenotype not only corroborated our hypothesis but, more importantly, showed the importance that IPC synthase has on the *in vitro* differentiation of epimastigotes into the mammal infective form found in the insect vector. In sum, these results demonstrate that the absence of this sphingolipid synthase greatly inhibits metacyclogenesis.

Impaired metacyclogenesis could be due to the inability of the KO parasites to perform critical developmental changes in their membrane composition, maintaining the parasite in the

epimastigote form despite the presence of environmental signals for differentiation. In fact, in epimastigotes, IPC has been found to anchor 92 – 98% of free GIPLs which form a dense glycocalyx covering the parasite surface (Nakayasu et al. 2009) while GPI-anchored glycoproteins are thought to be mainly tethered by alkylacyl-phosphatidylinositol (AAPI) in epimastigotes (Serrano et al. 1995). On the other hand, in metacyclic trypomastigotes, critical glycoprotein surface families such as trans-sialidases (TS) and mucins are GPI-anchored by IPC (Agusti et al. 1998; Serrano et al. 1995).

These GIPLs and GPI-anchored proteins are profoundly involved in different host-parasite interactions and pathogenesis itself (DosReis et al. 2002; Previato et al. 2004; Sergio Schenkman et al. 1993). A clear example of this developmental regulation occurs with the GPI-anchored mucin multigene family, which is anchored to the membrane by AAPI in epimastigotes. However, upon epimastigote transformation into metacyclic trypomastigotes, GPI lipid portion changes substantially to mostly IPC (~70 % of mucins) (Serrano et al. 1995). The inability of the KO parasites to remodel its surface mucins, and probably other GPI-anchored glycoproteins as TSs, could be causing or at least contributing substantially to the metacyclogenesis impairment. Furthermore, the reason why this structural change occurs is an object of discussion; nevertheless, it may be significant for cell infection, as the metacyclic trypomastigote sheds most of its mucins during host cell invasion (Schenkman et al. 1993). Also, GIPLs and GPI-anchored mucins are involved in epimastigote attachment to the vector's luminal midgut surface and rectal ampoule, respectively (Cámara et al. 2019; Nogueira et al. 2007). This adhesion step has been suggested as a triggering factor of metacyclogenesis *in vivo* and *in vitro* (De Souza, De Carvalho, and Barrias 2010), the metacyclogenesis delay observed could also be worsened by a defective adhesion process. Since metacyclogenesis occurs in the insect vector, it would be interesting to study *in vivo* metacyclogenesis of the KO parasites and how *TcIPCS* deletion affects this process, probably obtaining an exacerbated phenotype. The study of processes that affect such metabolic differentiation would be significant for therapeutic strategies for the vector.

Since the percentage of metacyclic trypomastigotes was greatly reduced and their membrane composition was expected to be configured differently, we asked if the metabolic and structural changes caused by the *TcIPCS* deletion attenuate the parasite infective capacity *in vitro* (detailed in Item 1.1 Figure 2). Thus, we took cultures in the stationary phase and infected LLC-MK2 monolayers using WT stationary phase cultures as controls (described in item 3.1). Under

these uncontrolled conditions, although we were able to find intracellular amastigotes followed by differentiation and release of trypomastigotes in the supernatant, there was an evident impairment of the KO clones infective capacity when compared with WT (data not shown).

To further characterize these observations under controlled conditions, we collected and purified TCTs from the KO clones and WT parasites and performed controlled infections in Vero cell monolayers with a multiplicity of infection (MOI) of 10:1 (for methods see item 3.17). To evaluate infective capacity, we incubated monolayers with TCTs for 4 hours, washed the infected cells and incubated for 24 h post-infection (hpi) in DMEM-2 before fixing and staining the cells (Figure 11D, E). Figure 11F showed a significant diminution in the percentage of infected cells by the *TcIPCS* KO clones compared with WT parasites. When we evaluated the numbers of intracellular amastigotes in monolayers infected for 24, 48, and 72 HPI (Figure 11D), we observed increased differences between WT and KO replication rates (Figure 11H). Since the differences in the numbers of intracellular amastigotes increased at 72 hpi we concluded that *TcIPCS* deletion also impairs amastigote intracellular proliferation.

The final part of the intracellular infection cycle, i.e., the differentiation of intracellular amastigotes into TCTs and their subsequent release into the supernatant after cell disruption was evaluated by infecting monolayers for 24 hours washed as before and incubated with DMEM-2 for 12 days to quantify, by direct counting, the number of TCTs in the supernatant (Figure 11G). Figure 11I showed significantly fewer TCTs released into the supernatant of the KO infections compared with the WT ones. Altogether, these results demonstrate the critical role IPC synthase plays in *T. cruzi*'s infective capacity. Interestingly, while quantifying TCTs in the supernatant of the KO infections, it was seen an increasing predominance of amastigote-like forms (up to 80% on day 10), commonly known as extracellular amastigotes (EA) (Figure 11J) (Bonfim-Melo et al. 2018). Although transformation of extracellular TCT into amastigote-like forms has been described to occur *in vivo* and *in vitro*, since we observed an increased differentiation with the *TcIPCS* KO parasites, it is possible that this was caused by the *TcIPCS* deletion (discussed below).

Even though *TcIPCS* gene showed not to be essential neither for survival nor for infection *in vitro*, its deletion has a great impact in the parasite fitness, causing the phenotype of an attenuated parasite similar to the avirulent *T. cruzi* clone CL-14 (Lima et al. 1991). Results indicated that IPC may be involved in metabolic processes that affects *i*) establishment of

infection; *ii*) intracellular proliferation; *iii*) TCT differentiation and release; and *iv*) extracellular TCT survival, re-infection, and dissemination.

Upon mammal invasion, *T. cruzi* provokes a quick immune response due to the interaction of the parasite with the complement system, which is followed by a coordinated innate and adaptive immune response (Reviewed in Acevedo, Girard, and Gómez 2018). Nevertheless, this orchestrated response is not effective enough to achieve complete clearance of the parasite (Tarleton and Zhang 1999). To cope with all these difficulties, *T. cruzi* has evolved a series of sophisticated strategies to evade the effect of both innate and adaptive immunity, while not seriously affecting its host. Such strategies have been shown to rely in the host-parasite interactions mainly regulated by the parasite through its surface GPI anchored glycoproteins (Valente et al. 2019).

The most elegant known mechanism throughout *T. cruzi* escapes from the mammal immune system is the poaching of sialic acid (SIA) molecules from host cells and transferring to its surface glycoproteins. It efficiently creates a molecular camouflage that entirely hides the parasite from phagocytic cells and interferes with an effective immune response (Argibay 2002; Freire-de-Lima et al. 2010; Gao, Wortis, and Pereira 2002). This process is mediated by the GPI-anchored TSs, responsible for SIA transfer, and the surface located mucins, which act as acceptors. Therefore, as the lipid anchor of TSs from metacyclic trypomastigotes, most TSs from TCTs and most mucins from metacyclic trypomastigotes, is composed by IPC (Agusti et al. 1997, 1998; Serrano et al. 1995), it is quite possible that *TcIPCS* KO parasites would not behave well when facing a healthy immune response, probably being incapable to successfully disseminating its infection. *In vivo* infections performed in mice would give a more realistic scenario of infection that will undoubtedly provide insights about the real impact of the *TcIPCS* deletion, probably raising the possibility of the use of the *TcIPCS* KO parasites as attenuated vaccines.

After the first encounter with the immune system, *T. cruzi* requires to internalize a cell in order to differentiate into the amastigote replicative form. This parasite can invade an extensive range of host cells relying on an array of molecular strategies. Traditionally, cell invasion has been divided into two different processes: adhesion, which involves the recognition and signaling of surface molecules from parasite and host cells, and internalization that may occur by phagocytosis or endocytosis (S. Schenkman and Mortara 1992; Vieira et al. 2002). Several GPI anchored

glycoproteins have been described as participants of the invasion process. These, include different mucins (Buscaglia et al. 2006; Di Noia, Sanchez, and Frasch 1995; Sibley and Andrews 2000; Villalta and Kierszenbaum 1984; Yoshida et al. 1989) and active and inactive TSs (Schenkman, Diaz, and Nussenzweig 1991), which shows the importance of these surface molecules in the host cell invasion.

Furthermore, the fact that most of those molecules are IPC anchored justifies the significant decrease in the percentage of infected cells. Also, this phenotype is not more pronounced probably because the parasite adapted its metabolism to the IPC absence by anchoring all its glycoproteins with only AAPI instead of both. Mass spectrometry analyses of the lipid portion of the GPI anchors could help clarify this hypothesis.

Once inside the host cell, parasites are restrained to the parasitophorous vacuole (PV); afterward, they escape to the cytoplasm and transform into the amastigote replicative form to start its proliferation by binary fission. During this process, especially the escape from the PV, it has been suggested that surface glycoproteins, especially TSs are majorly involved (Norma W. Andrews and Whitlow 1989; Stecconi-Silva, Andreoli, and Mortara 2003), but certainly, more research is needed. IPC showed not to be essential for this process to occur, as *TcIPCS* KO cells can complete the invasion process. Nonetheless, probably its absence could also be affecting the PV escape process, contributing to the impaired cell invasion.

The transformation from slender TCTs to round amastigotes has been suggested to occur accompanied by extensive remodeling of the parasite's membrane composition (Maria Laura Salto et al. 2003). Although little is known about the IPC metabolism in amastigotes, it has been shown that the synthesis of IPC accompanies differentiation of TCTs to intracellular amastigotes. Thus, IPC ends up constituting the lipid portion of the major part of the amastigote inositolphospholipids (IPLs) (Salto et al. 2002; 2003). During early amastigote differentiation, *Ssp4*, a stage-specific IPC anchored glycoprotein, is majorly expressed and progressively shed by the action of a unique *T. cruzi* phosphoinositide phospholipase C (PI-PLC) (Andrews et al. 1988; Bertello, Andrews, and De Lederkremer 1996). PI-PLC has been shown to play an essential role in the inositol phosphate/diacylglycerol signal transduction cascade (Berridge 1987; Irvine 1996). Although PI-PLC can also cleave AAPI anchored glycoproteins, the fact that *Ssp4*, probably the major surface glycoprotein of amastigotes (Andrews et al. 1988), is IPC anchored, and its shedding occurs

concomitantly with the peak of surface expression of the PI-PLC (Martins et al. 2010), suggest that the absence of IPC synthesis could be affecting the standard anchoring of the Ssp4 glycoprotein. Therefore, affecting the cascade initiated by the Ssp4 shedding and the following metabolic processes involved in amastigote maturation and duplication. This hypothesis is strengthened by the fact that a decreased expression of GPI-anchored glycoproteins causes a decreased rate of amastigote duplication and trypomastigote differentiation (Garg et al. 1997).

Once intracellular amastigotes have differentiated and started its proliferation by binary fission in the cytoplasm, they give rise to bloodstream trypomastigotes (TCTs, when differentiated *in vitro*), which rupture the cell and escape into the blood and lymph with the possibility to invade an extensive range of cells (Tyler and Engman 2001). In addition to this canonical life cycle, in the peripheral blood can also be observed rounded forms denominated extracellular amastigotes (EA) (Andrews et al. 1987). These forms are thought to come from bloodstream trypomastigotes that fail to invade a new cell undergoing sequentially morphological and biochemical changes, and from amastigote released from prematurely lysed infected cells (Andrews et al. 1987). In infected mice at the acute phase, EA constitutes up to 10% of the circulating parasites, and are capable of infecting cells and evade the complement system (Andrews et al. 1987; Iida, Whitlow, and Nussenzweig 1989; Ley et al. 1988). *In vitro*, different conditions have been described to induce EA transformation from trypomastigotes. Such conditions rely basically on acidic pHs (pH 5), nutrient components, and temperature (Andrews et al. 1987; Lanar 1979; Pan 1978; Tomlinson et al. 1995; F Villalta and Kierszenbaum 1984). More recently, *in vitro* treatment of TCTs with PI-PLC showed to rapidly induce EA differentiation producing quick morphological changes in the organization of the parasite cytoskeleton, followed by biochemical changes (Mortara et al. 2001). *In vitro* and *in vivo* EA showed to be biochemically identical to the intracellular counterparts.

Thus, the final evaluated parameter was TCT differentiation and supernatant release, which exhibits not only the parasite's capacity to differentiate from intracellular amastigote into TCT followed by host-cell disruption and supernatant release, but also a general perspective of the parasite's infective capacities; as it is influenced by the previous steps of the infection cycle (discussed above). Having this in mind, the results from the KO experiment showed the summation of the impaired infective capacities (discussed above) plus a defective TCT differentiation and

supernatant release, which altogether displayed a profoundly impacted infectivity. Such KO defective differentiation and release would be related with an impaired Ssp4 shed by the PI-PLC (Andrews et al. 1988; Bertello, Andrews, and De Lederkremer 1996) and a subsequent defect in the signal transduction cascades this process regulates (Berridge 1987; Irvine 1996); followed by a decreased trypanomastigote differentiation, as showed in parasites with decreased GPI anchored glycoprotein expression (Garg et al. 1997).

This defective TCT release phenotype was accompanied by an increasing percentage of EA. Such a phenotype may be the result of two different possibilities. On the one hand, the KO inability to infect neighboring cells for 24 h that end up initiating EA differentiation. On the other hand, a TCT membrane configuration caused by the IPC absence, which metabolically emulates late-stage TCTs that cannot maintain their form for long periods, thereby initiating EA differentiation. As our results showed a significant decrease in the KO infected cells (Figure 9F), this impairment certainly is contributing to the EA differentiation. Nevertheless, as that experiment was performed restricting infection to only 4 hours, and it is not the case of the present experiment, it is highly improbable that it accounts solely for the evidenced phenotype. Therefore, *TcIPCS* KO EA differentiation and predominance is probably the result of the combined effect of both possibilities.

Regarding the EA infective capacities, they were shown to infect different cell types by a distinct and less efficient mechanism than the one used by trypanomastigotes (Bonfim-Melo et al. 2018; A. B. Fernandes and Mortara 2004). It has been demonstrated that EAs must attach to the surface of host cells before their invasion (Bonfim-Melo et al. 2018; Ferreira et al. 2012). As one of the critical factors involved during this process is the IPC anchored glycoprotein Ssp4 (Barros et al. 1997; Florentino et al. 2018; Vieira da Silva et al. 2006), *TcIPCS* deletion may be also affecting the EA infective capacities, which contributes to the attenuation of the KO infectivity.

4.5 Generation of *T. cruzi* *IPCS* overexpressors and preliminary characterization

As *TcIPCS* deletion caused significant metabolic impacts that provoked the attenuation of the KO parasite, we next evaluated the effect that overexpressing the gene on the parasite's fitness. To generate stable *TcIPCS* overexpressing parasites we prepared a pROCK-Hygro expression vector

(DaRocha et al. 2004) cloned with the *TcIPCSI* CDS in-frame fused at the C-terminal end with the human influenza hemagglutinin tag (HA-tag) (Figure 12A, C) (see items 3.5 and 3.13 for details). The main advantage of this vector lies in its β -*tubulin* sequences that allow for the integration of the linearized vector into the parasite's genome by homologous recombination (HR) (Figure 12B). Thus, after cloning, the resultant pROCK-Hygro-IPCS::HA was gel-purified, and WT parasites were transfected, selected with hygromycin, and cloned. *TcIPCS* overexpression was confirmed in two selected clones at the mRNA level (Figure 12D). Since *T. cruzi* possesses various β -*Tubulin* gene copies (Maingon et al. 1988), the selected clones (i.e., CL15 and 17) showed a different level of expression probably due to the integration of the vector into a different number of tubulin loci. qPCR relative quantification showed that CL15 and CL17 clones have 4.6 and 10.8 times *TcIPCS* mRNA levels than the WT, respectively. It is important to note that the expression cassette contained by the pROCK vector is composed by a constitutive ribosomal promoter and the 5' and 3' UTR regions of the highly expressed genes *TcP2 β* and *GAPDH*, respectively, which contribute to the mRNA stability and translation efficiency, also enhancing the expression of each integrated pROCK plasmid (DaRocha et al. 2004). To verify *TcIPCS::HA* overexpression, we performed western blot with anti-HA antibodies. However, even after testing different western blot conditions we were not able to detect the tagged protein, most likely because TcIPCS is a TM protein and requires other methods to be visualized.

Since we showed by qPCR that we have obtained parasites over-expressing TcIPCS, we performed preliminary characterization of the two selected clones. As seen in the *TcIPCS* KO parasites, overexpressor (OE) epimastigotes showed to be viable with normal morphology (data not shown). Also, *TcIPCS* overexpression did not affect *in vitro* epimastigote duplication in supplemented LIT medium when compared with WT parasites (Figure 10E). In contrast, when evaluating *in vitro* metacyclogenesis, our preliminary results suggested that overexpression of *TcIPCS* causes a faster and enhanced metacyclic differentiation compared to WT (Figure 12F). Such phenotype was expected, since *TcIPCS* deletion causes a considerable impairment in the metacyclic differentiation (Figure 11C).

These results, although preliminary, suggest that the major effect of IPC synthase overexpression in epimastigote forms is related to the signals cascades that regulate triggering of metacyclogenesis. According to enzymatic characteristics, IPCSs have a bi-directional function capable of converting PI and CER into IPC and DAG and vice versa (Huitema et al. 2004; Tafesse

et al. 2006). Therefore, TcIPCS products participate not only in the host-parasite interactions but also may be crucial in the control of the balance between pro-apoptotic CER and pro-mitogenic DAG. As these latter compounds are potent modulators of cell behavior, it was expected that its dysregulation of expression could distort in any way the parasite proliferation. Surprisingly this was not the case, as OE parasites showed to grow at the same pace as a WT parasite. Such a result suggests that TcIPCS may be part of additional levels of control, probably interacting with regulatory proteins that manage their activation. According to the *in silico* topology analyses, the intrinsically disordered C-terminal region of 49 aa may be the site of interaction with these regulatory proteins. Nevertheless, a preliminary domain search using the InterProScan server (Zdobnov and Apweiler 2001) could only detect the SMS like domain, which is characteristic of the family but cannot account for the suggested interaction.

On the other hand, the metacyclogenesis, which was seen to be impaired by the *TcIPCS* deletion, was enhanced by the protein overexpression. This differentiation process may also be affected by the hypothesized protein regulation, though in a different way.

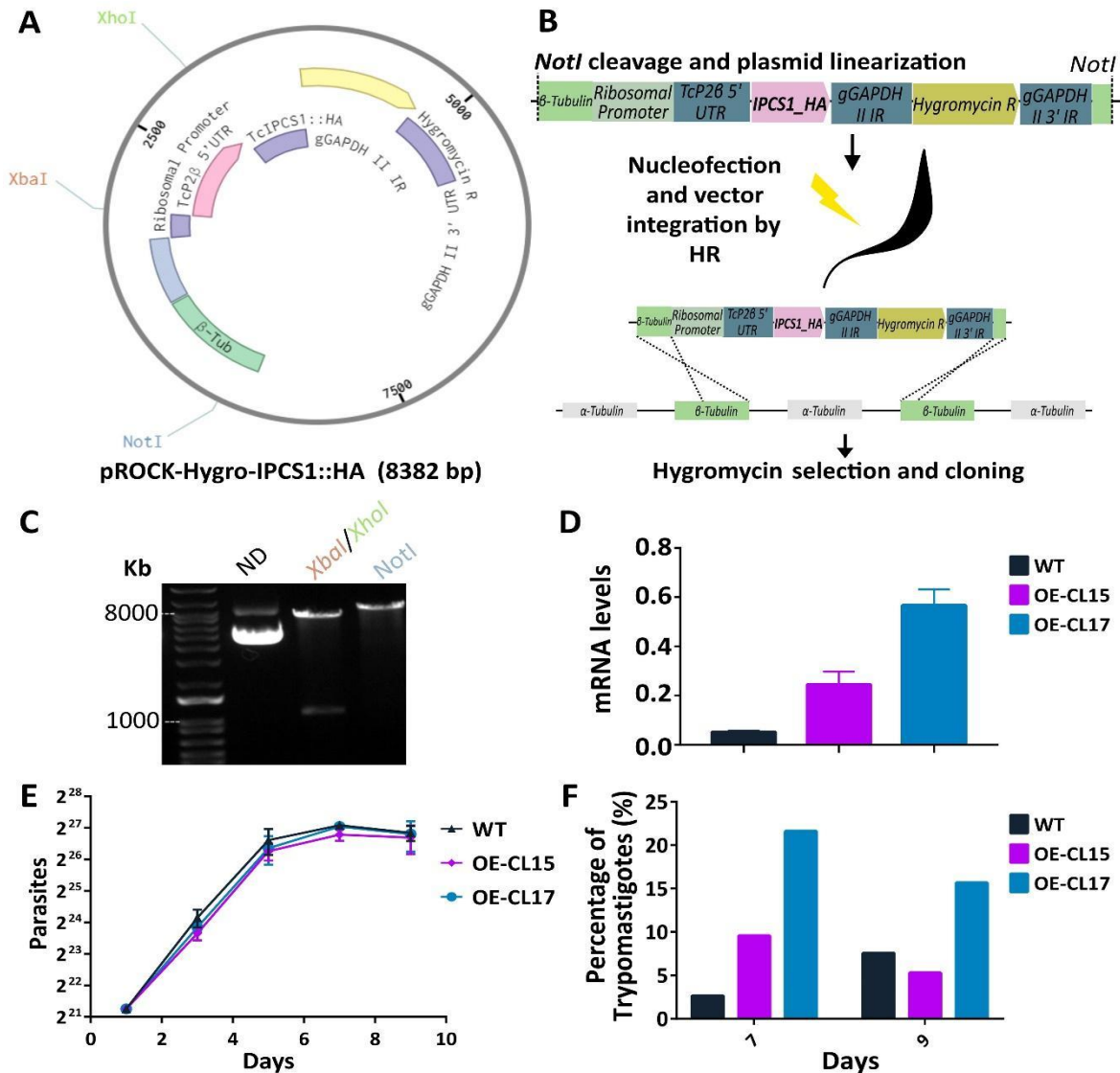


Figure 12. Generation of *TcIPCS* overexpressor parasites and preliminary characterization. **A.** Schematic representation of the pROCK-Hygro-IPCS::HA, an integrative vector for stable expression of *TcIPCS*::HA. **B.** Diagrammatic representation of the methodology used to obtain overexpressor (OE) parasites. **C.** Restriction mapping of the pROCK-Hygro-IPCS::HA plasmid to verify the integrity of the construction. Plasmid DNA was digested with either *XbaI/XhoI* or *NotI* and analyzed on 1% agarose gel electrophoresis. Restriction enzyme cutting sites are illustrated in A. ND: non-digested plasmid DNA. **D.** Quantitative PCR analysis of *TcIPCS* mRNA levels of wild type (WT) and OE clone 15 (CL15) and clone 17 (CL17) epimastigotes. Results were normalized against the *TcL9* control gene. **E.** Growth of WT, OE CL15, and CL17 epimastigotes in LIT medium. Parasites were diluted to a concentration of 2.5×10^6 cells/mL, and parasite density was determined over 9 days. No significant differences in growth rates were found using two-way ANOVA followed by Bonferroni post-test. Values are mean \pm SD; $n = 3$. **F.** Percentage of metacyclic trypomastigotes differentiated by nutritional stress in aged epimastigote cultures. Metacyclic differentiation was quantified by Giemsa staining to distinguish the position of the kinetoplastid by light microscopy. Values are the mean of two technical replicates.

As the OE parasites showed a peak of metacyclogenesis two days sooner from the WT parasites, we hypothesize that the overexpression stimulated the signal cascades that control metacyclogenesis, causing an earlier and improved differentiation. Furthermore, the percentage of

differentiated trypanomastigotes appeared to be related to the *TcIPCS* mRNA levels (Figure 12D, F), which is also in accordance with the stated before. As discussed in section 4.3, *T. cruzi* during metacyclogenesis performs important developmental changes in its membrane composition that are accompanied by signal transduction cascades, which launch this process. The overexpression of the *TcIPCS* probably produces an earlier commence of these processes and a faster transit into the metacyclic infective form. Moreover, *TcIPCS* OE may also sensitize the parasite membrane to the signals of the medium that signalizes metacyclogenesis start (e.g., nutrient starvation), producing a higher percentage of differentiating parasites.

Altogether, these preliminary results are in line with the findings obtained with the KO parasites showing from a different perspective the importance of *TcIPCS* for the normal metabolism of the parasite. As suggested with the KO parasites, it would be interesting to corroborate these results *in vivo*, possibly obtaining a more contrasting phenotype.

4.6 Recombinant *TcIPCS1* and C-terminal-*TcIPCS1* heterologous expression and purification for anti-TcIPCS polyclonal antiserum generation

To test the effect of compounds directly on the protein, we attempted to express and purify the TcIPCS in *E. coli*. We cloned the *TcIPCS1* CDS (see item 3.5 for details, Figure 13A) into the pET-28a (+) expression vector (Novagen) and, after transforming different *E. coli* strains (see item 3.8 and table 2) we induced the protein expression under various conditions (see item 3.14 for details). Unfortunately, probably due to the topology of the protein (Figure 7), none of the evaluated strains under the conditions assessed produced a perceptible induction, neither by coomassie blue staining nor by western blot analysis (data not shown), showing that all of our attempt to express the full-length sequence of the enzyme were unsuccessful. Reports from other laboratories also indicated that it was impossible to express in *E. coli* the full-length protein from *L. major* (personal communication with Professor Paul Denny, Durham University). These results led us to try to induce an immunogenic fraction of the protein so that we could generate antibodies to be used in the characterization studies of the enzyme. Such an immunogenic fraction was selected according to the B-cell epitope predictions made by the software Bepipred-2.0 (Jespersen et al. 2017), from the TcIPCS1 protein sequence (Figure 7).

Based on the software results and the predicted properties of the protein (Figure 13C, D), we selected a C-terminal fraction of 177 aa that included the last three predicted TMDs, flanked by the loop b (thought to be important for substrate recognition), the catalytic triad, and the disordered region located at the c-terminal part of the protein. Therefore, we cloned into the pET-28a (+) expression vector the selected *C-terminal-TcIPCSI* sequence (Figure 13B), transformed different *E. coli* strains (see item 3.8 and table 2) and induced the heterologous expression at various temperatures (10, 20, 30 and 37°C), times of induction (4, 16, 24 and 48h) and IPTG concentrations (0.1 and 0.5 mM) (see item 3.14 for details). Probably due to hydrophobic properties of the recombinant protein (Figure 13D), expression was only achieved in the *E. coli* ArcticExpress (DE3) strain at low temperatures ($\leq 13^{\circ}\text{C}$) and after 16 hours of induction (Figure 14B, C). Such result was possibly obtained because of the cold-adapted Cpn10 and Cpn60 chaperonins co-expressed by this strain, which highly enhances recombinant protein yield at low temperatures, outperforming the capacity to promote disulfide bonding by Shuffle T7 and Origami™ 2(DE3) strains or the OverExpress™ C41(DE3) tolerance to toxic proteins (Results from Shuffle T7 and OverExpress™ C41(DE3) are not shown).

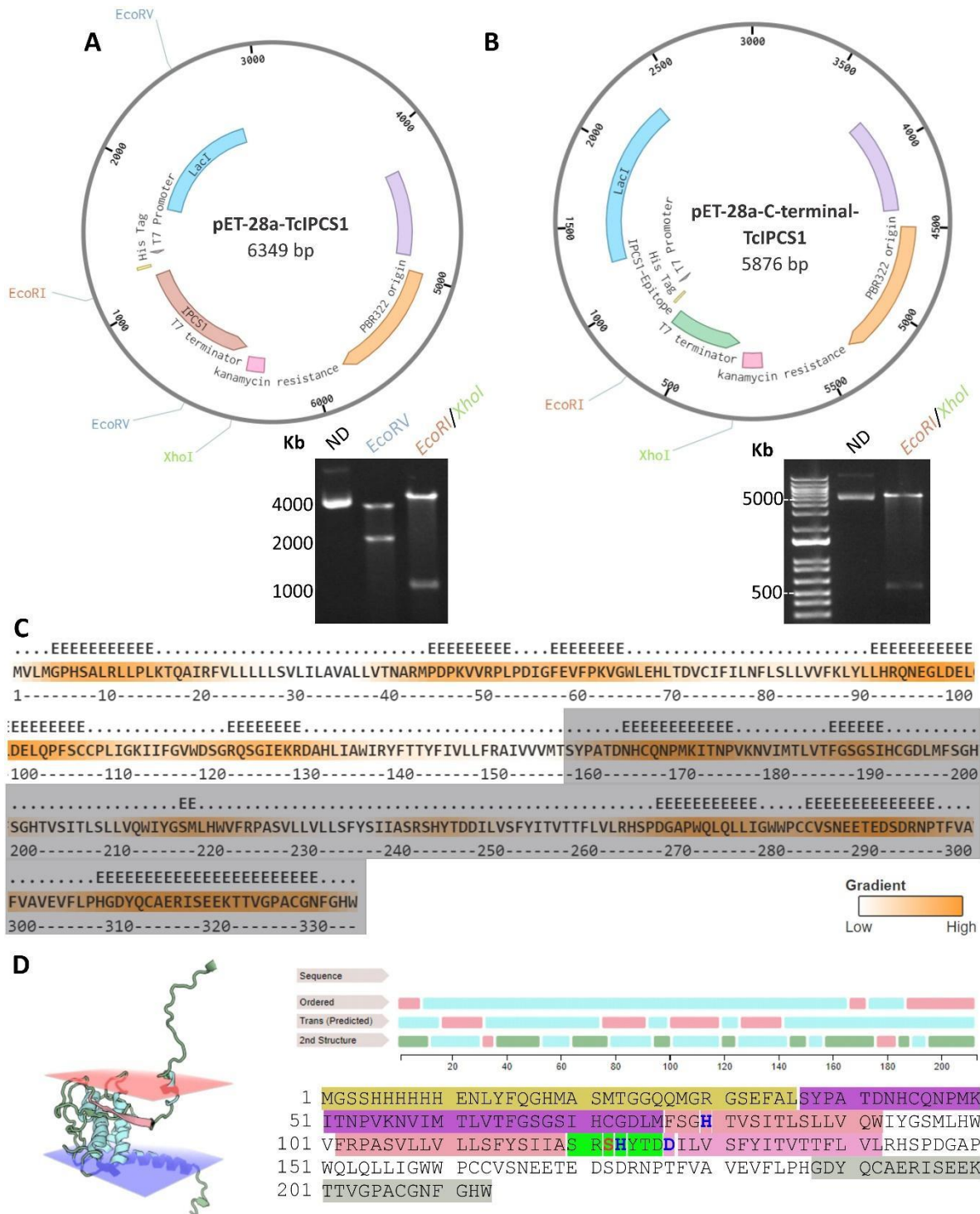


Figure 13. pET28a-TcIPCS1 and pET28a-C-terminal-TcIPCS1 vector construction and *in silico* analysis of the expected rC-terminal-TcIPCS1. A, B. (On top) Schematic representation of the pET28a-TcIPCS and pET28a-C-terminal-TcIPCS vectors. (Bottom part) Restriction mapping of each plasmid to verify the integrity of the constructions. Plasmid DNAs were digested with either *EcoRV* or *EcoRI/XhoI* and analyzed on 1% agarose gel electrophoresis. Restriction enzyme cutting sites are illustrated in the vector diagrams. ND: non-digested plasmid DNA. C. B-cell epitope prediction performed by BepiPred-2.0 for the amino acid (aa) of TcIPCS1. The orange gradient

shows the epitope score of each aa. E letters over the protein sequence represent positions above the epitope threshold set at 0.5. Gray shaded sequence exhibits the selected TcIPCS C-terminal fraction to be heterologous expressed. **D.** (On the left) Best *de novo* constructed 3D model of the His-tagged rC-terminal-TcIPCS1, according to the energy function of CNS. To see the five predicted models with their information access to <http://predmp.com:3001/#/detail/1906232205079>. The color palette illustrates the 3-state secondary structure prediction. Light blue: α -helix; pink: β -strand; green: coil. (On the upper right) Summary of the topology prediction results. The first row shows ordered (light blue) and disordered regions (pink). The second row shows transmembrane domains (pink). The third row shows the secondary structure, as described above. (On the bottom right) The amino acid sequence of the r-C-terminal TcIPCS1. The exact position of the translated pET28a sequence, each TMD, loop b, loop c, and C-terminal region, are indicated in golden, pink, purple, green, and grey, respectively. Blue letters indicate the catalytic triad.

After establishing the induction conditions, the protein was expressed in a larger scale, and lysing conditions were analyzed as they have been shown to affect protein yield and solubility (Miskiewicz and Macphee 2019; Peach et al. 2015). After evaluating cell lysis by high-pressure homogenization and sonication in phosphate lysis buffer (PLB) (see methodology details in item 3.14), we achieved better results with the sonication method (Figure 14D). The whole lysed derived from 250 mL of cultures that were induced for 16 h with IPTG (0.5mM) was centrifuged to separate soluble and insoluble fractions. After analyzing the fractions by SDS-PAGE, we observed that the protein was present in the insoluble fraction (Figure 14E). To address this issue, we evaluated different buffers, finally achieving solubilization of the protein extract by using the solubilization buffer (SB) proposed by Schlager and collaborators (2012) (Figure 12F). Since SB buffer contains 1% SDS, which interferes with the His-tagged protein interaction with the NI columns, it was removed before application into the affinity chromatography system (see item 3.14 for details). Finally, the rC-terminal-TcIPCS1 was mainly eluted in fractions 19 to 21 that accounted for 1.14 mg of purified protein (Figure 12G). This purified extract will be used to immunize mice for the generation of anti-TcIPCS polyclonal antisera.

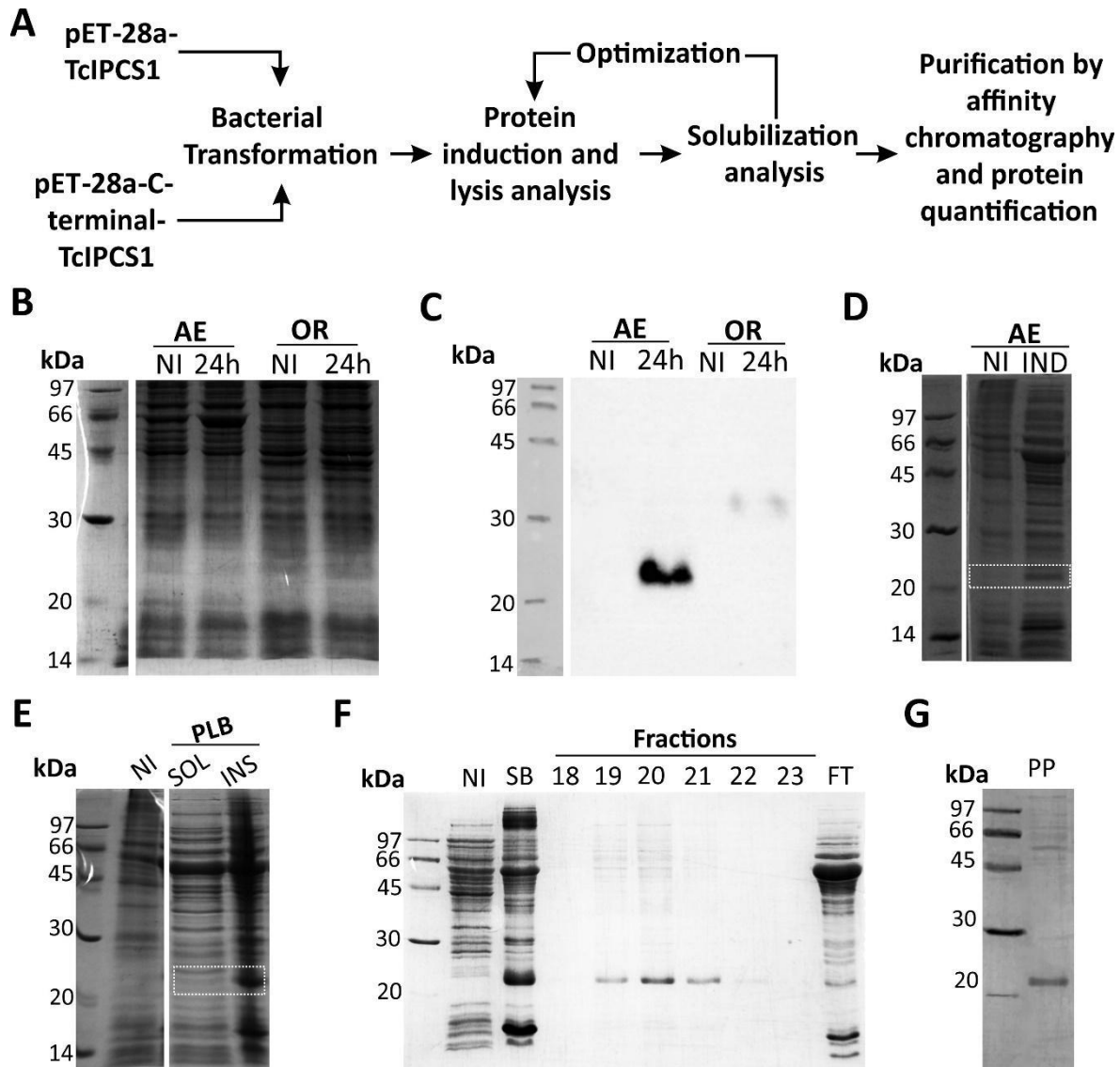


Figure 14. Heterologous expression of rTcIPCS1 (38.68 kDa) and rC-terminal-TcIPCS1 (23.87 kDa), and purification by affinity chromatography. **A.** Schematic workflow of the methodology followed to generate purified recombinant protein extracts. **B, C.** *rC-terminal-TcIPCS1* induction was only achieved in ArcticExpress (DE3) (AE). AE and Origami2 (DE3) (OR) cells were transformed with pET28a-C-terminal-TcIPCS1, induced for 24 h at 10 °C, lysed in Laemmli buffer, syringed to shred genomic DNA, and analyzed either by 12.5% SDS-PAGE stained with coomassie blue or by western blot using a monoclonal anti-His antibody (Invitrogen). **D.** Cell lysis standardization. AE cultures were induced and lysed by sonication in phosphate lysis buffer (PLB). A clear band corresponding to the rC-terminal-TcIPCS1 was distinguished only in the induced (IND) protein extract (dotted square). **E.** Induced protein extract was centrifuged to separate the soluble (SOL) and insoluble (INS) fractions. rC-terminal-TcIPCS1 was located in the insoluble fraction. **F.** Standardization of solubility conditions and purification by affinity chromatography. Solubilization of the rC-terminal-TcIPCS1 was achieved by resuspension of the INS fraction in a solubilization buffer (SB) proposed by Schlager et al.(2012). After SDS removal (see item 3.14), the solubilized extract was purified by affinity chromatography using His-Trap columns and the ÄKTA prime system (GE Healthcare, USA). Fractions 19, 20, and 21 show the elution of the purified rC-terminal-TcIPCS1 protein. FT: flowthrough. **G.** rC-terminal-TcIPCS1 purified protein extract (PP). Mixed fractions 19, 20 and 21 accounted for 1.14 mg of purified protein. Unless stated differently, all protein extracts were separated in 12.5% SDS-PAGE and stained with coomassie blue. NI = Non-induced.

4.7 Determination of inhibitory concentrations (IC₅₀) of tamoxifen and benzazepanes for *TcIPCS* KO and wild type epimastigotes

Since the identification of the different SLS orthologues on fungi and the neglected kinetoplastid parasites, extensive efforts have been made for the identification of specific inhibitors that could be used to treat these organisms (Aoyagi et al. 2007; Mandala et al. 1997; Norcliffe et al. 2018; Ohnuki et al. 2009; Sugimoto, Sakoh, and Yamada 2004; Trinconi et al. 2018). In particular, for the kinetoplastids, an IPCS complementary assay established in yeast has been the commonly used strategy to perform these screenings (e.g., Norcliffe et al. 2018). Unfortunately, the *T. cruzi* enzyme was not able to complement the yeast enzyme (Cardoso et al. 2013); hence, it is impossible to use this model for *T. cruzi*. Thus, one of our main reasons to develop the genetically modified parasites (i.e., *TcIPCS* KO and OE clones), was to produce valid models that can be used to identify TcIPCS specific inhibitors in different cell screening platforms.

As indicated in the Introduction (item 1.7), the *Leishmania* IPCS orthologue was subject of yeast-based HTS that led to the identification and refining of the benzazepanes, as potent anti-*IPCS* compounds (Norcliffe et al. 2018). Moreover, a known estrogen receptor antagonist used in the treatment of breast cancer, denominated Tamoxifen (TAM), was also recently identified as a specific inhibitor of the *Leishmania* IPCS enzyme (Trinconi et al. 2018) (see item 3.18 and Table 3 for more details of the compounds). As the *Leishmania* enzyme presents topology conservation and 70% of similarity (Figure 8), it could be possible that these drugs also present anti-TcIPCS activity. Therefore, we established a sensitivity analysis using resazurin as an indicator of cell viability to evaluate these drugs (Figure 15A).

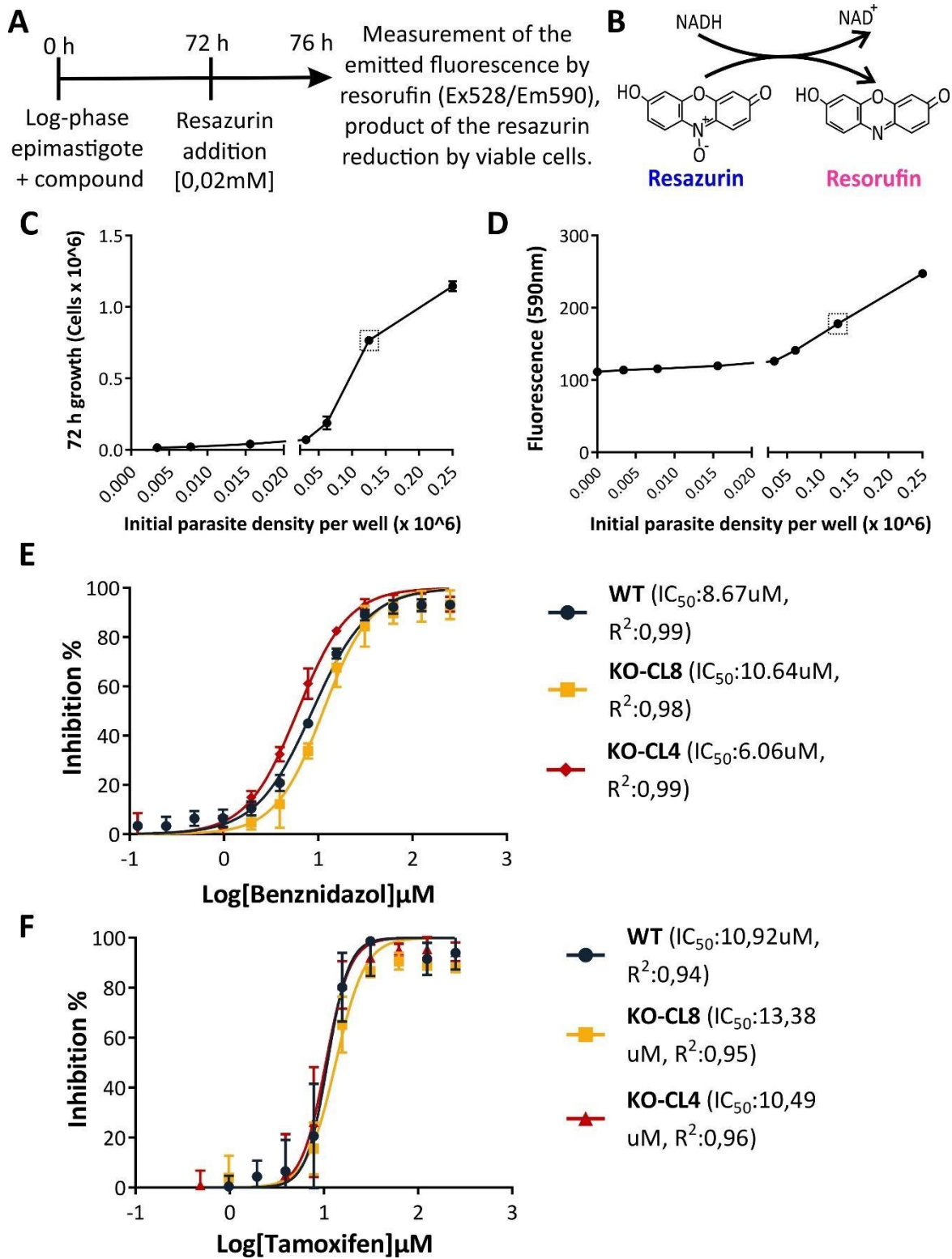


Figure 15. Establishment of a resazurin cell viability assay to evaluate *TcIPCS* KO epimastigote sensitivity to potential *TcIPCS* inhibitory molecules. **A.** Diagrammatic representation of the standardized resazurin reduction cell viability assay. **B.** Structure of resazurin substrate and the fluorescent resorufin product resulting from its reduction in metabolically active viable parasites. **C, D.** Determination of initial parasite density for the viability assay. Log-phase wild type (WT) CL Brener epimastigotes were cultured at different initial densities for 72 h, and growth was determined by the resazurin assay or by direct counting in a Neubauer chamber. An initial parasite density of 0.125 x

10^6 parasites/well was selected for assays with compounds. **E.** Validation of the established resazurin cell viability assay with the known anti-*T. cruzi* benznidazole (BZ). The half-maximal inhibitory concentration (IC_{50}) of BZ (twelve 2-fold serial dilutions from 250 μ M top concentration) against WT, *TcIPCS* KO CL4, and CL8 was calculated using GraphPad Prism 7 (log (inhibitor) vs. normalized response - Variable slope). Values are from at least three independent replicates. Error bars represent standard deviation (not visible were very small). Each concentration was normalized against the respective vehicle (DMSO) concentration. **F.** The activity of tamoxifen (TAM) against WT and *TcIPCS* KO CL4 and CL8 epimastigotes. IC_{50} of TAM (ten 2-fold serial dilutions from 250 μ M top concentration) was calculated as above.

Resazurin is a cell-permeable redox indicator that is commonly used to monitor viable cell number by its addition to the culture (Riss et al. 2013). The assay relies on the resazurin reduction by the metabolically active cells into resorufin, a pink fluorescent product (Figure 15B). Thus, the quantity of resorufin produced is proportional to the number of viable cells that can be quantified using a fluorometer equipped with the right filter set (for more details, see item 3.19). Due to its simplicity and high sensitivity, numerous reports are using this assay for different screening applications (e.g., Norcliffe et al. 2018; Shum et al. 2008).

Because these assays must be standardized for each type of cell, cell density per well, culture medium, and other conditions, before evaluating the drugs we established the experimental parameters of the assay. Resazurin working solution (2.5 mM) and incubation time (4 h at 28°C) were chosen according to the results previously obtained by Rolón and co-workers in the standardization of a resazurin microtiter assay using the *T. cruzi* Y strain (Rolón et al. 2006). The initial parasite density and incubation time before resazurin addition were tested by seeding different inocula of log-phase WT epimastigote culture ranging from 0.039 to 0.25 x 10^6 /well in 96-well plates, incubated them for 72 or 96 h at 28 °C and calculated the parasite density by direct counting or by the resazurin reduction assay (Figure 15C, D; data for 96 h of incubation is not shown). Since similar growth curves were obtained with both methods, because the resazurin assay is much faster and can be done with large numbers of samples we decided to use it instead of direct counting. To select the initial parasite density for drug testing, we chose a density at which the parasite showed growth with a steeper slope because it guarantees that the parasite will maintain its logarithmic growth rate during the incubation time.

To test our method, we determined, in WT epimastigotes, the half-maximal inhibitory concentration (IC_{50}) of the most commonly used drug to treat CD, the benznidazole (BZ). Figure 15E showed a dose-response assay with 12 BZ concentrations between 0.12 μ M and 250 μ M, which resulted in an IC_{50} similar to the previously published (Luna et al., 2009). We also evaluated

the effect of BZ in the *TcIPCS* KO, obtaining the same results as with WT parasites, suggesting that the BZ action mechanism is independent of the metabolic processes regulated by the IPC synthase.

Table 3 shows all the compounds with a potential anti-TcIPCS activity we evaluated. It has been suggested that Tamoxifen (TAM), which has proven anti-*Leishmania* IPCS activity (Trinconi et al., 2018), acts on the enzymes involved with *T. cruzi*'s sphingolipid pathway, since an increased level of CER was observed after TAM treatment, triggering an apoptotic-like cell death (Landoni et al. 2019). We evaluated TAM concentrations between 0.48 μM and 250 μM , in WT and *TcIPCS* KO parasites (Figure 15F). The dose-response assay resulted in an IC_{50} of 10.92 μM for WT epimastigotes, similar to the values published in the literature (Landoni et al. 2019; Miguel et al., 2010). The KO clones showed IC_{50} s similar to what was obtained with the WT parasites (KO-CL4: 10.49 μM , KO-CL8: 13.38 μM), showing that TAM has no specific inhibitory effect on the *T. cruzi* IPC synthase activity. Besides the CER increased levels, Landoni and co-workers (2019) also reported a ten times increase of IPC concentration after TAM treatment. Such an increase would indicate a greater susceptibility of the KO clones to the drug, which neither was the case. Altogether, results suggest that, although *T. cruzi* activates its SL biosynthetic pathway after TAM treatment, *TcIPCS* deletion does not sensitize the parasite to the drug. Therefore, the existence of additional endpoints of the SL pathway that are rescuing the TcIPCS absence in the KO parasites is a reasonable possibility.

We also evaluated various benzazepanes (compounds 2, 7, and 7a) that have common scaffolds with few chemical modifications and were proven to be specific to the *Leishmania* enzyme in a biochemical *in vitro* assay (Norcliffe et al. 2018) (Figure 16A-D). Furthermore, molecule 7 was also evaluated against WT and *lcb2* *L. major* mutant, showing selectivity for the WT over the mutant. As *lcb2* deletion causes a lack of serine palmitoyltransferase activity, which is the first enzyme of the SL pathway, such effect was interpreted as a redundant anti-*LmjFIPCS* because of the substrate absence. Compound 7a presents a slight modification that confers higher solubility and stability than compound 7. The dose-response curves assayed against WT parasites resulted in an IC_{50} of 34 μM for compound 2, which is much higher than the IC_{50} of 2 μM found against *L. donovani* infected THP-1 macrophages. The IC_{50} obtained for *TcIPCS* KO *T. cruzi* did not present an evident selectivity (KO-CL4: 39.13 μM , KO-CL8: 52.9 μM). Similar results were obtained with compound 7a, which displayed a WT IC_{50} of 19.5 μM and KO IC_{50} of 18.87 and

22.2 for KO-CL4 and KO-CL8, respectively. IC₅₀ for compound 7, which showed selectivity for the WT *L. major* (IC₅₀ of 3.1 μM) over the *lcb2* mutant (IC₅₀ >10 μM), was only slightly different when *T. cruzi*, WT and *TcIPCS* KO clones were tested (IC₅₀: KO-CL4: 23.97 μM, KO-CL8: 31.3 μM compared to WT parasites IC₅₀ of 48.01 μM).

In summary, benzazepanes showed low anti-*T. cruzi* activity up to 7.81 μM, which rapidly increased their growth inhibitory effects from 15.62 μM onwards. Moreover, none of these compounds exhibited an evident anti-TcIPCS activity, as KO clones displayed either similar or greater susceptibility to the benzazepanes when compared with WT parasites. Nevertheless, the *TcIPCS* KO higher sensibility to compound 7 may be related to an effect directed for the SL biosynthesis, probably affecting the metabolic processes previous to the action of the IPC synthase. Such a hypothesis is in line with the resistant phenotype displayed by the *lcb2* *L. major* mutant reported by Norcliffe and co-workers (2018), as these parasites lack serine palmitoyltransferase activity, which absence is expected to impair the whole pathway due to substrate unavailability. Indeed, *in vitro* infection tests could be the best assay to evaluate TAM and benzazepanes anti-*TcIPCS* effect. However, as the epimastigote form was evidenced to be the phase with higher activity (Figueiredo et al. 2005), it was expected to be the form that would be more impacted by any anti-TcIPCS compounds. Moreover, although sensibility can dramatically vary between forms, the moderate micro molar anti-*T. cruzi* epimastigote activity, showed mainly by the benzazepanes, suggests an effect not much different if assayed in a platform with the other parasite forms (i. e., metacyclic trypomastigotes, TCTs or amastigotes).

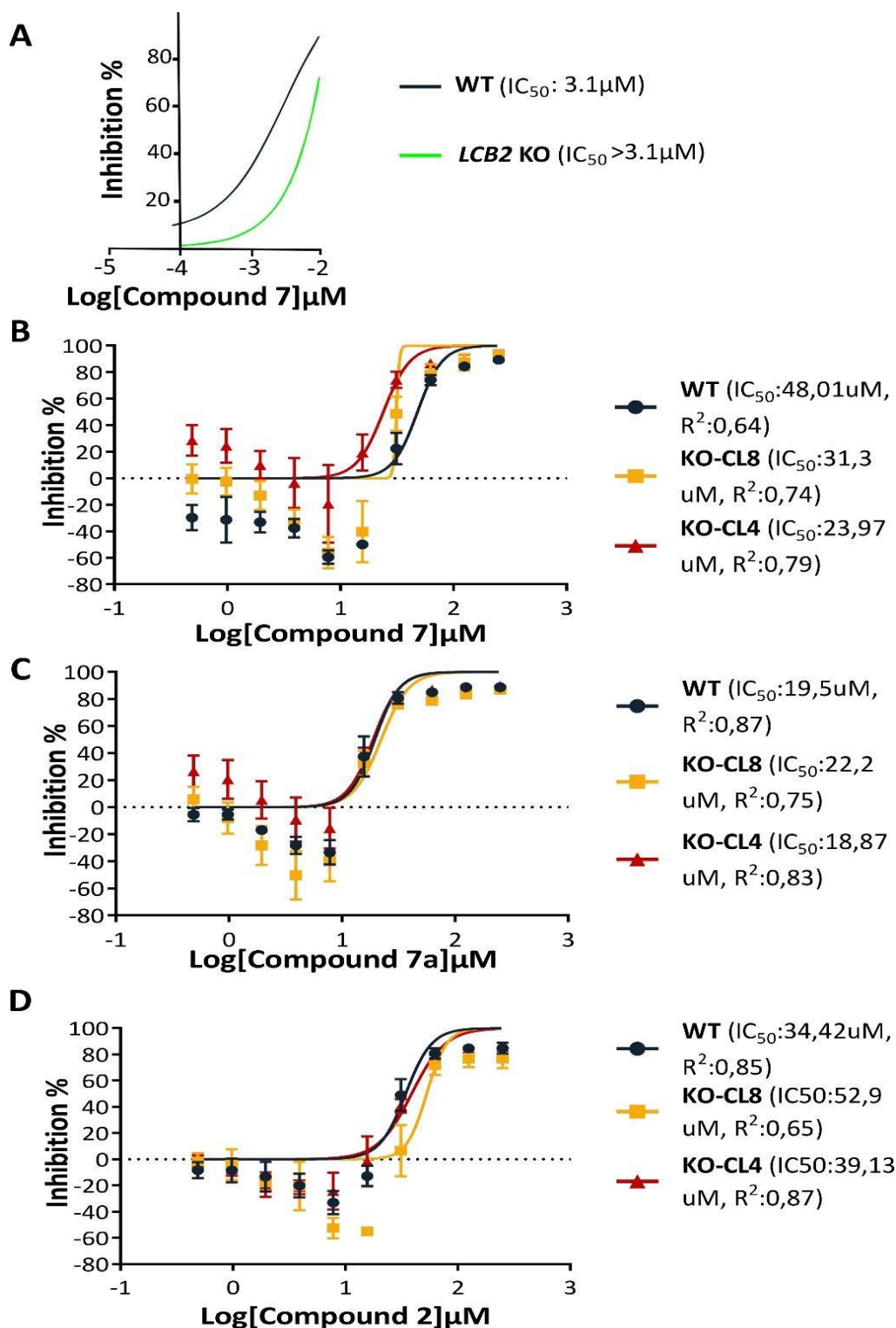


Figure 16. Effect of benzazepanes against wild type and *TcIPCS* KO epimastigotes. A. The activity of compound 7 against wild type *Leishmania major* and *lcb2* KO parasites. Values are from at least 3 independent experiments. Taken from Norcliffe et al. (2018). **B, C, D.** Activity of compound 7 (**B**), compound 7a (**C**), and compound 2 (**D**) against wild type *T. cruzi* CL Brener and *TcIPCS* KO CL4 and CL8. The Half-maximal inhibitory concentration (IC_{50}) of each compound (ten 2-fold serial dilutions from 250 μM top concentration) was calculated using GraphPad Prism 7

(log (inhibitor) vs. normalized response - Variable slope). Values are from at least three independent replicates. Error bars represent standard deviation (not visible were very small). Each concentration was normalized against the respective vehicle (DMSO) concentration.

5. Concluding Remarks and Perspectives

The fact that nowadays there is still no effective treatment against Chagas disease demonstrates the metabolic complexity of *Trypanosoma cruzi* and the host-pathogen interplay during the disease development. Moreover, it also proves the necessity to tackle the disease from innovative perspectives, apart from the traditional ones which a long time ago have been repeatedly proven to be wrong. The unexpected complexity of the bioactive SLs and the pivotal roles they play in most of the major biological responses, make SL metabolism a highly promising pathway for drug intervention. In this study, we molecularly characterize TcIPCS, the only known end-point of the SL biosynthetic pathway of *T. cruzi*. Although our results indicated that this enzyme is not essential, we should not discard TcIPCS as a possible target for drug discovery, since the phenotypic characterizations of the *TcIPCS* null mutants strongly suggested a crucial role of the protein for the successful establishment of infection. In brief, our data demonstrated a direct impact of the TcIPCS in the metacyclogenesis process, as it was considerably impaired or stimulated depending on the absence or overexpression of the protein. Furthermore, *in vitro* infections showed not only a general impairment of the cycle of infection (i.e., cell infection, amastigote intracellular proliferation and TCT differentiation and release) but also demonstrated the stimulation of extracellular amastigote differentiation, a particular phenotype caused by the *TcIPCS* deletion, which certainly affected the parasite fitness. It is important to note that these infection assays are performed in ideal conditions that eliminate the role of the host immune response and the parasite defense mechanisms, which may also be affected by the *TcIPCS* deletion. Therefore, the TcIPCS null mutants may be unable to establish infection *in vivo*; hence, TcIPCS is still a valid target of study for the development of alternative anti-trypanosomal therapies. On the other hand, regarding the evaluation of the *Leishmania* IPCS inhibitors, tamoxifen, and benzazepanes, results exposed the clear evolutionary divergence between both parasites and their enzymes. Making evident the fact that anti-*Leishmania* does not necessarily mean anti-*Trypanosoma*.

Our future perspectives for a comprehensive characterization of the *TcIPCS* protein includes the evaluation of the *TcIPCS* KO capacity to successfully establish *in vivo* infections and the evaluation of the sphingolipidomics of the genetically modified parasites, with emphasis on the GPI anchors. Such infections will commence soon, and lipid extracts from the *TcIPCS* KO and WT

parasite forms (i.e., epimastigotes, TCTs and amastigotes) are currently under evaluation by liquid chromatography and mass spectrometry. Moreover, mice immunizations will also commence soon, in order to produce polyclonal antiserum for various applications, including the evaluation of the protein expression pattern.

If the *in vivo* infections corroborate the validity of the TcIPCS as a promising target for drug development, we are planning to establish an HTS platform to assay compound libraries aiming to identify anti-TcIPCS molecules. Due to the enzyme properties, a miniaturized yeast-based system would be a tractable strategy to develop the assay; nevertheless, Cardoso and co-workers showed that TcIPCS is not able to complement an auxotrophic *Saccharomyces cerevisiae* mutant (Cardoso et al. 2013). Another exciting possibility may be *in vitro* TcIPCS directed screening using a biochemical assay established with purified soluble protein. According to our results, the heterologous expression of an active TcIPCS in bacteria or eukaryotic model may not be an easy task. Thus, in collaboration with the post-doctoral fellow Gabriela Burle, from Durham University, we are devising to express the protein in a cell-free synthesis approach followed by the establishment of a biochemical assay platform adapted to HTS as previously published by Mina and co-workers (2011). One of the limitations of this kind of assays is the lack of cellular context, which we will overcome by the subsequent test of the identified hits in the established cell viability resazurin assay.

6. Bibliography

- Acevedo, Gonzalo R., Magalí C. Girard, and Karina A. Gómez. 2018. “The Unsolved Jigsaw Puzzle of the Immune Response in Chagas Disease.” *Frontiers in Immunology* 9 (August): 1929. <https://doi.org/10.3389/fimmu.2018.01929>.
- Agusti, Rosalía, Alicia S. Couto, Oscar E. Campetella, Alberto C.C. Frasch, and Rosa M. De Lederkremer. 1997. “The Trans-sialidase of *Trypanosoma cruzi* Is Anchored by Two Different Lipids.” *Glycobiology* 7 (6): 731–35. <https://doi.org/10.1093/glycob/7.6.731>.
- Agusti, Rosalía, Alicia S. Couto, Oscar Campetella, Alberto C.C. Frasch, and Rosa M. De Lederkremer. 1998. “Structure of the Glycosylphosphatidylinositol-Anchor of the Trans-Sialidase from *Trypanosoma cruzi* Metacyclic Trypomastigote Forms.” *Molecular and Biochemical Parasitology* 97 (1–2): 123–31. [https://doi.org/10.1016/S0166-6851\(98\)00137-6](https://doi.org/10.1016/S0166-6851(98)00137-6).
- Andrews, N W, E S Robbins, V Ley, K S Hong, and V Nussenzweig. 1988. “Developmentally Regulated, Phospholipase C-Mediated Release of the Major Surface Glycoprotein of Amastigotes of *Trypanosoma cruzi*.” *Journal of Experimental Medicine* 167 (February): 300–314.
- Andrews, Norma W., and Michael B. Whitlow. 1989. “Secretion by *Trypanosoma cruzi* of a Hemolysin Active at Low PH.” *Molecular and Biochemical Parasitology* 33 (3): 249–56. [https://doi.org/10.1016/0166-6851\(89\)90086-8](https://doi.org/10.1016/0166-6851(89)90086-8).
- Andrews, Norma W, Kyong-su Hong, Edith S Robbins, and Victor Nussenzweig. 1987. “Stage-Specific Surface Antigens Expressed during the Morphogenesis of Vertebrate Forms of *Trypanosoma cruzi*.” *Experimental Parasitology* 64: 474–84.
- Aoyagi, Azusa, Tatsuya Yano, Shiho Kozuma, and Toshio Takatsu. 2007. “Pleofungins, Novel Inositol Phosphorylceramide Synthase Inhibitors, from Phoma Sp. SANK 13899 II. Structural Elucidation.” *Journal of Antibiotics* 60 (2): 143–52. <https://doi.org/10.1038/ja.2007.14>.
- Argibay, P. F. 2002. “*Trypanosoma Cruzi* Surface Mucin TcMuc-E2 Expressed on Higher Eukaryotic Cells Induces Human T Cell Anergy, Which Is Reversible.” *Glycobiology* 12 (1): 25–32. <https://doi.org/10.1093/glycob/12.1.25>.
- Barros, Helena C., Newton V. Verbisck, Solange Da Silva, Marcia F. Araguth, and Renato A. Mortara. 1997. “Distribution of Epitopes of *Trypanosoma Cruzi* Amastigotes during the Intracellular Life Cycle within Mammalian Cells.” *Journal of Eukaryotic Microbiology* 44 (4): 332–44.

<https://doi.org/10.1111/j.1550-7408.1997.tb05675.x>.

- Belew, A. Trey, Caroline Junqueira, Gabriela F. Rodrigues-Luiz, Bruna M. Valente, Antonio Edson R. Oliveira, Rafael B. Polidoro, Luciana W. Zuccherato, et al. 2017. “Comparative Transcriptome Profiling of Virulent and Non-Virulent *Trypanosoma Cruzi* Underlines the Role of Surface Proteins during Infection.” *PLoS Pathogens* 13 (12): 1–23. <https://doi.org/10.1371/journal.ppat.1006767>.
- Beneke, Tom, Ross Madden, Laura Makin, Jessica Valli, Jack Sunter, and Eva Gluenz. 2017. “A CRISPR Cas9 High-Throughput Genome Editing Toolkit for Kinetoplastids.” *Royal Society Open Science* 4 (5): 1–16. <https://doi.org/10.1098/rsos.170095>.
- Berridge, Michael J. 1987. “Inositol Trisphosphate and Diacylglycerol: Two Interacting Second Messengers.” *Annual Review of Biochemistry* 56: 159–93.
- Bertello, L. E., M. F. Goncalvez, W. Colli, and R. M. De Lederkremer. 1995. “Structural Analysis of Inositol Phospholipids from *Trypanosoma Cruzi* Epimastigote Forms.” *Biochemical Journal* 310 (1): 255–61. <https://doi.org/10.1042/bj3100255>.
- Bertello, Laura E., Norma W. Andrews, and Rosa M. De Lederkremer. 1996. “Developmentally Regulated Expression of Ceramide in *Trypanosoma Cruzi*.” *Molecular and Biochemical Parasitology* 79 (2): 143–51. [https://doi.org/10.1016/0166-6851\(96\)02645-X](https://doi.org/10.1016/0166-6851(96)02645-X).
- Bhat, Basharat, Nazir A. Ganai, Syed Mudasir Andrabi, Riaz A. Shah, and Ashutosh Singh. 2017. “TM-Aligner: Multiple Sequence Alignment Tool for Transmembrane Proteins with Reduced Time and Improved Accuracy.” *Scientific Reports* 7 (1): 1–8. <https://doi.org/10.1038/s41598-017-13083-y>.
- Bonfim-Melo, Alexis, Eden R. Ferreira, Pilar T.V. Florentino, and Renato A. Mortara. 2018. “Amastigote Synapse: The Tricks of *Trypanosoma Cruzi* Extracellular Amastigotes.” *Frontiers in Microbiology* 9 (JUN): 1–7. <https://doi.org/10.3389/fmicb.2018.01341>.
- Brünger, Axel T., Paul D. Adams, G. Marius Clore, Warren L. Delano, Piet Gros, Ralf W. Grosse-Kunstleve, Jian Sheng Jiang, et al. 1998. “Crystallography & NMR System: A New Software Suite for Macromolecular Structure Determination.” *Acta Crystallographica Section D: Biological Crystallography* 54 (5): 905–21. <https://doi.org/10.1107/S0907444998003254>.
- Burle-Caldas, Gabriela Assis, Viviane Grazielle-Silva, Melissa Soares-Simões, Gabriela Schumann Burkard, Isabel Roditi, Wanderson Duarte DaRocha, and Santuza M. Teixeira. 2017. “Editing the *Trypanosoma Cruzi* Genome with Zinc Finger Nucleases.” *Molecular and Biochemical Parasitology* 212: 28–32. <https://doi.org/10.1016/j.molbiopara.2017.01.002>.

- Burle-Caldas, Gabriela Assis, Melissa Soares-Simões, Laiane Lemos-Pechnicki, Wanderson Duarte DaRocha, and Santuza M.R. Teixeira. 2018. "Assessment of Two CRISPR-Cas9 Genome Editing Protocols for Rapid Generation of *Trypanosoma cruzi* Gene Knockout Mutants." *International Journal for Parasitology* 48 (8): 591–96. <https://doi.org/10.1016/j.ijpara.2018.02.002>.
- Buscaglia, Carlos A., Vanina A. Campo, Alberto C.C. Frasch, and Javier M. Di Noia. 2006. "*Trypanosoma cruzi* Surface Mucins: Host-Dependent Coat Diversity." *Nature Reviews. Microbiology* 4 (3): 229–36. <https://doi.org/10.1038/nrmicro1351>.
- Cámara, María de los Milagros, Virginia Balouz, Camila Centeno Cameán, Carmen R. Cori, Gustavo A. Kashiwagi, Santiago A. Gil, Natalia Paula Macchiaverna, et al. 2019. "*Trypanosoma cruzi* Surface Mucins Are Involved in the Attachment to the *Triatoma infestans* Rectal Ampoule." *PLoS Neglected Tropical Diseases* 13 (5): 1–23. <https://doi.org/10.1371/journal.pntd.0007418>.
- Camargo, Ep. 1964. "Growth and Differentiation in *Trypanosoma cruzi*. I. Origin of Metacyclic Trypanosomes in Liquid Media." *Rev Inst Med São Paulo* 6 (3): 93-100.
- Cardoso, Mariana S., Caroline Junqueira, Ricardo C. Trigueiro, Hosam Shams-Eldin, Cristiana S. Macedo, Patrícia R. Araújo, Dawidson A. Gomes, et al. 2013. "Identification and Functional Analysis of *Trypanosoma cruzi* Genes That Encode Proteins of the Glycosylphosphatidylinositol Biosynthetic Pathway." *PLoS Neglected Tropical Diseases* 7 (8). <https://doi.org/10.1371/journal.pntd.0002369>.
- Costa, Fernanda Cristina, Amanda Fortes Francisco, Shiromani Jayawardhana, Simone Guedes Calderano, Michael D. Lewis, Francisco Olmo, Tom Beneke, et al. 2018. "Expanding the Toolbox for *Trypanosoma cruzi*: A Parasite Line Incorporating a Bioluminescence-Fluorescence Dual Reporter and Streamlined CRISPR/Cas9 Functionality for Rapid in Vivo Localisation and Phenotyping." *PLoS Neglected Tropical Diseases* 12 (4): 1–21. <https://doi.org/10.1371/journal.pntd.0006388>.
- Couto, Alicia S., R M De Lederkremer, Walter Collo, M. Julia M. Alves. 1993. "The Glycosylphosphatidylinositol Anchor of the Trypomastigote-Specific Tc-85 Glycoprotein from *Trypanosoma cruzi*" *European Journal of Biochemistry*, 217, 597–602.
- Cuvillier, Olivier. 2002. "Sphingosine in Apoptosis Signaling." *Biochimica et Biophysica Acta - Molecular and Cell Biology of Lipids* 1585 (2–3): 153–62. [https://doi.org/10.1016/S1388-1981\(02\)00336-0](https://doi.org/10.1016/S1388-1981(02)00336-0).
- DaRocha, Wanderson D., Rosiane A. Silva, Daniella C. Bartholomeu, Simone F. Pires, Jorge M. Freitas, Andrea M. Macedo, Martin P. Vazquez, Mariano J. Levin, and Santuza M.R. Teixeira. 2004. "Expression of Exogenous Genes in *Trypanosoma cruzi*: Improving Vectors and Electroporation

- Protocols.” *Parasitology Research* 92 (2): 113–20. <https://doi.org/10.1007/s00436-003-1004-5>.
- Denny, Paul W., Hosam Shams-Eldin, Helen P. Price, Deborah F. Smith, and Ralph T. Schwarz. 2006. “The Protozoan Inositol Phosphorylceramide Synthase: A Novel Drug Target That Defines a New Class of Sphingolipid Synthase.” *Journal of Biological Chemistry* 281 (38): 28200–209. <https://doi.org/10.1074/jbc.M600796200>.
- DosReis, George A., Lígia M.T. Peçanha, Maria Bellio, José O. Previato, and Lúcia Mendonça-Previato. 2002. “Glycoinositol Phospholipids from *Trypanosoma cruzi* Transmit Signals to the Cells of the Host Immune System through Both Ceramide and Glycan Chains.” *Microbes and Infection* 4 (9): 1007–13. [https://doi.org/10.1016/S1286-4579\(02\)01616-7](https://doi.org/10.1016/S1286-4579(02)01616-7).
- El-sayed, Najib M, Peter J Myler, Daniella C Bartholomeu, Daniel Nilsson, Gautam Aggarwal, Scott J Westenberger, Anh-nhi Tran, et al. 2005. “The Genome Sequence of *Trypanosoma cruzi* , Etiologic Agent of Chagas Disease.” *Science* 309: 409–15.
- Engels, Dirk, and Lorenzo Savioli. 2006. “Reconsidering the Underestimated Burden Caused by Neglected Tropical Diseases.” *Trends in Parasitology* 22 (8): 363–66. <https://doi.org/10.1016/j.pt.2006.06.004>.
- Fernandes, Adriana B., and Renato A. Mortara. 2004. “Invasion of MDCK Epithelial Cells with Altered Expression of Rho GTPases by *Trypanosoma cruzi* Amastigotes and Metacyclic Trypomastigotes of Strains from the Two Major Phylogenetic Lineages.” *Microbes and Infection* 6 (5): 460–67. <https://doi.org/10.1016/j.micinf.2004.01.009>.
- Fernandes, Maria Cecilia, and Norma W. Andrews. 2012. “Host Cell Invasion by *Trypanosoma cruzi*: A Unique Strategy That Promotes Persistence.” *FEMS Microbiology Reviews* 36 (3): 734–47. <https://doi.org/10.1111/j.1574-6976.2012.00333.x>.
- Ferreira, Éden R., Alexis Bonfim-Melo, Renato A. Mortara, and Diana Bahia. 2012. “*Trypanosoma cruzi* Extracellular Amastigotes and Host Cell Signaling: More Pieces to the Puzzle.” *Frontiers in Immunology* 3 (NOV): 1–6. <https://doi.org/10.3389/fimmu.2012.00363>.
- Figueiredo, Juliana M., Wagner B. Dias, Lucia Mendonça-Previato, José O. Previato, and Norton Heise. 2005. “Characterization of the Inositol Phosphorylceramide Synthase Activity from *Trypanosoma cruzi*.” *Biochemical Journal* 387 (2): 519–29. <https://doi.org/10.1042/BJ20041842>.
- Florentino, Pilar T.V., Fernando Real, Cristina M. Orikaza, Julia P.C. da Cunha, Francisca N.L. Vitorino, Esteban M. Cordero, Tiago J.P. Sobreira, and Renato A. Mortara. 2018. “A Carbohydrate Moiety of Secreted Stage-Specific Glycoprotein 4 Participates in Host Cell Invasion by *Trypanosoma cruzi*

- Extracellular Amastigotes.” *Frontiers in Microbiology* 9 (APR): 1–14. <https://doi.org/10.3389/fmicb.2018.00693>.
- Freire-de-Lima, Leonardo, Frederico Alisson-Silva, Sebastião T. Carvalho, Christina M. Takiya, Maurício M. Rodrigues, George A. DosReis, Lucia Mendonça-Previato, José O. Previato, and Adriane R. Todeschini. 2010. “*Trypanosoma cruzi* Subverts Host Cell Sialylation and May Compromise Antigen-Specific CD8⁺ T Cell Responses.” *Journal of Biological Chemistry* 285 (18): 13388–96. <https://doi.org/10.1074/jbc.M109.096305>.
- Gao, Wenda, Henry H. Wortis, and Miercio A. Pereira. 2002. “The *Trypanosoma cruzi* Trans-Sialidase Is a T Cell-Independent B Cell Mitogen and an Inducer of Non-Specific Ig Secretion.” *International Immunology* 14 (3): 299–308. <https://doi.org/10.1093/intimm/14.3.299>.
- Garg, N., M. Postan, K. Mensa-Wilmot, and R. L. Tarleton. 1997. “Glycosylphosphatidylinositols Are Required for the Development of *Trypanosoma cruzi* Amastigotes.” *Infection and Immunity* 65 (10): 4055–60.
- Gascon, Joaquim, Caryn Bern, and María-jesús Pinazo. 2010. “Chagas Disease in Spain, the United States and Other Non-Endemic Countries.” *Acta Tropica* 115: 22–27. <https://doi.org/10.1016/j.actatropica.2009.07.019>.
- Gazos-Lopes, Felipe, Jessica L. Martin, Peter C. Dumoulin, and Barbara A. Burleigh. 2017. “Host Triacylglycerols Shape the Lipidome of Intracellular Trypanosomes and Modulate Their Growth.” *PLoS Pathogens* 13 (12): 1–22. <https://doi.org/10.1371/journal.ppat.1006800>.
- Georgopapadakou, N. H. 2000. “Antifungals Targeted to Sphingolipid Synthesis: Focus on Inositol Phosphorylceramide Synthase.” *Expert Opinion on Investigational Drugs* 9 (8): 1787–96. <https://doi.org/10.1517/13543784.9.8.1787>.
- Goren, Michael A., Brian G. Fox, and James D. Bangs. 2011. “Amino Acid Determinants of Substrate Selectivity in the *Trypanosoma Brucei* Sphingolipid Synthase Family.” *Biochemistry* 50 (41): 8853–61. <https://doi.org/10.1021/bi200981a>.
- Guan, Xue Li, and Pascal Mäser. 2017. “Comparative Sphingolipidomics of Disease-Causing Trypanosomatids Reveal Unique Lifecycle- and Taxonomy-Specific Lipid Chemistries.” *Scientific Reports* 7 (1): 1–13. <https://doi.org/10.1038/s41598-017-13931-x>.
- Guhl, F. 2017. *Geographical Distribution of Chagas Disease. American Trypanosomiasis Chagas Disease: One Hundred Years of Research: Second Edition*. Second Edi. Elsevier Inc.

<https://doi.org/10.1016/B978-0-12-801029-7.00005-8>.

- Guther, M. L.S., M. L.C. De Almeida, N. Yoshida, and M. A.J. Ferguson. 1992. "Structural Studies on the Glycosylphosphatidylinositol Membrane Anchor of *Trypanosoma cruzi* 1G7-Antigen. The Structure of the Glycan Core." *Journal of Biological Chemistry* 267 (10): 6820–28.
- Hannun, Yusuf A., and Lina M. Obeid. 2018. "Sphingolipids and Their Metabolism in Physiology and Disease." *Nature Reviews Molecular Cell Biology* 19 (3): 175–91. <https://doi.org/10.1038/nrm.2017.107>.
- Heise, Norton, M. Lucia Cardoso de Almeida, and Michael A.J. Ferguson. 1995. "Characterization of the Lipid Moiety of the Glycosylphosphatidylinositol Anchor of *Trypanosoma cruzi* 1G7-Antigen." *Molecular and Biochemical Parasitology* 70 (1–2): 71–84. [https://doi.org/10.1016/0166-6851\(95\)00009-P](https://doi.org/10.1016/0166-6851(95)00009-P).
- Hernández-Corbacho, María José, Mohamed F. Salama, Daniel Canals, Can E. Senkal, and Lina M. Obeid. 2017. "Sphingolipids in Mitochondria." *Biochimica et Biophysica Acta - Molecular and Cell Biology of Lipids* 1862 (1): 56–68. <https://doi.org/10.1016/j.bbailip.2016.09.019>.
- Huitema, Klazien, Joep Van Den Dikkenberg, Jos F.H.M. Brouwers, and Joost C.M. Holthuis. 2004. "Identification of a Family of Animal Sphingomyelin Synthases." *EMBO Journal* 23 (1): 33–44. <https://doi.org/10.1038/sj.emboj.7600034>.
- Huwiler, Andrea, Thomas Kolter, Josef Pfeilschifter, and Konrad Sandhoff. 2000. "Physiology and Pathophysiology of Sphingolipid Metabolism and Signaling." *Biochimica et Biophysica Acta - Molecular and Cell Biology of Lipids* 1485 (2–3): 63–99. [https://doi.org/10.1016/S1388-1981\(00\)00042-1](https://doi.org/10.1016/S1388-1981(00)00042-1).
- Iida, Kyoko, Michael B Whitlow, and Victor Nussenzweig. 1989. "Amastigotes of *Trypanosoma cruzi* Escape Destruction by the Terminal Complement Components." *Journal of Experimental Medicine* 169 (March): 881–91.
- Irvine, Robin. 1996. "Taking Stock of PI-PLC." *Nature*. <https://doi.org/10.1038/380581a0>.
- Jackson, Yves, Angie Pinto, and Sarah Pett. 2014. "Chagas Disease in Australia and New Zealand : Risks and Needs for Public Health Interventions." *Tropical Medicine and International Health* 19 (2): 212–18. <https://doi.org/10.1111/tmi.12235>.
- Jespersen, Martin Closter, Bjoern Peters, Morten Nielsen, and Paolo Marcatili. 2017. "BepiPred-2.0: Improving Sequence-Based B-Cell Epitope Prediction Using Conformational Epitopes." *Nucleic*

- Acids Research* 45 (W1): W24–29. <https://doi.org/10.1093/nar/gkx346>.
- Knott, Gavin J., and Jennifer A. Doudna. 2018. “CRISPR-Cas Guides the Future of Genetic Engineering.” *Science* 361 (6405): 866–69. <https://doi.org/10.1126/science.aat5011>.
- Kol, Matthijs, Radhakrishnan Panatala, Mirjana Nordmann, Leoni Swart, Leonie Van Suijlekom, Birol Cabukusta, Angelika Hilderink, et al. 2017. “Switching Head Group Selectivity in Mammalian Sphingolipid Biosynthesis by Active-Site-Engineering of Sphingomyelin Synthases.” *Journal of Lipid Research* 58 (5): 962–73. <https://doi.org/10.1194/jlr.M076133>.
- Lanar, David E. 1979. “Growth and Differentiation of *Trypanosoma cruzi* Cultivated with a Triatoma Infestans Embryo Cell Line.” *The Journal of Protozoology* 26 (3): 457–62.
- Lander, Noelia, and Miguel A. Chiurillo. 2019. “State-of-the-Art CRISPR/Cas9 Technology for Genome Editing in Trypanosomatids.” *Journal of Eukaryotic Microbiology* 66 (6): 981–91. <https://doi.org/10.1111/jeu.12747>.
- Landoni, Malena, Tamara Piñero, Luciana L. Soprano, Facundo Garcia-Bournissen, Laura Fichera, Monica I. Esteva, Vilma G. Duschak, and Alicia S. Couto. 2019. “Tamoxifen Acts on *Trypanosoma cruzi* Sphingolipid Pathway Triggering an Apoptotic Death Process.” *Biochemical and Biophysical Research Communications*, 1–7. <https://doi.org/10.1016/j.bbrc.2019.06.149>.
- Lederkremer, R. De, and L. Bertello. 2001. “Glycoinositolphospholipids, Free and as Anchors of Proteins, in *Trypanosoma cruzi*.” *Current Pharmaceutical Design* 7 (12): 1165–79. <https://doi.org/10.2174/1381612013397519>.
- Levine, N. D., J. O. Corliss, F. E.G. Cox, G. Deroux, J. Grain, B. M. Honigberg, G. F. Leedale, et al. 1980. “A Newly Revised Classification of the Protozoa.” *The Journal of Protozoology* 27 (1): 37–58. <https://doi.org/10.1111/j.1550-7408.1980.tb04228.x>.
- Ley, Victoria, N W Andrews, E S Robbins, and V Nussenzweig. 1988. “Amastigotes of *Trypanosoma cruzi* Sustain an Infective Cycle in Mammalian Cells.” *Journal of Experimental Medicine* 168 (August): 649–59. https://doi.org/10.1007/978-3-662-49054-9_3656-1.
- Li, Zhiqiang, Inamul Kabir, Gladys Tietelman, Chongmin Huan, Jianglin Fan, Tilla Worgall, and Xian Cheng Jiang. 2018. “Sphingolipid de Novo Biosynthesis Is Essential for Intestine Cell Survival and Barrier Function.” *Cell Death and Disease* 9 (2): 1–13. <https://doi.org/10.1038/s41419-017-0214-1>.
- Lidani, Kárita Cláudia Freitas, Fabiana Antunes Andrade, Lorena Bavia, Flávia Silva Damasceno, Marcia Holsbach Beltrame, Iara J. Messias-Reason, and Thaisa Lucas Sandri. 2019. “Chagas Disease: From

- Discovery to a Worldwide Health Problem.” *Journal of Physical Oceanography* 49 (6): 1–13. <https://doi.org/10.3389/fpubh.2019.00166>.
- Lima, M. T., A. M. Jansen, E. Rondinelli, and C. R. Gattass. 1991. “*Trypanosoma cruzi*: Properties of a Clone Isolated from CL Strain.” *Parasitology Research* 77 (1): 77–81. <https://doi.org/10.1007/BF00934390>.
- Livak, K J, and T D Schmittgen. 2001. “Analysis of Relative Gene Expression Data Using Real-Time Quantitative PCR and the $2(-\Delta\Delta C(T))$ Method.” *Methods (San Diego, Calif.)* 25 (4): 402–8. <https://doi.org/10.1006/meth.2001.1262>.
- Maingon, Rhaiza, Roger Gerke, Margarita Rodriguez, Julio Urbina, Janet Hoenicka, Stefania Negri, Tania Aguirre, Jan Nehlin, Teresa Knapp, and Julian Crampton. 1988. “The Tubulin Genes of *Trypanosoma cruzi*.” *European Journal of Biochemistry* 171 (1–2): 285–91. <https://doi.org/10.1111/j.1432-1033.1988.tb13788.x>.
- Mandala, Suzanne M., Rosemary A. Thornton, Mark Rosenbach, James Milligan, Margarita Garcia-Calvo, Herbert G. Bull, and Myra B. Kurtz. 1997. “Khafrefungin, a Novel Inhibitor of Sphingolipid Synthesis.” *Journal of Biological Chemistry* 272 (51): 32709–14. <https://doi.org/10.1074/jbc.272.51.32709>.
- Martins, Vicente De Paulo, Michael Okura, Danijela Maric, David M. Engman, Mauricio Vieira, Roberto Docampo, and Silvia N.J. Moreno. 2010. “Acylation-Dependent Export of *Trypanosoma cruzi* Phosphoinositide-Specific Phospholipase C to the Outer Surface of Amastigotes.” *Journal of Biological Chemistry* 285 (40): 30906–17. <https://doi.org/10.1074/jbc.M110.142190>.
- Meer, Gerrit Van, and Quirine Lisman. 2002. “Sphingolipid Transport: Rafts and Translocators.” *Journal of Biological Chemistry* 277 (29): 25855–58. <https://doi.org/10.1074/jbc.R200010200>.
- Menna-barreto, Rubem Figueiredo Sadok, and Solange Lisboa De Castro. 2017. “Clear Shot at Primary Aim: Susceptibility of *Trypanosoma cruzi* Organelles, Structures and Molecular Targets to Drug Treatment.” *Current Topics in Medicinal Chemistry*, 17, 1212–1234. <https://doi.org/10.2174/156802661666616102>
- Mina, John G., Jackie A. Mosely, Hayder Z. Ali, Paul W. Denny, and Patrick G. Steel. 2011. “Exploring Leishmania Major Inositol Phosphorylceramide Synthase (LmjIPCS): Insights into the Ceramide Binding Domain.” *Organic and Biomolecular Chemistry* 9 (6): 1823–30. <https://doi.org/10.1039/c0ob00871k>.

- Mina, John G., Jackie A. Mosely, Hayder Z. Ali, Hosam Shams-Eldin, Ralph T. Schwarz, Patrick G. Steel, and Paul W. Denny. 2010. "A Plate-Based Assay System for Analyses and Screening of the Leishmania Major Inositol Phosphorylceramide Synthase." *International Journal of Biochemistry and Cell Biology* 42 (9): 1553–61. <https://doi.org/10.1016/j.biocel.2010.06.008>.
- Mina, John G.M., and P. W. Denny. 2018. "Everybody Needs Sphingolipids, Right! Mining for New Drug Targets in Protozoan Sphingolipid Biosynthesis." *Parasitology* 145 (2): 134–47. <https://doi.org/10.1017/S0031182017001081>.
- Miskiewicz, Ewa I, and Daniel J Macphee. 2019. "Chapter 5: Lysis Buffer Choices Are Key Considerations to Ensure Effective Sample Solubilization for Protein Electrophoresis." In *Electrophoretic Separation of Proteins: Methods and Protocols*, 1855:61–72.
- Mortara, Renato A., Lindamar M.S. Minelli, Filip Vandekerckhove, Victor Nussenzweig, and F. Juarez Ramalho-Pinto. 2001. "Phosphatidylinositol-Specific Phospholipase C (PI-PLC) Cleavage of GPI-Anchored Surface Molecules of *Trypanosoma cruzi* Triggers in Vitro Morphological Reorganization of Trypomastigotes." *Journal of Eukaryotic Microbiology* 48 (1): 27–37. <https://doi.org/10.1111/j.1550-7408.2001.tb00413.x>.
- Moult, John, Fidelis, Krzysztof, Andriy Kryshchak, Torsten Schwede, and Anna Tramontano. 2018. "Critical Assessment of Methods of Protein Structure Prediction (CASP) – Round XII." *Proteins* 86 (1): 7–15. <https://doi.org/10.1002/prot.25415>.
- Müller Kratz, Jadel, Facundo Garcia Bournissen, Colin J. Forsyth, and Sergio Sosa-Estani. 2018. "Clinical and Pharmacological Profile of Benznidazole for Treatment of Chagas Disease." *Expert Review of Clinical Pharmacology* 11 (10): 943–57. <https://doi.org/10.1080/17512433.2018.1509704>.
- Nagiec, M. Marek, Elzbieta E. Nagiec, Julie A. Baltisberger, Gerald B. Wells, Robert L. Lester, and Robert C. Dickson. 1997. "Sphingolipid Synthesis as a Target for Antifungal Drugs. Complementation of the Inositol Phosphorylceramide Synthase Defect in a Mutant Strain of *Saccharomyces Cerevisiae* by the AUR1 Gene." *Journal of Biological Chemistry* 272 (15): 9809–17. <https://doi.org/10.1074/jbc.272.15.9809>.
- Nakayasu, Ernesto S., Dmitry V. Yashunsky, Lilian L. Nohara, Ana Claudia T Torrecilhas, Andrei V. Nikolaev, and Igor C. Almeida. 2009. "GPIomics: Global Analysis of Glycosylphosphatidylinositol-Anchored Molecules of *Trypanosoma cruzi*." *Molecular Systems Biology* 5 (261): 1–17. <https://doi.org/10.1038/msb.2009.13>.
- Neuwald, Andrew F. 1997. "An Unexpected Structural Relationship between Integral Membrane

- Phosphatases and Soluble Haloperoxidases.” *Protein Science* 6 (8): 1764–67. <https://doi.org/10.1002/pro.5560060817>.
- Nogueira, Nadir F.S., Marcelo S. Gonzalez, José Eugênio Gomes, Wanderley de Souza, Eloi S. Garcia, Patricia Azambuja, Lilian L. Nohara, Igor C. Almeida, Bianca Zingales, and Walter Colli. 2007. “*Trypanosoma cruzi*: Involvement of Glycoinositolphospholipids in the Attachment to the Luminal Midgut Surface of *Rhodnius Prolixus*.” *Experimental Parasitology* 116 (2): 120–28. <https://doi.org/10.1016/j.exppara.2006.12.014>.
- Noia, J. M. Di, D. O. Sanchez, and A. C.C. Frasch. 1995. “The Protozoan *Trypanosoma cruzi* Has a Family of Genes Resembling the Mucin Genes of Mammalian Cells.” *Journal of Biological Chemistry* 270 (41): 24146–49. <https://doi.org/10.1074/jbc.270.41.24146>.
- Norcliffe, Jennifer L., John G. Mina, Emilio Alvarez, Juan Cantizani, Francisco De Dios-Anton, Gonzalo Colmenarejo, Silva Gonzalez Del Valle, et al. 2018. “Identifying Inhibitors of the Leishmania Inositol Phosphorylceramide Synthase with Antiprotozoal Activity Using a Yeast-Based Assay and Ultra-High Throughput Screening Platform.” *Scientific Reports* 8 (1): 1–10. <https://doi.org/10.1038/s41598-018-22063-9>.
- Ohanian, J., and V. Ohanian. 2001. “Sphingolipids in Mammalian Cell Signalling.” *Cellular and Molecular Life Sciences* 58 (14): 2053–68. <https://doi.org/10.1007/PL00000836>.
- Ohnuki, Takashi, Tatsuya Yano, Yasunori Ono, Shiho Kozuma, Toshihiro Suzuki, Yasumasa Ogawa, and Toshio Takatsu. 2009. “Haplofungins, Novel Inositol Phosphorylceramide Synthase Inhibitors, from *Lauriomyces Bellulus* SANK 26899 I. Taxonomy, Fermentation, Isolation and Biological Activities.” *Journal of Antibiotics* 62 (10): 545–49. <https://doi.org/10.1038/ja.2009.72>.
- Pan, S. Chia Tung. 1978. “*Trypanosoma cruzi*: Intracellular Stages Grown in a Cell-Free Medium at 37 C.” *Experimental Parasitology* 45 (2): 215–24. [https://doi.org/10.1016/0014-4894\(78\)90062-0](https://doi.org/10.1016/0014-4894(78)90062-0).
- Peach, M, N Marsh, Ewa I Miskiewicz, and Daniel J Macphee. 2015. “Chapter 8: Solubilization of Proteins: The Importance of Lysis Buffer Choice.” In *Western Blotting: Methods and Protocols*, 1312:1–509. <https://doi.org/10.1007/978-1-4939-2694-7>.
- Pratt, Steven, Nilu K. Wansadhipathi-Kannangara, Catherine R. Bruce, John G. Mina, Hosam Shams-Eldin, Josefina Casas, Kentaro Hanada, Ralph T. Schwarz, Sabrina Sonda, and Paul W. Denny. 2013. “Sphingolipid Synthesis and Scavenging in the Intracellular Apicomplexan Parasite, *Toxoplasma Gondii*.” *Molecular and Biochemical Parasitology* 187 (1): 43–51. <https://doi.org/10.1016/j.molbiopara.2012.11.007>.

- Previato, JO, R Wait, C Jones, GA DosReis, AR Todeschini, N Heise, and LM Previato. 2004. "Glycoinositolphospholipid from *Trypanosoma cruzi*: Structure, Biosynthesis and Immunobiology." *Adv Parasitol.* 56: 1–41.
- Rassi, Jr Anis, Anis Rassi, and Joffre Marcondes de Rezende. 2012. "American Trypanosomiasis (Chagas Disease)." *Infect Dis Clin North Am* 26: 275–91. <https://doi.org/10.1016/j.idc.2012.03.002>.
- Rassi Jr, Anis, Anis Rassi, and José Antonio Marin-Neto. 2010. "Seminar Chagas Disease." *Lancet* 375 (9723): 1388–1402. [https://doi.org/10.1016/S0140-6736\(10\)60061-X](https://doi.org/10.1016/S0140-6736(10)60061-X).
- Rios, Lizette E., Juan Carlos Vázquez-Chagoyán, Antonio Ortega Pacheco, M. Paola Zago, and Nisha J. Garg. 2019. "Immunity and Vaccine Development Efforts against *Trypanosoma cruzi*." *Acta Tropica* 200: 105168. <https://doi.org/10.1016/j.actatropica.2019.105168>.
- Riss, Terry L, Richard A Moravec, Andrew L Niles, Sarah Duellman, Hélène A Benink, Tracy J Worzella, and Lisa Minor. 2013. "Cell Viability Assays." In *Assay Guidance Manual*, 1–25. <http://www.ncbi.nlm.nih.gov/pubmed/23805433>.
- Rodríguez-Morales, Olivia, Víctor Monteón-Padilla, Silvia C. Carrillo-Sánchez, Martha Rios-Castro, Mariana Martínez-Cruz, Alejandro Carabarin-Lima, and Minerva Arce-Fonseca. 2015. "Experimental Vaccines against Chagas Disease: A Journey through History." *Journal of Immunology Research* 2015. <https://doi.org/10.1155/2015/489758>.
- Rolón, Miriam, Celeste Vega, José A. Escario, and Alicia Gómez-Barrio. 2006. "Development of Resazurin Microtiter Assay for Drug Sensibility Testing of *Trypanosoma cruzi* Epimastigotes." *Parasitology Research* 99 (2): 103–7. <https://doi.org/10.1007/s00436-006-0126-y>.
- Romano, Julia D., Sabrina Sonda, Emily Bergbower, Maria Elisa Smith, and Isabelle Coppens. 2013. "Toxoplasma Gondii Salvages Sphingolipids from the Host Golgi through the Rerouting of Selected Rab Vesicles to the Parasitophorous Vacuole." *Molecular Biology of the Cell* 24 (12): 1974–95. <https://doi.org/10.1091/mbc.E12-11-0827>.
- Salto, Maria Laura, Laura E. Bertello, Mauricio Vieira, Roberto Docampo, Silvia N.J. Moreno, and Rosa M. De Lederkremer. 2003. "Formation and Remodeling of Inositolphosphoceramide during Differentiation of *Trypanosoma cruzi* from Trypomastigote to Amastigote." *Eukaryotic Cell* 2 (4): 756–68. <https://doi.org/10.1128/EC.2.4.756-768.2003>.
- Salto, María Laura, Tetsuya Furuya, Silvia N. Moreno, Roberto Docampo, and Rosa M. De Lederkremer. 2002. "The Phosphatidylinositol-Phospholipase C from *Trypanosoma cruzi* Is Active on

- Inositolphosphoceramide.” *Molecular and Biochemical Parasitology* 119 (1): 131–33. [https://doi.org/10.1016/S0166-6851\(01\)00392-9](https://doi.org/10.1016/S0166-6851(01)00392-9).
- Schenkman, S., and R. A. Mortara. 1992. “HeLa Cells Extend and Internalize Pseudopodia during Active Invasion by *Trypanosoma cruzi* Trypomastigotes.” *Journal of Cell Science* 101 (4): 895–905.
- Schenkman, Sergio, Carmen Diaz, and Victor Nussenzweig. 1991. “Attachment of *Trypanosoma cruzi* Trypomastigotes to Receptors at Restricted Cell Surface Domains.” *Experimental Parasitology* 72 (1): 76–86. [https://doi.org/10.1016/0014-4894\(91\)90123-E](https://doi.org/10.1016/0014-4894(91)90123-E).
- Schenkman, Sergio, Michael A.J. Ferguson, Norton Heise, Maria Lucia Cardoso de Almeida, Renato A. Mortara, and Nobuko Yoshida. 1993. “Mucin-like Glycoproteins Linked to the Membrane by Glycosylphosphatidylinositol Anchor Are the Major Acceptors of Sialic Acid in a Reaction Catalyzed by Trans-Sialidase in Metacyclic Forms of *Trypanosoma cruzi*.” *Molecular and Biochemical Parasitology* 59 (2): 293–303. [https://doi.org/10.1016/0166-6851\(93\)90227-O](https://doi.org/10.1016/0166-6851(93)90227-O).
- Schlager, Benjamin, Anna Straessle, and Ernst Hafen. 2012. “Use of Anionic Denaturing Detergents to Purify Insoluble Proteins after Overexpression.” *BMC Biotechnology* 12 (1): 1. <https://doi.org/10.1186/1472-6750-12-95>.
- Serrano, Alvaro Acosta, Sergio Schenkman, Nobuko Yoshida, Angela Mehlert, Julia M. Richardson, and Michael A.J. Ferguson. 1995. “The Lipid Structure of the Glycosylphosphatidylinositol-Anchored Mucin-like Sialic Acid Acceptors of *Trypanosoma cruzi* Changes during Parasite Differentiation from Epimastigotes to Infective Metacyclic Trypomastigote Forms.” *Journal of Biological Chemistry* 270 (45): 27244–53. <https://doi.org/10.1074/jbc.270.45.27244>.
- Sevova, Elitza S., Michael A. Goren, Kevin J. Schwartz, Fong Fu Hsu, John Turk, Brian G. Fox, and James D. Bangs. 2010. “Cell-Free Synthesis and Functional Characterization of Sphingolipid Synthases from Parasitic Trypanosomatid Protozoa.” *Journal of Biological Chemistry* 285 (27): 20580–87. <https://doi.org/10.1074/jbc.M110.127662>.
- Shum, David, Constantin Radu, Earl Kim, Muriel Cajuste, Yufang Shao, Venkatraman E. Seshan, and Hakim Djaballah. 2008. “A High Density Assay Format for the Detection of Novel Cytotoxic Agents in Large Chemical Libraries.” *Journal of Enzyme Inhibition and Medicinal Chemistry* 23 (6): 931–45. <https://doi.org/10.1080/14756360701810082>.
- Sibley, L. David, and Norma W. Andrews. 2000. “Cell Invasion by Un-Palatable Parasites.” *Traffic* 1 (2): 100–106. <https://doi.org/10.1034/j.1600-0854.2000.010202.x>.

- Souza, Wanderley De, Tecia Maria Ulisses De Carvalho, and Emile Santos Barrias. 2010. "Review on *Trypanosoma cruzi*: Host Cell Interaction." *International Journal of Cell Biology* 2010. <https://doi.org/10.1155/2010/295394>.
- Stank, Antonia, Daria B. Kokh, Jonathan C. Fuller, and Rebecca C. Wade. 2016. "Protein Binding Pocket Dynamics." *Accounts of Chemical Research* 49 (5): 809–15. <https://doi.org/10.1021/acs.accounts.5b00516>.
- Stecconi-Silva, R. B., W. K. Andreoli, and R. A. Mortara. 2003. "Parameters Affecting Cellular Invasion and Escape from the Parasitophorous Vacuole by Different Infective Forms of *Trypanosoma cruzi*." *Memorias Do Instituto Oswaldo Cruz* 98 (7): 953–58. <https://doi.org/10.1590/S0074-02762003000700016>.
- Studier, F. William, and Barbara A. Moffatt. 1986. "Use of Bacteriophage T7 RNA Polymerase to Direct Selective High-Level Expression of Cloned Genes." *Journal of Molecular Biology* 189 (1): 113–30. [https://doi.org/10.1016/0022-2836\(86\)90385-2](https://doi.org/10.1016/0022-2836(86)90385-2).
- Sugimoto, Yuichi, Hiroki Sakoh, and Koji Yamada. 2004. "IPC Synthase as a Useful Target for Antifungal Drugs." *Current Drug Targets - Infectious Disorders* 4 (4): 311–22. <https://doi.org/10.2174/1568005043340597>.
- Sutterwala, Shaheen S., Caleb H. Creswell, Sumana Sanyal, Anant K. Menon, and James D. Bangs. 2007. "De Novo Sphingolipid Synthesis Is Essential for Viability, but Not for Transport of Glycosylphosphatidylinositol-Anchored Proteins, in African Trypanosomes." *Eukaryotic Cell* 6 (3): 454–64. <https://doi.org/10.1128/EC.00283-06>.
- Sutterwala, Shaheen S., Fong Fu Hsu, Elitza S. Sevova, Kevin J. Schwartz, Kai Zhang, Phillip Key, John Turk, Stephen M. Beverley, and James D. Bangs. 2008. "Developmentally Regulated Sphingolipid Synthesis in African Trypanosomes." *Molecular Microbiology* 70 (2): 281–96. <https://doi.org/10.1111/j.1365-2958.2008.06393.x>.
- Tafesse, Fikadu Geta, Philipp Ternes, and Joost C M Holthuis. 2006. "The Multigenic Sphingomyelin Synthase Family." *Journal of Biological Chemistry* 281 (40): 29421–25. <https://doi.org/10.1074/jbc.R600021200>.
- Tarleton, Rick L., and L. Zhang. 1999. "Chagas Disease Etiology: Autoimmunity or Parasite Persistence?" *Parasitology Today* 15 (3). [https://doi.org/10.1016/S0169-4758\(99\)01398-8](https://doi.org/10.1016/S0169-4758(99)01398-8).
- Tomlinson, S., F. Vandekerckhove, U. Frevert, and V. Nussenzweig. 1995. "The Induction of *Trypanosoma*

- cruzi* Trypomastigote to Amastigote Transformation by Low PH.” *Parasitology* 110 (5): 547–54. <https://doi.org/10.1017/S0031182000065264>.
- Trinconi, Cristiana T., Danilo C. Miguel, Ariel M. Silber, Christopher Brown, John G.M. Mina, Paul W. Denny, Norton Heise, and Silvia R.B. Uliana. 2018. “Tamoxifen Inhibits the Biosynthesis of Inositolphosphorylceramide in *Leishmania*.” *International Journal for Parasitology: Drugs and Drug Resistance* 8 (3): 475–87. <https://doi.org/10.1016/j.ijpddr.2018.10.007>.
- Tyler, K. M., and D. M. Engman. 2001. “The Life Cycle of *Trypanosoma cruzi* Revisited.” *International Journal for Parasitology* 31 (5–6): 472–81. [https://doi.org/10.1016/S0020-7519\(01\)00153-9](https://doi.org/10.1016/S0020-7519(01)00153-9).
- Uhrig, María Laura, Alicia S. Couto, Walter Colli, and Rosa M. De Lederkremer. 1996. “Characterization of Inositolphospholipids in *Trypanosoma Cruzi* Trypmastigote Forms.” *Biochimica et Biophysica Acta - Lipids and Lipid Metabolism* 1300 (3): 233–39. [https://doi.org/10.1016/0005-2760\(96\)00021-5](https://doi.org/10.1016/0005-2760(96)00021-5).
- Valente, Maria, Víctor M. Castillo-Acosta, Antonio E. Vidal, and Dolores González-Pacanowska. 2019. “Overview of the Role of Kinetoplastid Surface Carbohydrates in Infection and Host Cell Invasion: Prospects for Therapeutic Intervention.” *Parasitology*, 1–12. <https://doi.org/10.1017/s0031182019001355>.
- Vieira da Silva, Claudio, Alejandro O. Luquetti, Anis Rassi, and Renato Arruda Mortara. 2006. “Involvement of Ssp-4-Related Carbohydrate Epitopes in Mammalian Cell Invasion by *Trypanosoma cruzi* Amastigotes.” *Microbes and Infection* 8 (8): 2120–29. <https://doi.org/10.1016/j.micinf.2006.03.016>.
- Vieira, Mauricio, Juliana M.F. Dutra, Tecia M.U. Carvalho, Narcisa L. Cunha-e-Silva, Thaïs Souto-Padrón, and Wanderley Souza. 2002. “Cellular Signaling during the Macrophage Invasion by *Trypanosoma cruzi*.” *Histochemistry and Cell Biology* 118 (6): 491–99. <https://doi.org/10.1007/s00418-002-0477-0>.
- Villalta, F, and F Kierszenbaum. 1984. “Host-cell Invasion by *Trypanosoma cruzi*: Role Of Cell Surface Galactose Residues.” *Biochemical and Biophysical Research Communications* 119 (1): 228–35.
- Villalta, Fernando, and Girish Rachakonda. 2019. “Advances in Preclinical Approaches to Chagas Disease Drug Discovery.” *Expert Opinion on Drug Discovery* 14 (11): 1–14. <https://doi.org/10.1080/17460441.2019.1652593>.
- Wang, Sheng, Shiyang Fei, Zongan Wang, Yu Li, Jinbo Xu, Feng Zhao, and Xin Gao. 2018. “PredMP: A Web Server for de Novo Prediction and Visualization of Membrane Proteins.” *Bioinformatics*, no.

- August: 1–3. <https://doi.org/10.1093/bioinformatics/bty684>.
- Wang, Zongan, John M. Jumper, Karl F. Freed, and Tobin R. Sosnick. 2016. “Including H-Bonding in Depth-Dependent Membrane Burial Potentials for Improving Folding Simulations.” *Biophysical Journal* 110 (3): 58a. <https://doi.org/10.1016/j.bpj.2015.11.378>.
- WHO. 2015. “Chagas Disease in Latin America: An Epidemiological Update Based on 2010 Estimates.” *Weekly Epidemiological Record* 90: 33–44.
- World Health Organization. 2012. “Research Priorities for Chagas Disease, Human African Trypanosomiasis and Leishmaniasis.” *World Health Organization Technical Report Series*, no. 975.
- Yoshida, N., R. A. Mortara, M. F. Araguth, J. C. Gonzalez, and M. Russo. 1989. “Metacyclic Neutralizing Effect of Monoclonal Antibody 10D8 Directed to the 35- and 50-Kilodalton Surface Glycoconjugates of *Trypanosoma cruzi*.” *Infection and Immunity* 57 (6): 1663–67.
- Zdobnov, E. M., and R. Apweiler. 2001. “InterProScan - An Integration Platform for the Signature-Recognition Methods in InterPro.” *Bioinformatics* 17 (9): 847–48. <https://doi.org/10.1093/bioinformatics/17.9.847>.
- Zhang, Ou, Mattie C. Wilson, Wei Xu, Fong Fu Hsu, John Turk, F. Matthew Kuhlmann, Yingwei Wang, et al. 2009. “Degradation of Host Sphingomyelin Is Essential for Leishmania Virulence.” *PLoS Pathogens* 5 (12). <https://doi.org/10.1371/journal.ppat.1000692>.
- Zingales, Bianca. 2018. “*Trypanosoma cruzi* Genetic Diversity: Something New for Something Known about Chagas Disease Manifestations, Serodiagnosis and Drug Sensitivity.” *Acta Tropica* 184 (September 2017): 38–52. <https://doi.org/10.1016/j.actatropica.2017.09.01>